

โครงสร้างขอลเวชันและพลวัตของไอออนไนเตรต (NO_3^-) ในน้ำ : การจำลอง
พลวัตเชิงโมเลกุลที่ผสมผสานกลศาสตร์ควอนตัมและกลศาสตร์โมเลกุล

นางปิยะวัน ตั้งควรรณวานิช

วิทยานิพนธ์นี้เป็นส่วนหนึ่งของการศึกษาตามหลักสูตรปริญญาวิทยาศาสตรดุษฎีบัณฑิต
สาขาวิชาเคมี
มหาวิทยาลัยเทคโนโลยีสุรนารี
ปีการศึกษา 2549

**SOLVATION STRUCTURE AND DYNAMICS OF
NITRATE ANION (NO₃⁻) IN WATER : AB INITIO
QM/MM MOLECULAR DYNAMICS SIMULATIONS**

Piyawan Tangkawanwanit

**A Thesis Submitted in Partial Fulfillment of the Requirements
for the Degree of Doctor of Philosophy in Chemistry**

Suranaree University of Technology

Academic Year 2006

**SOLVATION STRUCTURE AND DYNAMICS OF NITRATE
ANION (NO₃⁻) IN WATER : AB INITIO QM/MM MOLECULAR
DYNAMICS SIMULATIONS**

Suranaree University of Technology has approved this thesis submitted in partial fulfillment of the requirements for the Degree of Doctor of Philosophy.

Thesis Examining Committee

(Assoc. Prof. Dr. Malee Tangsathitkulchai)

Chairperson

(Assoc. Prof. Dr. Anan Tongraar)

Member (Thesis Advisor)

(Prof. Dr. Kritsana Sagarik)

Member

(Prof. Dr. Supot Hannongbua)

Member

(Asst. Prof. Dr. Visit Vao-Soongnern)

Member

(Assoc. Prof. Dr. Saowanee Rattanaphani)

Vice Rector for Academic Affairs

(Assoc. Prof. Dr. Sompong Thammathaworn)

Dean of Institute of Science

ปิยะวัน ดังควรรณวานิช : โครงสร้างซอลเวชันและพลวัตของไอออนไนเตรต (NO_3^-) ในน้ำ : การจำลองพลวัตเชิงโมเลกุลที่ผสมผสานกลศาสตร์ควอนตัมและกลศาสตร์โมเลกุล (SOLVATION STRUCTURE AND DYNAMICS OF NITRATE ANION (NO_3^-) IN WATER : AB INITIO QM/MM MOLECULAR DYNAMICS SIMULATIONS) อาจารย์ที่ปรึกษา: รองศาสตราจารย์ ดร.อนันต์ ทองระอา, 113 หน้า.

สมบัติเชิงโครงสร้างและเชิงพลวัตของไอออนไนเตรตในสารละลายน้ำได้ถูกศึกษาโดยการจำลองพลวัตเชิงโมเลกุลที่ผสมผสานกลศาสตร์ควอนตัมและกลศาสตร์โมเลกุลที่แตกต่างกันสองการจำลอง ได้แก่ HF/MM และ B3LYP/MM โดยส่วนของไอออนและน้ำที่อยู่ล้อมรอบไอออนถูกอธิบายด้วยกลศาสตร์ควอนตัมในระดับ HF และ B3LYP ตามลำดับ โดยใช้เบซิสเซตชนิด DZV+ บนพื้นฐานของทั้งวิธี HF และ B3LYP พบว่า ไอออนไนเตรตสามารถเกิดชั้นไฮเดรชันได้ชัดเจน แต่ชั้นไฮเดรชันดังกล่าวค่อนข้างยืดหยุ่น และพันธะไฮโดรเจนระหว่างไอออนไนเตรตกับน้ำค่อนข้างอ่อน จากข้อมูลการวิเคราะห์การจัดตัวและการสั่นของไอออนไนเตรต พบว่าน้ำที่อยู่ล้อมรอบไอออนได้เหนี่ยวนำให้ไอออนมีการสลายสมมาตร (symmetry breaking) ซึ่งลักษณะดังกล่าว สอดคล้องกับผลการทดลองเป็นอย่างดี นอกจากนี้ ข้อมูลด้านพลวัต เช่น การบิดเบือนของพันธะ และการเลื่อนของความถี่ที่เกิดจากการสั่น รวมทั้งเวลาการอยู่เฉลี่ย (mean residence time) ของน้ำรอบไอออน ได้ชี้ให้เห็นความสามารถการสลายโครงสร้าง (structure-breaking) ของไอออนไนเตรตในสารละลายน้ำได้อย่างชัดเจน ในส่วนของวิธีทางกลศาสตร์ควอนตัมที่เลือกใช้นั้น ดูเหมือนว่าวิธี HF และ B3LYP สามารถอธิบายการเกิดชั้นไฮเดรชันของไอออนได้ไม่แตกต่างกันมากนัก อย่างไรก็ตาม ข้อมูลด้านพลวัตชี้ให้เห็นว่า วิธี HF มีความเหมาะสมมากกว่าวิธี B3LYP

PIYAWAN TANGKAWANWANIT : SOLVATION STRUCTURE AND DYNAMICS OF NITRATE ANION (NO_3^-) IN WATER : AB INITIO QM/MM MOLECULAR DYNAMICS SIMULATIONS. THESIS ADVISOR : ASSOC. PROF. ANAN TONGRAAR, Ph.D. 113 PP.

NITRATE/STRUCTURE-BREAKING/MRT/WATER EXCHANGE

The structural and dynamical properties of NO_3^- in dilute aqueous solution have been investigated by means of two combined quantum mechanics/molecular mechanics (QM/MM) molecular dynamics simulations, namely HF/MM and B3LYP/MM, in which the ion and its surrounding water molecules were treated at HF and B3LYP levels of accuracy, respectively, using DZV+ basis set. On the basis of both HF and B3LYP methods, a well-defined first hydration shell of NO_3^- is obtainable, but the shell is quite flexible and the hydrogen-bond interactions between NO_3^- and water are rather weak. With respect to the detailed analysis of the geometrical arrangement and vibrations of NO_3^- , the experimentally observed solvent-induced symmetry breaking of the ion is well reflected. In addition, the dynamical information, *i.e.*, the bond distortions and shifts in the corresponding bending and stretching frequencies as well as the mean residence time of water molecules surrounding the NO_3^- ion, clearly indicate the “structure-breaking” ability of this ion in aqueous solution. From a methodical point of view it seems that both HF and B3LYP methods are not too different in describing this hydrated ion by means of a QM/MM simulation. However, the detailed analysis of the dynamics properties indicates a better suitability of the HF method compared to the B3LYP-DFT approach.

School of Chemistry

Student's Signature _____

Academic Year 2006

Advisor's Signature _____

ACKNOWLEDGEMENTS

Firstly, it is very difficult to overstate my gratitude to my Ph.D. supervisor, Assoc. Prof. Dr. Anan Tongraar for his enthusiasm, his inspiration, and his great efforts to explain things clearly and simply, as well as making computational chemistry fun for me. He has provided encouragement, sound advice, good teaching, good company and lots of good ideas throughout my thesis-writing and course work periods.

I am thankful to all of thesis examining committee namely Prof. Dr. Kritsana Sagarik, Prof. Dr. Supot Hannongbua, Assoc. Prof. Dr. Malee Tangsathitkulchai and Asst. Prof. Dr. Visit Vao-soongnern for their useful suggestions.

I wish to thank all chemistry friends for their friendships, especially Supaporn Dokmaisrijan, Weenawan Somphon and Jittima Chaodamrongsakul for helping me get through the difficult times and for all the emotional support, comradeship and fun entertainment. I wish to thank my family, my parents, my brothers, my sister and my child for their love and for understanding me.

Finally, I would like to thanks School of Chemistry, Suranaree University of Technology. My apologies to the others who I have not mentioned by name, I am indebted to them for everything they have helped.

Piyawan Tangkawanwanit

CONTENTS

	Page
ABSTRACTS IN THAI.....	I
ABSTRACTS IN ENGLISH.....	II
ACKNOWLEDGEMENTS.....	IV
CONTENTS.....	V
LIST OF TABLES.....	VIII
LIST OF FIGURES.....	IX
LIST OF ABBREVIATIONS.....	XII
CHAPTER	
I INTRODUCTION.....	1
II COMPUTATIONAL METHODS.....	10
2.1 Quantum chemistry.....	10
2.1.1 Schrödinger equation.....	10
2.1.2 Born-Oppenheimer approximation.....	12
2.1.3 Molecular orbital (MO) theory.....	13
2.1.4 Basis functions.....	16
2.1.5 Basis sets.....	18
2.1.6 Variation principle.....	19
2.1.7 Hartree-Fock (HF) method.....	20
2.1.8 Electron correlation.....	24

CONTENTS (Continued)

	Page
2.1.9 Density functional theory (DFT).....	25
2.2 Computer simulation methods.....	27
2.2.1 Statistical mechanics.....	27
2.2.2 Correlation functions.....	28
2.2.1.1 Radial distribution functions (RDFs).....	28
2.2.1.2 Time correlation functions.....	29
2.2.3 Classical MD method.....	30
2.2.3.1 Intermolecular potentials.....	32
2.2.3.2 Time integration algorithms.....	33
2.2.3.3 Periodic boundary conditions.....	37
2.2.3.4 Cut-off limit and potential at cut-off.....	38
2.2.3.5 Non-bonded neighbor lists.....	40
2.2.3.6 Long-range interactions.....	41
2.3 Combined <i>ab initio</i> QM/MM MD simulation.....	42
III RESULTS AND DISCUSSION	45
3.1 Computational details.....	45
3.1.1 Construction of NO ₃ ⁻ -H ₂ O pair potential.....	45
3.1.2 Selection of QM method, basis set and QM size.....	53
3.1.3 Simulation protocol.....	56
3.2 Structural details.....	57

CONTENTS (Continued)

	Page
3.3 Dynamical details.....	65
3.3.1 Intramolecular geometry and vibration of NO_3^-	65
3.3.2 Intramolecular geometry and vibrations of water molecules in the hydration shell of NO_3^-	70
3.3.3 Translational motion and exchange process of water molecular in the hydration shell of NO_3^-	73
IV CONCLUSION	81
REFERENCES	83
APPENDIX CIRRICULUM VITAE	102
Appendix A Publication.....	103
CIRRICULUM VITAE	113

LIST OF TABLES

Table		Page
3.1	Optimized parameters of the analytical pair potential for the interaction of water with NO_3^- (interaction energies in kcal.mol^{-1} and distances in \AA)	51
3.2	Stabilization energies and some selected structural parameters of the optimized NO_3^- - H_2O complex, calculated at HF, B3LYP, MP2 and CCSD methods using DZV+ and aug-cc-pvdz (data in parentheses) basis sets.....	55
3.3	Vibrational frequencies of NO_3^-	69
3.4	Vibrational frequencies of water molecules in the bulk and in the hydration sphere of NO_3^- . Numbers in parentheses correspond to the data obtained by B3LYP/MM-based simulations.....	73
3.5	Diffusion coefficients of water molecules in the bulk and in the hydration shell of NO_3^-	74
3.6	Mean residence time of water molecules in the bulk and in the vicinity of NO_3^- oxygens, calculated within the $\text{O}_\text{N}--\text{O}_\text{w}$ distance of 3.5 \AA	79

LIST OF FIGURES

Figure	Page
2.1 The schematic of MD simulation.....	31
2.2 Periodic boundary conditions in two dimensions.....	37
2.3 Cut-off limit.....	38
2.4 Verlet neighbor list.....	40
2.5 System's partition.....	43
2.6 Smoothing of force at transition between QM and MM regions.....	44
3.1 Variation of NO_3^- - H_2O configurations.....	46
3.2 Variation of water's orientations.....	46
3.3 Plot of stabilization energies between the NO_3^- ion and water molecule, for $\theta = 0^\circ$ and $\phi = 0^\circ$	47
3.4 Plot of stabilization energies between the NO_3^- ion and water molecule, for $\theta = 15^\circ$ and $\phi = 0^\circ$	47
3.5 Plot of stabilization energies between the NO_3^- ion and water molecule, for $\theta = 30^\circ$ and $\phi = 0^\circ$	48
3.6 Plot of stabilization energies between the NO_3^- ion and water molecule, for $\theta = 45^\circ$ and $\phi = 0^\circ$	48

LIST OF FIGURES (Continued)

Figure	Page
3.7 Plot of stabilization energies between the NO_3^- ion and water molecule, for $\theta = 60^\circ$ and $\phi = 0^\circ$	49
3.8 Plot of stabilization energies between the NO_3^- ion and water molecule, for $\theta = 60^\circ$ and $\phi = 30^\circ$	49
3.9 Plot of stabilization energies between the NO_3^- ion and water molecule, for $\theta = 60^\circ$ and $\phi = 60^\circ$	50
3.10 Comparison of the interaction energies obtained from the MP2 calculations with and without basis set superposition error (BSSE) correction, ΔE_{MP2} and ΔE_{BSSE} , and from the fitted potential function, ΔE_{FIT} , using the parameters given in Table 3.1 for some values of θ and ϕ	52
3.11 a) N-O_w , b) N-H_w , c) $\text{O}_N\text{-O}_w$ and d) $\text{O}_N\text{-H}_w$ radial distribution functions and their corresponding integration numbers.....	58
3.12 Distributions of the angle α between the vector perpendicular to NO_3^- plane and the vector along $\text{N}\cdots\text{O}_w$ distance, calculated within the first minimum of N-O_w RDFs.....	59
3.13 Arrangements of $\text{NO}_3^-(\text{H}_2\text{O})_n$ complexes obtained at 0, 1, 2, 3 and 4 ps of the HF/MM and B3LYP/MM simulations, plotted within the $\text{O}_N\cdots\text{H}_w$ distance of 2.5 Å.....	61

LIST OF FIGURES (Continued)

Figure	Page
3.14 a) O-O, b) O-H, c) H-O and d) H-H radial distribution functions and their corresponding integration numbers. The first atom of each pair refers to the atoms of the water molecule, whose oxygen position was defined as center of the QM region during the QM/MM simulation.....	62
3.15 Distributions of the $\text{N-O}_\text{N}\text{---H}_\text{w}$ angle, calculated within the $\text{O}_\text{N}\text{---H}_\text{w}$ distance of 2.5 Å.....	64
3.16 Distributions of the $\text{O}_\text{N}\text{---H}_\text{w}\text{-O}_\text{w}$ angle, calculated within the $\text{O}_\text{N}\text{---H}_\text{w}$ distance of 2.5 Å.....	64
3.17 Distributions of the angle θ between the $\text{O}_\text{w}\text{---O}_\text{N}$ vector and the vector of water's dipole moment, calculated within the $\text{O}_\text{N}\text{---H}_\text{w}$ distance of 2.5 Å.....	65
3.18 Distributions of a) N-O bond length and b) O-N-O angle of NO_3^-	67
3.19 Distributions of ϕ , as defined by a vector along any N-O bond and a vector pointing outwards between the other two N-O bonds.....	68
3.20 Distributions of a) O-H bond length and b) H-O-H angle of water molecules in the bulk and in hydration shell of NO_3^-	72
3.21 Time dependence of $\text{O}_\text{N}\text{---O}_\text{w}$ distances, selecting only for the first 10 ps of the HF/MM simulation.....	76
3.22 Time dependence of $\text{O}_\text{N}\text{---O}_\text{w}$ distances, selecting only for the first 10 ps of the B3LYP/MM simulation.....	77

LIST OF ABBREVIATIONS

MC	=	Monte Carlo
MD	=	Molecular Dynamics
PCM	=	Polarizable Continuum Model
QM	=	Quantum Mechanics
MM	=	Molecular Mechanics
QM/MM	=	Combined Quantum Mechanical/Molecular Mechanical Method
HF	=	Hartree-Fock
SCF	=	Self-Consistent Field
B3LYP	=	Becke's Three-Parameters Hybrid Functional Combined with Lee-Yang-Parr Correlation Function
DFT	=	Density Functional Theory
MP2	=	Second-Order Møller-Plesset Perturbation Theory
CCSD	=	Coupled Cluster with Single and Double Excitations
LCAO-MO	=	Linear Combination of Atomic Orbital to Molecular Orbital
MO	=	Molecular Orbital
AO	=	Atomic Orbital
STO	=	Slater-Type Orbital
GTO	=	Gaussian-Type Orbital

LIST OF ABBREVIATIONS (Continued)

ECP	=	Effective Core Potentials
aug-cc-pvdz	=	Additional Diffuse Basis Function and Correlation Consistent Polarized Valence Double Zeta
DZV+	=	Double Zeta Valence plus Diffuse Function
BJH	=	A Flexible Water Model Developed by Bopp, Jancsó, and Heinzinger
CF2	=	Central Force Model Version 2
NO ₃ ⁻	=	Nitrate Anion
H ₂ O	=	Water
$\Delta E_{NO_3^- - H_2O}$	=	Pair Potential Energy between NO ₃ ⁻ and H ₂ O
q	=	Point Charge
r_{ij}	=	Distances between the i -th Site and the j -th Site Atoms
MPA	=	Mulliken Population Analysis
BSSE	=	Basis Set Superposition Error
RDF	=	Radial Distribution Function
ADF	=	Angular Distribution Function
VACF	=	Velocity Autocorrelation Function
MRT	=	Mean Residence Time
CN	=	Coordination Number
NVT	=	Canonical Ensemble
K	=	Kelvin

LIST OF ABBREVIATIONS (Continued)

ps	=	Pico Second
°	=	Degree
Å	=	Angström
kcal.mol ⁻¹	=	Kilocalorie/Mole
cm ² s ⁻¹	=	Square Centimeter per Second
fs	=	Femto Second
expt.	=	Experiment
E_{tot}	=	Total Interaction Energy
E_{MM}	=	Interactions within MM Region
E_{QM-MM}	=	Interactions between QM and MM Regions
$\langle \Psi_{QM} \hat{H} \Psi_{QM} \rangle$	=	Interactions within QM Region
F_i	=	Force on each Particle
$S_m(r)$	=	Smoothing Function
F_{QM}	=	Quantum Mechanical Force
F_{MM}	=	Molecular Mechanical Force
D	=	Self-Diffusion Coefficient
r_1	=	Distance Characterizing the Start of QM Region
r_0	=	Distance Characterizing the End of QM Region
$g_{\alpha\beta}(r)$	=	Site-Site Pair Correlation Functions
$n_{\alpha\beta}(r)$	=	Site-Site Integration Number
ρ_β	=	Average Number Density of β Site in the Liquid

LIST OF ABBREVIATIONS (Continued)

$N_{\alpha\beta}(r)$	=	Average of β Site Located in the Shell ($r, r+\Delta r$) Centered on α Site
$C(t)$	=	Time Correlation Function
t_{sim}	=	Simulation Time
CN_{av}	=	Average Number of Nearest-Neighbor Water Molecules
N_{ex}	=	Number of Exchange Events
A	=	Associative Exchange Mechanism
D	=	Dissociative Exchange Mechanism
I	=	Interchange Mechanism
I_a	=	Associative Interchange Mechanism
I_d	=	Dissociative Interchange Mechanism
$\tau_{H_2O}(O_i)$	=	MRT of Water Molecules at each of Oxygen Atoms of NO_3^-
$\tau_{H_2O}(H_2O)$	=	MRT of Water Molecules in the Bulk

CHAPTER I

INTRODUCTION

Characteristics of ions solvated in aqueous electrolyte solutions have long been an interesting subject for chemists and biologists in order to understand the role of these ions in chemical and biological processes (Frank, 1956; Robinson and Stokes, 1959; William, 1971; Hille, 1992). Consequently, a number of experimental and theoretical studies have been carried out to obtain detailed knowledge about solvation structure and dynamics of ions in aqueous solutions (Ohtaki and Radnai, 1993; Remsungnern and Rode, 2004; Tongraar, Hannongbua, and Rode, 1997; Caminiti, Licheri, Paschina, Piccaluga, and Pinna, 1980; Mezei and Beveridge, 1981; Skipper and Neilson, 1989; Lee and Rasaiah, 1995; Obst and Bradaczek, 1996; Texler, Holdway, Neilson, and Rode, 1998). In experiments, several techniques such as X-ray and neutron diffractions as well as infrared and Raman spectroscopy have been employed to provide detailed information on the structure and dynamics of several hydrated ions. In conjunction with experiment, computer simulations have been an alternative approach to elucidate such data. The results from computer simulations can in principle provide a more detailed interpretation and prediction of experimental observations at molecular level, in particular where the experimental results are prone to large errors.

In terms of computer simulations, Monte Carlo (MC) and molecular dynamics (MD) simulations are well-established tools for studying a wide variety of ion-solvent

complexes. However, it is known that quality and accuracy of the simulation results depend crucially on the quality of potential function employed in the simulations. In past decades, most of earlier simulation works had relied on classical pair potentials for describing interactions of each interacting atoms or molecules in the system. It has been shown that classical pair potentials, although providing rather accurate structural details, often fail to correctly predict the dynamics properties of such systems (Elrod and Saykally, 1994; Tongraar, Sagarik, and Rode, 2001; Tongraar, Sagarik, and Rode, 2002; Rode, Schwenk, and Tongraar, 2004).

To more accurately describe the properties of hydrated ions, it has been demonstrated that the interaction potentials must include polarizability and many-body non-additive contributions (Martínez, Hernández-Cobos, Saint-Martin, Pappalardo, Ortega-Blake, and Marcos, 1994; Tongraar, Liedl, and Rode, 1997; Tongraar, Liedl, and Rode, 1998; Tongraar and Rode, 2003; Salvador, Curtis, Tobias, and Jungwirth, 2003). The non-additive contributions in ion-water complexes are generally related to the strength of binding between the ion and water. These many-body effects have been demonstrated to be large for the case of highly charge ions or strongly interacting systems (Remsungnern and Rode, 2004). It has been shown that the neglect of these terms in the potentials resulted in wrong structural and dynamical properties of the hydrated ions, particularly in the first hydration shell (Tongraar, 1998; Tongraar and Rode, 2004; Tongraar, Liedl, and Rode, 1998). With regard to this point, various schemes have been proposed, for example, the polarizable continuum model (PCM) (Tomasi and Persico, 1994), which incorporates the many-body interactions in an average way, or a direct approach by calculating the energy hypersurface of many-body interactions and then fitting them to an analytical function

(Probst, Spohr, Heinzinger, and Bopp, 1991; Hannongbua, 1997). In general, both exemplary models can provide significant improvement of the results. However, for the PCM model, a major weakness is that it can not reproduce specific interaction with the surrounding solvent, such as hydrogen bonds (Earras-Hanauer, Clark, and van Eldik, 2003). For the second model, the construction of many-body potentials is rather difficult, and is hardly feasible for large molecular systems because of their complicated orientation dependence (Hannongbua, 1997; Texler and Rode, 1997; Schwenk, Loeffler, and Rode, 2001; Yagüe, Mohammed, Loeffler, and Rode, 2001).

In principle, *ab initio* quantum mechanical methods can be seen as an ideal method for a correct treatment of multiple intermolecular interactions of the systems. However, the performance of quantum mechanics for a condensed-phase system comprising a large number of molecules is still beyond the current computational feasibility. Thus, an alternative approach is to apply a so-call combined *ab initio* quantum mechanical and molecular mechanical (QM/MM) method (Singh and Kollman, 1986; Field, Bash, and Karplus, 1990). In recent years, several hybrid QM/MM models have been proposed, incorporating either semiempirical (Field *et al.*, 1990; Cummins and Gready, 1997; Gao, 1996), density functional (Stanton, Hartsough, and Merz, 1995; Car and Parrinello, 1985; Murphy, Philipp, and Friesner, 2000), valence bond (Bernardi, Olivucci, and Robb, 1992; Åqvist and Warshel, 1993), or even *ab initio* Hartree-Fock (Singh and Kollman, 1986; Muller and Warshel, 1995) methodology with commonly used molecular mechanical force fields. Consequently, a “Born-Oppenheimer *ab initio* QM/MM MD technique” has been introduced and applied for studying the structural and dynamical properties of various ions in solutions (Kerdcharoen, Liedl, and Rode, 1996; Tongraar and Rode, 1999; Tongraar

and Rode, 2001; Tongraar and Rode, 2004; Tongraar and Rode, 2001; Loeffler, Yagiie, and Rode, 2002; Inada, Loeffler, and Rode, 2002; Loeffler, Yagiie, and Rode, 2002; Schwenk, Loeffler, and Rode, 2003; Remsungnern and Rode, 2003; Kritayakornupong, Plankensteiner, and Rode, 2003; Armunanto, Schwenk, and Rode, 2003; Armunanto, Schwenk, and Rode, 2004; Armunanto, Schwenk, Setiaji, and Rode, 2003; Armunanto, Schwenk, Randolph, and Rode, 2004). Based on the QM/MM approach, the active-site region (*i.e.*, the solvation shell around the ion) is treated quantum mechanically, while the environment consisting of further solvent molecules is described by classical molecular mechanical potentials. By this technique, the complicated many-body contributions as well as the polarization effects within the solvation sphere of the ion can be reliably included. The QM/MM results have clearly shown the important role of non-additive contributions and that inclusion of higher-order interaction terms is essential for the correct description of the solvated ions, even for monovalent ions where many-body interactions could be expected to be weaker than in the case of di- and trivalent ions (Tongraar and Rode, 2003; Tongraar, 1998; Tongraar and Rode, 2004; Tongraar and Rode, 1999; Tongraar and Rode, 2001; Tongraar and Rode, 2001). For example, the QM/MM simulations of Na^+ and K^+ in aqueous solution have provided a clear evidence for the background of the experimentally observed transition from “structure-making” to “structure-breaking” behavior from Na^+ to K^+ (Tongraar *et al.*, 1998). This finding proved of essential importance for the interpretation of the functionality of the potassium-specific ion channels in cell membranes. Another example, where classical simulations, even three-body corrected ones, have failed to reproduce is the Jahn-Teller effect of hydrated Cu^{2+} and Ti^{3+} : the typical distortion of the octahedral $\text{M}^{n+}(\text{H}_2\text{O})_6$ structure

observed experimentally for these ions both in the solid and in the liquid states. It has been reported that this effect could be only revealed by the quantum mechanical treatment of the solvated ion, and to a full extent only after including two complete hydration shells through the *ab initio* QM/MM simulations (Rode *et al.*, 2004).

During the past decades, the QM/MM method has been successfully applied to various ions in aqueous solution (Kerdcharoen *et al.*, 1996; Tongraar and Rode, 1999; Tongraar and Rode, 2001; Tongraar and Rode, 2004; Tongraar and Rode, 2001; Loeffler *et al.*, 2002; Inada *et al.*, 2002; Loeffler *et al.*, 2002; Schwenk *et al.*, 2003; Remsungnern and Rode, 2003; Kritayakornupong *et al.*, 2003; Armunanto *et al.*, 2003; Armunanto, Schwenk, and Rode, 2004; Armunanto, Schwenk, and Rode, 2003; Armunanto *et al.*, 2004). Nevertheless, it is quite rare for the case of anions, except for F⁻ and Cl⁻ (Tongraar and Rode, 2003). The main reasons can be attributed to the fact that a satisfactory description of highly polarizable systems, like solvated anions, requires additional diffuse basis functions as well as electron correlations, thus increasing the computational time.

In general, most of cations usually have simple solvated geometries due to their strong binding energies between ion and water molecules. Unlike cations, anion solvation is more complicated since most of anion-water interactions are generally weaker than those of cations and energetically comparable with the water-water interactions. As a consequence, a delicate balance between anion-water and water-water interactions is crucial in determining bulk *vs.* surface solvation, *i.e.*, structures with the anion on the “surface” of water clusters. For small anions, such as F⁻ and Cl⁻, the QM/MM results have shown the important role of quantum mechanical treatment for obtaining a more realistic picture of these solvated anions (Tongraar and Rode,

2003). The QM/MM study has predicted average coordination numbers of 4.6 and 5.6 for F^- and Cl^- , respectively, in contrast to the corresponding values of 5.8 and 5.9 resulting from the classical pair potential simulations. The QM/MM results of F^- indicated more flexibility of the first hydration shell complex in which the $F^- \cdots H-O$ bond appeared to be linear. In the first hydration shell of Cl^- , although the classical simulation supplied an almost identical coordination number, the orientation of solvent molecules was considerably changed by ‘quantum effects’, which reflect in a combination of linear and bridged forms of the hydrated Cl^- complex, together with a competition between the hydration of the ion and hydrogen bonding among water molecules. In addition, with respect to detailed analysis on the dynamics of these hydrated ions, it has been demonstrated that F^- clearly acted as a “structure-maker”, while the characteristics of Cl^- solvation led to a more flexible structure with frequent re-arrangements of the hydrogen bonds. These observed details are of great importance since a correct geometrical description is a precondition for reliable dynamics data.

In this study, the QM/MM method has been applied to a more complicated aqueous anionic system, namely nitrate anion (NO_3^-) in water. The NO_3^- ion has been considered as one of great important ions in solution chemistry and biology, which is frequently encountered as a terminal anion in the series of reactions involving nitrogen in inorganic compounds (Shen, Xie, Deakyne, and Schaefer, 1990; Berendren, Postma, van Gunsteren, and Hermans, 1981; Ferguson, Fehsenfeld, and Albritton, 1979; Carravetta and Clementi, 1984; Kato, Machida, Oobatake, and Hayashi, 1988; Kato, Machida, Oobatake, and Hayashi, 1990; Guilbaud and Wipff, 1993). In gas-phase, the isolated NO_3^- ion is nominally planar and has D_{3h} symmetry.

In polar solvents, however, its D_{3h} symmetry is expected to be broken by the influence of solvent environment. These effects have already been explored *via* resonance Raman spectroscopy studies (Waterland and Kelley, 2000; Waterland, Stockwell, and Kelley, 2001). In terms of theoretical studies, several *ab initio* calculations on the structure of $\text{NO}_3^-(\text{H}_2\text{O})_n$ (where $n = 1$ (Shen *et al.*, 1990), $n = 1,2$ (Waterland *et al.*, 2001), $n = 1-3$ (Howell, Sapse, Singman, and Synder, 1982) and $n = 1-6$ (Wang, Yang, Wang, and Nicholas, 2002)) have been carried out. In the latter study (Wang *et al.*, 2002), the calculations indicated that the first three waters form a first hydration shell around NO_3^- , giving rise to a high symmetry C_{3h} $\text{NO}_3^-(\text{H}_2\text{O})_3$ complex. The C_{3h} $\text{NO}_3^-(\text{H}_2\text{O})_3$ complex was found to be a rather robust hydration structure since it is largely preserved as the fourth to sixth waters form a second hydration shell without direct contact with the NO_3^- ion. Consequently, the authors suggested that the first hydration shell of NO_3^- in bulk aqueous nitrate solution might also involve only three water molecules.

In aqueous solution, the hydration shell structure of NO_3^- has been studied both by experiments and computer simulations (Nicholas and Wasylishen, 1985; Rosi and Fontana, 1987; Burke, Adya, and Neilson, 1991; Nakahara and Emi, 1993; Aker, Zhang, and Nichols, 1999; Waterland and Kelley, 2000; Jakobsen, Bildsøe, Skibsted, and Giavani, 2001; Kapinus, Revelsky, Ulogov, and Lyalikov, 2004). Experimental studies, in particular neutron and X-ray diffractions (Ohtaki and Radnai, 1993; Jakobsen *et al.*, 2001; Ikushima, Saito, and Arai, 1998), have reported a wide variety of coordination numbers, ranging from about 2 to 18. The observed large discrepancy has been attributed to the interference of counterions. Besides the experimental data, computer simulations of aqueous solutions containing NO_3^- have provided structural

and dynamical details of this solvated ion at molecular level. However, most of the previous computer simulations of NO_3^- in aqueous solution have been carried out using a wide variety of standard potentials (Laaksonen and Kovacs, 1994; Kataoka, 1993; Guilbaud and Wipff, 1993; Kato, Hayashi, Oobatake, and Machida, 1993). For instance, the hydrated silver nitrate has been studied by Laaksonen and Kovacs (1994) using rigid simple point charge (SPC) for water and rigid model with Lennard-Jones force field for NO_3^- (Berendsen *et al.*, 1981). In another simulation, Kataoka (1993) employed a Caravetta-Clementi water model (Caravetta and Clementi, 1984) and an empirical potential for the nitrate interactions. Later, a MD simulation using pairwise additive *ab initio* interaction potentials has been carried out for a dilute aqueous solution of potassium nitrate (Ebner, Sansone, Hengrasmee, and Probst, 1999). It was found that the details of the hydration shell as well as the orientations of water surrounding the NO_3^- ion depend quite sensitively on the interaction potentials employed in the simulations. Recently, MD simulation of NO_3^- embedded in 124 water molecules has been performed using a hybrid QM-TIP4P-FQ scheme (Lebrero, Bikiel, Elola, and Estrin, 2002). Nevertheless, this work had employed quantum mechanics method only for the treatment of NO_3^- , thus no improvement for the description of nitrate-water as well as water-water interactions.

Since detailed information on the structure and dynamics of NO_3^- in aqueous solution is still not clear, it is of particular interest to perform a sophisticated *ab initio* QM/MM MD simulation in order to provide better knowledge of this hydrated ion. In the present study, two combined QM/MM MD simulations, namely HF/MM and B3LYP/MM, have been performed. The detailed analysis with respect to the HF/MM

and B3LYP/MM results will be discussed and compared to available experimental data and those previous theoretical studies.

CHAPTER II

COMPUTATIONAL METHODS

2.1 Quantum chemistry

Conceptually, a molecule of all matter is described as a group of atoms that hold together with chemical bonds. In terms of quantum mechanics, the molecule is a group of particles consisting of nuclei and electrons. The energy and other properties of a molecule can be derived from wavefunction, *i.e.*, the function which characterizes the particle's motion. Accordingly, the starting point for any discussion of quantum mechanics is Schrödinger equation (Schrödinger, 1926). On the other hand, the system's properties can be obtained by solving the Schrödinger equation.

2.1.1 Schrödinger equation

The time-independent Schrödinger equation can be written as

$$\hat{H}\Psi = E\Psi, \quad (2.1)$$

where Ψ and E are eigenfunction and eigenvalue, respectively, and \hat{H} is Hamiltonian operator. To solve the Schrödinger equation it is necessary to find values of E and function Ψ such that when the wavefunction is operated upon by the Hamiltonian, it returns the wavefunction multiplied by the energy.

The Hamiltonian operator is composed of two parts, namely kinetic energy operator for each particle in the molecule and potential energy operator describing the electrostatic interactions between each pair of particles in the molecule:

$$\hat{H} = \sum_i^{\text{nuclei}} \hat{T}(i) + \sum_j^{\text{electrons}} \hat{T}(j) + \sum_j^n \sum_k^e \hat{V}(j, k) + \sum_l^e \sum_{m>l}^e \hat{V}(l, m) + \sum_o^n \sum_{p>o}^n \hat{V}(o, p). \quad (2.2)$$

With respect to equation (2.2), the five terms on the right hand side refer to kinetic energy operator for each nucleus, kinetic energy operator for each electron, potential energy operator for each electron-nucleus pair, potential energy operator for each electron pair and potential energy operator for each nucleus pair, respectively.

The kinetic energy operator can be expressed as

$$\hat{T}(i) = -\frac{\hbar^2}{2m_i} \nabla^2(i), \quad (2.3)$$

where \hbar is Plank's constant, m refers to mass of the particle i and $\nabla^2(i)$ is second derivatives of Laplacian operator, which can be calculated with respect to the coordinates of the particle i .

The potential energy operator can be written as

$$\hat{V}(i, j) = \frac{q_i q_j}{r_{ij}}, \quad (2.4)$$

where q defines the charge of each particle and r is the distance between the two particles.

2.1.2 Born-Oppenheimer approximation

To solve Schrödinger equation for multi-electron systems, Born-Oppenheimer approximation (Born and Oppenheimer, 1927) is one of several approximations made. The Born-Oppenheimer approximation considers the nuclei to be stationary phase relative to the electron due to much heavier mass. Under this approximation, the nuclei wavefunction can be separated and the electron distribution in a field of fixed nuclei depends only on the instantaneous positions of the nuclei and not on their momenta. Therefore, the kinetic energy operator for each nucleus is zero and the potential energy operator for each nucleus pair, which depends only on the molecular geometry, can be treated as constant value. The electronic energy, E_{elec} , is obtained as the eigenvalue of the electronic Schrödinger equation:

$$\hat{H}_{elec} \Psi_{elec} = E_{elec} \Psi_{elec}, \quad (2.5)$$

where Ψ_{elec} is a function of electron coordinates and \hat{H}_{elec} is an electronic Hamiltonian, which can be written as

$$\hat{H}_{elec} = \sum_j^{electrons} \hat{T}(j) + \sum_j^n \sum_k^e \hat{V}(j,k) + \sum_l^e \sum_{m>l}^e \hat{V}(l,m) + \sum_o^n \sum_{p>o}^n \hat{V}(o,p), \quad (2.6)$$

or

$$\hat{H}_{elec} = -\frac{1}{2} \sum_i^{electrons} \nabla^2(i) - \sum_j^n \sum_k^e \frac{Z_j}{r_{jk}} + \sum_l^e \sum_{m>l}^e \frac{1}{r_{lm}} + \sum_o^n \sum_{p>o}^n \frac{Z_o Z_p}{R_{op}}. \quad (2.7)$$

According to equation (2.7), the atomic units are applied by combining all the constants into one constant, where Z_j is the atomic number of nucleus j and r is the distance between the particles. In addition, the last term on the right hand side is also a constant value.

2.1.3 Molecular orbital (MO) theory

Molecular orbital (MO) theory is widely used in quantum chemistry, making use of sets of atomic orbital (AO) to construct an appropriate MO. The full wavefunction for a single electron is called spin orbital, which is the product of a molecular orbital that depends on the electron's Cartesian coordinates and a spin function (*e.g.* $+1/2$ or $-1/2$), designated as $\alpha(s)$ and $\beta(s)$. These two states correspond to alignment along or opposite to the external magnetic field, often called as up spin and down spin, respectively. As a consequence, the spin orbital can be written as

$$\chi_i = \psi_i(x_i, y_i, z_i) \alpha(\sigma_i), \quad (2.8)$$

or

$$\chi_i = \psi_i(x_i, y_i, z_i) \beta(\sigma_i). \quad (2.9)$$

For N -electron system, the simplest form of wavefunction can be written as:

$$\Psi = \chi_1(1)\chi_2(2)\dots\chi_N(N), \quad (2.10)$$

where $\chi_i(i)$ is the spin orbitals of the i -th electron. However, this product is not acceptable since it does not allow the antisymmetry property, *i.e.*, a sign of interchanging coordinates of any two electrons in the wavefunction cannot lead to different wavefunction. To satisfy the antisymmetric principle, the electronic wavefunction is usually written in terms of Slater determinant (Slater, 1929). By this scheme, the wavefunction can be expressed as single determinant,

$$\Psi = (N!)^{-1/2} \begin{vmatrix} \chi_1(1) & \chi_2(1) & \dots & \chi_N(1) \\ \chi_1(2) & \chi_2(2) & \dots & \chi_N(2) \\ \vdots & \vdots & \vdots & \vdots \\ \chi_1(N) & \chi_2(N) & \dots & \chi_N(N) \end{vmatrix}, \quad (2.11)$$

where the columns of the determinant represent the single electronic wavefunctions (orbitals) and the rows of the determinant are the electron coordinates.

Considering a two-electron system, the spin orbitals can be written in terms of a 2×2 determinant. Thus, the determinant wavefunction can be expressed as

$$\Psi = \frac{1}{\sqrt{2}} \begin{vmatrix} \chi_1(1) & \chi_2(1) \\ \chi_1(2) & \chi_2(2) \end{vmatrix} = \frac{1}{\sqrt{2}} [\chi_1(1)\chi_2(2) - \chi_1(2)\chi_2(1)]. \quad (2.12)$$

Here, when the coordinates of the two electrons are interchanged, it turns to be

$$\Psi' = \frac{1}{\sqrt{2}} \begin{vmatrix} \chi_1(2) & \chi_2(2) \\ \chi_1(1) & \chi_2(1) \end{vmatrix} = \frac{1}{\sqrt{2}} [\chi_1(2)\chi_2(1) - \chi_1(1)\chi_2(2)], \quad (2.13)$$

which corresponds to $\Psi' = -\Psi$. If the electrons occupy the same spin orbital ($\chi_1 = \chi_2$), then

$$\Psi = \frac{1}{\sqrt{2}} \begin{vmatrix} \chi_1(2) & \chi_1(2) \\ \chi_1(1) & \chi_1(1) \end{vmatrix} = \frac{1}{\sqrt{2}} [\chi_1(2)\chi_1(1) - \chi_1(1)\chi_1(2)] = 0, \quad (2.14)$$

which implies that the determinant vanishes. This also satisfies the Pauli exclusion principle (Pauli, 1925), which states that the two electrons in the same spin cannot be situated in a single MO. In addition, the spin orbitals must have orthonormal properties. First, the orthogonal property is possible when the spin orbitals is written as

$$S_{ij} = \int \chi_i^* \chi_j d\tau = 0, \quad \text{for } i \neq j, \quad (2.15)$$

and the spin orbitals may be normalized,

$$S_{ij} = \int \chi_i^* \chi_j d\tau = 1, \quad (2.16)$$

which correspond to requirement that the probability of finding the electron somewhere in the universe is unity.

2.1.4 Basis functions

MO of a system can be constructed through a schematic called Linear Combination of Atomic Orbitals to Molecular Orbitals (LCAO-MO) method. Thus, the MOs are composed of a set of atomic orbitals (basis functions), which can be expressed as

$$\psi_i = \sum_{\mu=1}^n c_{\mu i} \phi_{\mu}, \quad (2.17)$$

where ψ_i refers to the i -th molecular orbital, $c_{\mu i}$ are set of coefficients weighting the contributions of the atomic orbital to the molecular orbitals, ϕ_{μ} defines the μ -th atomic orbital and n is number of atomic basis functions. The $c_{\mu i}$ can be calculated using various methods, where overall such methods are based on linear variation principle.

In general, accuracy of the representation of the true MO depends on increasing the number of atomic basis functions in the approximation. With respect to the type of basis function, one of the popular choices is Exponential or Slater-type orbitals (STOs) (Slater, 1930). The STOs are described by the function depending on spherical coordinates:

$$\phi_i(\zeta, n, l, m; r, \theta, \phi) = Nr^{n-1}e^{-\zeta r}Y_{lm}(\theta, \phi), \quad (2.18)$$

where N is a normalization constant, ζ refers to exponent, which determines the size of the orbital. The r , θ and ϕ are the spherical coordinates and Y_{lm} defines the angular momentum part (function for describing orbital shape). The n , l and m are quantum numbers referring to principal, angular momentum and magnetic, respectively.

The STOs are used as basis function due to their similarity to the atomic orbitals of the hydrogen atom. However, the STOs are not suitable for solving the integrals of the wave equation because they are rather time consuming. As a consequence, Gaussian-type orbitals (GTOs) (Boys, 1950) are introduced since they are simpler to manipulate mathematically, and of course they are less accurate than the STOs. Thus, the shape of STO function can be estimated from a linear combination of GTO functions with different set of exponents and coefficients. The GTOs is sometimes called as Cartesian gaussian or gaussian primitives, these functions can be written as

$$\phi_i(\alpha, l, m, n; x, y, z) = Ne^{-\alpha r^2}x^l y^m z^n, \quad (2.19)$$

where N is a normalization constant, α defines the exponent and x , y and z are Cartesian coordinates. The l , m and n are now not quantum numbers, but simply integral exponents at Cartesian coordinates, $r^2 = x^2 + y^2 + z^2$.

2.1.5 Basis sets

The basis sets are group of numerical constants used in the wavefunctions. Nowadays, several standard basis sets are commonly used in the quantum mechanical calculations (Hehre, Stewart, and Pople, 1969; Collins, Schleyer, Stephen Binkley, and Pople, 1976). The minimal basis set (SZ) is only one basis function per atomic orbital. The problem of this basis set is that it often inefficient to describe the chemical bonding. If the basis set is formed by doubling the number of basis functions in the minimal basis set, it is usually called as extended or double-zeta (DZ) basis set. As a matter of fact that valence shell electrons are most essential for interaction between atoms, *i.e.*, double-zeta basis set of inner shell electrons doesn't gain much accuracy, a split-valence basis set is more efficient. In several cases, the basis sets are frequently augmented with polarization and diffuse functions. The polarization functions are important for reproducing chemical bonding, while the diffuse functions are usually necessary for anion or weak interacting systems. In practice, the polarization and diffuse functions can directly be added into the basis set to achieve better performance, but it is time consuming.

For heavy atoms, since the calculations for two-electron integral are very computational demanding (*e.g.* with respect to the number of basis functions), Effective Core Potentials (ECP) (Kahn, Baybutt, and Truhlar, 1976) or Pseudopotentials (Dolg, Stoll, Preuss, and Pitzer, 1993) are introduced. This type of basis set considers the inner shell electrons as if they were the average potential. The objective of the ECP method is to construct potentials which are solely dependent upon the coordinates of the valence electrons, but approximate the influence of the

inner core electrons. Obviously, the ECP's are not actual orbitals but are a modified form which encourages the Hamiltonian to take an advantage of fast calculation.

2.1.6 Variation principle

The variation principle has been applied to determine the lowest energy, which represents the ground state of the system. By this scheme, if a trial wavefunction, Φ , is appropriately chosen, then an expectation value (average value) of the energy, \bar{E} , can then be obtained. To apply the variation principle, the Φ often multiplies with N so that $N\Phi$ is normalized:

$$\bar{E} = |N|^2 \int \Phi^* \hat{H} \Phi d\tau, \quad (2.20)$$

where

$$\int (N\Phi)^* N\Phi d\tau = 1, \quad (2.21)$$

in which the expectation energy can be determined by calculating the following integral,

$$\bar{E} = \frac{\int \Phi^* \hat{H} \Phi d\tau}{\int \Phi^* \Phi d\tau}, \quad (2.22)$$

where the two-integrals are performed for all coordinates of all electrons, and the asterisk denotes complex conjugation. From this calculation, the expectation energy is always higher than or equal to the exact energy, but it will never be less than the exact energy,

$$\bar{E} \geq E, \quad (2.23)$$

where \bar{E} refers to the expectation energy and E is the exact energy of the ground state wavefunction corresponding to the given Hamiltonian. According to this principle, the lowest expectation energy can be achieved by trying several trial wavefunctions and then look for the one that gives the lowest the expectation energy. On the other hand, we require the best set of coefficients for a given functions ϕ_i (the basis set) and a given Slater determinant wavefunction such that

$$\frac{\partial \bar{E}}{\partial c_{\mu i}} = 0 \quad \text{for all } \mu \text{ and } i. \quad (2.24)$$

2.1.7 Hartree-Fock (HF) method

In principle, the variation method can be used to determine the minimum energy from best wavefunction. At a minimum, the first derivative of the energy, $\partial \bar{E}$ will be zero. By imposing this condition, all of the modern MO computational methods (*ab initio* and semiempirical) make use of Hartree-Fock (HF) method which is more effective in approximating molecular wavefunction. By means of the HF method, the Hamiltonian considers each electron in the average field of all

other electrons in the molecule. The one-electron Hamiltonian operator contains three terms appropriate as core, Coulomb and exchange operators that represent the contributions to the energy of spin orbital. The Hamiltonian for describing approximation is called Fock operator, F . For a closed-shell system (no unpaired electrons), the Fock operator can be written as

$$F(1) = \hat{H}^{core}(1) + \sum_{j=1}^{N/2} (2\hat{J}_j(1) - \hat{K}_j(1)), \quad (2.25)$$

where $\hat{H}^{core}(1)$ is the core Hamiltonian operator,

$$\hat{H}^{core}(1) = -\frac{1}{2}\nabla_1^2 - \sum_{A=1}^{N/2} \frac{Z_A}{r_{1A}}, \quad (2.26)$$

where \hat{J}_j and \hat{K}_j are Coulomb and exchange integral operators, respectively,

$$\hat{J}_j(1)\chi_i(1) = \left[\int d\tau_2 \chi_j(2) \frac{1}{r_{12}} \chi_j(2) \right] \chi_i(1) \quad (2.27)$$

and

$$\hat{K}_j(1)\chi_i(1) = \left[\int d\tau_2 \chi_j(2) \frac{1}{r_{12}} \chi_i(2) \right] \chi_j(1). \quad (2.28)$$

The difference between the Fock operator and exact Hamiltonian is the Coulomb integral operator represents the electrostatic repulsion energy between two electrons meaning the average interaction potential of the electron j due to all of the other electrons. The exchange integral operator involves the exchange of the electron between MOs. According to the HF method, the greater basis set will always provide the better wavefunction and the lower energy. In practice, however, the wavefunction expansion in terms of the basis set had led to a limitation of the *ab initio* HF method. The derivation of HF equations for molecular system was proposed by Roothaan-Hall equations, which can be written as

$$\sum_{\nu=1}^N (F_{\mu\nu} - \varepsilon_i S_{\mu\nu}) c_{\nu i} = 0 \quad \mu = 1, 2, \dots, N, \quad (2.29)$$

where N is the number of basis functions, ε_i is the one-electron energy of wavefunction and $S_{\mu\nu}$ is overlap integral between the basis functions μ and ν ,

$$S_{\mu\nu} = \int d\nu_1 \phi_{\mu}(1) \phi_{\nu}(1). \quad (2.30)$$

The expression for each element $F_{\mu\nu}$ of Fock matrix elements for a closed-shell system of N electrons becomes:

$$F_{\mu\nu} = H_{\mu\nu}^{core} + \sum_{\lambda=1}^K \sum_{\sigma=1}^K P_{\lambda\sigma} \left[(\mu\nu|\lambda\sigma) - \frac{1}{2}(\mu\nu|\lambda\sigma) \right]. \quad (2.31)$$

This is the standard form of Fock matrix in the Roothaan-Hall equations. $H_{\mu\nu}^{core}$ is a one-electron integral that can be written as

$$H_{\mu\nu}^{core} = \int d\nu_1 \phi_\mu(1) H^{core}(1) \phi_\nu(1), \quad (2.32)$$

in which

$$H^{core}(1) = -\frac{1}{2} \nabla^2 - \sum_{A=1}^M \frac{Z_A}{|r_1 - R_A|}. \quad (2.33)$$

Here, Z_A is the atomic number of atom A . $P_{\lambda\sigma}$ refers to an element of density matrix,

$$P_{\lambda\sigma} = 2 \sum_{i=1}^{N/2} c_{\lambda i} c_{\sigma i}. \quad (2.34)$$

The quantities of $(\mu\nu|\lambda\sigma)$ and $(\mu\lambda|\nu\sigma)$ are two-electron repulsion integrals. The total energy of the molecule can be expressed as

$$E_{molecule} = E_{elec} + E_{nuc}. \quad (2.35)$$

The electronic energy and nuclear repulsion are given by

$$E_{elec} = \frac{1}{2} \sum_{\mu=1}^K \sum_{\nu=1}^K P_{\mu\nu} (H_{\mu\nu}^{core} + F_{\mu\nu}) \quad (2.36)$$

and

$$E_{nuc} = \sum_{A=1}^N \sum_{B=1}^N \frac{Z_A Z_B}{R_{AB}}. \quad (2.37)$$

In practice, solution of the HF equations for the two-electron integrals over atomic basis functions require time consuming and also their storage on disk for the large systems. To reduce these problems, the direct self-consistent field (SCF) method (Haser and Ahlrichs, 1989) is introduced by working iteratively. By this approach, the two-electron integrals are not stored but recalculated as required.

2.1.8 Electron correlation

It is known that motions of electrons are correlated and they tend to repel each electron which gives a lower energy. According to the HF method, each electron moves in the static electric field created by all of the other electrons in the system. On the other hand, the electron cannot see other electrons during the HF calculation. Thus, the significant deficiency of the HF method is that it fails to adequately treat the correlation between motions of electrons. The effects of electron correlation were usually neglected in the Hamiltonian in the previous section. This leads to limitation of the calculated HF energies. The difference between HF and exact (nonrelativistic) energies is the correlation energy,

$$E_{exact} = E_{HF} + E_{correlation}. \quad (2.38)$$

In several cases, the neglect of electron correlation effects can lead to some anomalous of qualitative information. As a consequence, the Ψ and E cannot be used to correctly predict atomic properties without somewhere accounting for electron correlation.

According to this point, many attempts have been proposed to correct the effects of electron correlation, such as Density functional theory (DFT) (Jones and Gunnarrson, 1989), Coupled cluster (CC) (Bartlett, 1989), Many-body Perturbation (MP) (Møller and Plesset, 1934) and Configuration interaction (CI) (Bauschlicher, Langhoff, and Taylor, 1990) methods.

2.1.9 Density functional theory (DFT)

Density functional theory (DFT) is an approach to the electronic structure of atoms and molecules which has enjoyed a dramatic surge of interest since the 1980's (Parr, 1983; Wimmer, 1991). The approach is based upon a theory presented by Hohenberg and Kohn (1964) which states that all the ground-state properties of a system are functions of the charge density. The Hohenberg-Kohn theorem thus enables us to write the total electronic energy as a function of the electron density ρ :

$$E(\rho) = E_{KE}(\rho) + E_C(\rho) + E_H(\rho) + E_{XC}(\rho). \quad (2.39)$$

$E_{KE}(\rho)$ is the kinetic energy, $E_C(\rho)$ is the electron-nuclear interaction term, $E_H(\rho)$ is the electron-electron Coulombic energy and $E_{XC}(\rho)$ contains the exchange

and correlation contributions. All of electron-electron interactions are thus contained within the $E_H(\rho)$ and $E_{xc}(\rho)$ terms. A crucial conclusion from the Hohenberg-Kohn theorem is that the ground-state properties of a system are determined by the density. An incorrect density gives an energy above the true energy. To perform a density functional calculation it is necessary to write the various terms in equation (2.39) in terms of the density and then optimize the energy with respect to the density, subject to any constraints on the system.

In practice, Kohn-Sham theory can be applied in several distinct ways depending on what is being investigated. In solid state calculations, the local density approximations are still commonly used along with plane wave basis sets, as an electron gas approach is more appropriate for an infinite solid. In molecular calculations, however, more sophisticated functionals are needed, and a huge variety of exchange-correlation functionals have been developed for chemical applications. Some of these are inconsistent with the uniform electron gas approximation, however, they must reduce to LDA in the electron gas limit. In the chemistry community, one popular functional is known as BLYP (from the names Becke, Lee, Yang and Parr), but even more widely used is B3LYP (Becke, 1993; Lee, Yang, and Parr, 1988; Stephens, Devlin, Chabalowski, and Frisch, 1994) which is a hybrid method in which the DFT exchange functional, in this case from BLYP, is combined with the exact exchange functional from Hartree-Fock theory. These hybrid functionals carry adjustable parameters which are generally fitted to a 'training set' of molecules. Unfortunately, although the results obtained with these functionals are usually sufficiently accurate for most applications, there is no systematic way of improving them (in contrast to some of the traditional wavefunction-based methods like

configuration interaction or coupled cluster theory). Hence in the current DFT approach it is not possible to estimate the error of the calculations without comparing them to other methods or experiment.

2.2 Computer simulation methods

2.2.1 Statistical mechanics

In statistical mechanics, the experimental observables are represented in terms of time averages of property A , *i.e.*, the property that is expressed as a function of the momenta, p , and the positions, r , of all particles in the system. The property A can be measured throughout infinite time, giving the time average,

$$\langle A \rangle_{time} = \lim_{\tau \rightarrow \infty} \frac{1}{\tau} \int_{t=0}^{\tau} A(p^N(t), r^N(t)) dt \approx \frac{1}{M} \sum_{t=1}^M A(p^N, r^N), \quad (2.40)$$

where τ is the simulation time, M is the number of time steps in the simulation and $A(p^N, r^N)$ is the instantaneous value of property A .

In practice, since the system is usually composed of a large number of particles, it is not feasible to generate even an initial system's configuration. Then, a concept of ensemble average is proposed. The ensembles are a collection of points in phase space under the conditions of a particular thermodynamic state such as temperature (T) energy (E) volume (V) pressure (P) and number of particles (N). In conjunction with an ergodic hypothesis, it is assumed that an estimation of time average can be obtained over a large number of replicas of the system considered simultaneously,

$$\langle A \rangle_{time} = \langle A \rangle_{ensemble} = \int \int dp^N dr^N A(p^N, r^N) \rho(p^N, r^N). \quad (2.41)$$

The probability density of the ensemble, $\rho(p^N, r^N)$, is given by

$$\rho(p^N, r^N) = \frac{1}{Q} \exp[-H(p^N, r^N)/k_B T], \quad (2.42)$$

where H is the Hamiltonian, T is the temperature, k_B is Boltzmann's constant and Q is the partition function.

$$Q = \int \int dp^N dr^N \exp[-H(p^N, r^N)/k_B T]. \quad (2.43)$$

2.2.2 Correlation functions

2.2.2.1 Radial distribution functions (RDFs)

The radial distribution functions (also known as pair correlation functions) are probability of finding a pair of the atom at a distance r from a central atom,

$$g_{\alpha\beta}(r) = N_{\alpha\beta}(r)/(4\pi r^2 \Delta r \rho_\beta), \quad (2.44)$$

where $N_{\alpha\beta}(r)$ is the average number of β sites located in the shell $(r, r + \Delta r)$ centered on site α , and $\rho_\beta = \frac{N_\beta}{V}$ is the average number density of β sites in the liquid. Consequently, the corresponding integration number can be defined as

$$n_{\alpha\beta}(r) = 4\pi\rho_\beta \int_0^r g_{\alpha\beta}(r')r'^2 dr'. \quad (2.45)$$

2.2.2.2 Time correlation functions

In MD simulation, the time dependent properties are often calculated in terms of time correlation functions, since they can give a clear view of the dynamic property of the liquid. The relation between two different properties, $A(x)$ and $B(x)$, known as a cross-correlation function, can be written as

$$C_{AB} = \frac{\langle A(0)B(t) \rangle}{\langle A(0)B(0) \rangle}, \quad (2.46)$$

where $A(0)$ is the property of A obtained at initial time and $B(t)$ is the property of B obtained at a time t later. If $A(x)$ and $B(x)$ are the same property, it is called an autocorrelation function,

$$C_{AB} = \frac{\langle A(0)B(t) \rangle}{\langle A(0)A(0) \rangle} = \frac{\langle A(0)B(t) \rangle}{\langle A(0)^2 \rangle}. \quad (2.47)$$

The autocorrelation functions have been used to calculate many dynamics properties. For example, the evaluation spectral properties such as librational and vibrational frequencies of water molecule motions was carried out using velocity autocorrelation functions (VACFs), $C(t)$, described as

$$C(t) = \frac{\sum_i^{N_t} \sum_j^N \vec{v}_j(t_i) \vec{v}_j(t_i + t)}{N_t N \sum_i^{N_t} \sum_j^N \vec{v}_j(t_i) \vec{v}_j(t_i)}, \quad (2.48)$$

where N and N_t are the number of particles and the number of time origins t_i , respectively, and \vec{v}_j refers to a certain velocity component of particle j . The power spectrum of the VACF can be calculated by Fourier transformation that may also often be related to the experimental spectra.

2.2.3 Classical MD method

The common scheme of classical MD simulation is summarized in Figure 2.1.

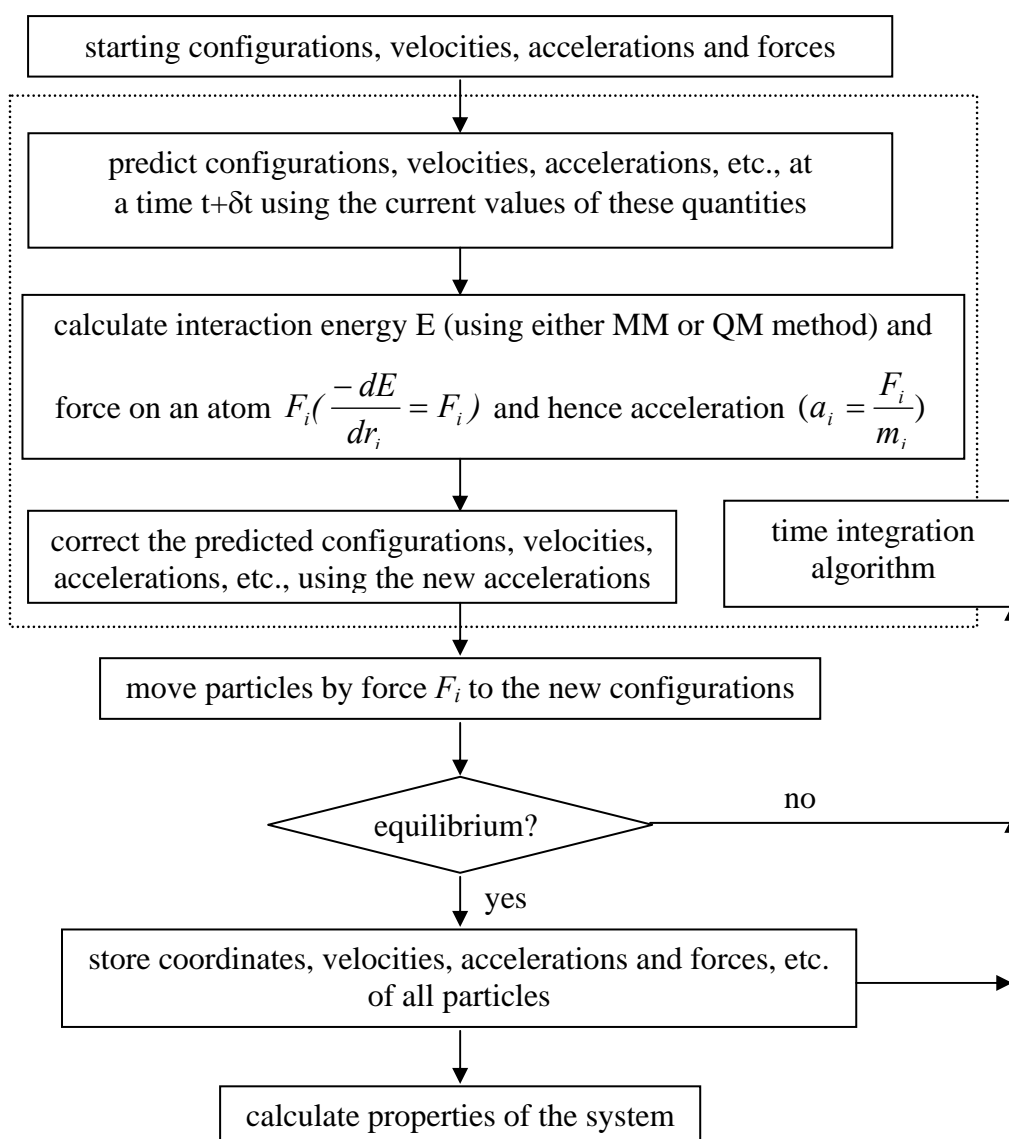


Figure 2.1 The schematic of MD simulation.

The actual simulation starts with reading in the starting configurations, velocities, accelerations and forces. The initial configuration has two simple forms, one using the random configurations and the other starting from a lattice. The essential condition of the simulation is that there are no explicitly time-dependent or velocity dependent forces that shall act on the system. In practice, the trajectories

cannot be directly obtained from Newton's equation. Therefore, the time integration algorithm will be used to obtain the knowledge of positions, velocities and accelerations of two successive time steps. The energy of the system can be calculated using either MM or QM method. The force on an atom can be calculated from derivative of the energy with respect to change in the atom's position. The particles will be moved by their new forces to new configurations and the steps will be repeated until the system reaches equilibrium. Then the coordinates, velocities, accelerations, forces and so on are collected for further structural and dynamical property calculations. In general, only positions and velocities are usually stored since most of the important and interesting properties can be obtained from these two quantities.

2.2.3.1 Intermolecular potentials

The intermolecular interaction of the system is most described by intermolecular potential. To correctly describe the system's interactions, we need to have a suitable potential function for describing all of pair, three-body, four-body up to N -body interactions,

$$V_{total} = \sum V(i, j) + \sum V(i, j, k) + \dots + \sum V(i, j, k, \dots, N). \quad (2.49)$$

The first term on the right hand side is the two-body interaction and the remaining terms of the series are termed many-body interactions. In most classical simulation, the higher order interactions (three, four, ..., N -body) are usually neglected since they are assumed to converge rather slowly, i.e., the terms tend to have alternating signs

(Kistenmacher, Popkie, and Clementi, 1974). As a consequence, it is assumed that the interactions of the system are approximately equal to only the summation of all two-body interaction, *i.e.* the interaction between species i and j is expressed as

$$V_{pair} = \sum_{i < j}^N V_{ij}(|r_i - r_j|), \quad (2.50)$$

where r_i and r_j are the position of species i and j , respectively.

2.2.3.2 Time integration algorithms

In MD simulation, system's trajectory can be generated using finite difference methods, assuming that the positions, velocities and so on can be expressed in terms of Taylor series expansions,

$$\begin{aligned} r(t + \delta t) &= r(t) + v(t)\delta t + \frac{1}{2}a(t)\delta t^2 + \frac{1}{6}b(t)\delta t^3 + \frac{1}{24}c(t)\delta t^4 + \dots \\ v(t + \delta t) &= v(t) + a(t)\delta t + \frac{1}{2}b(t)\delta t^2 + \frac{1}{6}c(t)\delta t^3 + \dots \\ a(t + \delta t) &= a(t) + b(t)\delta t + \frac{1}{2}c(t)\delta t^2 \dots \\ b(t + \delta t) &= b(t) + c(t)\delta t + \dots \end{aligned} \quad (2.51)$$

Two popular integration algorithms are Verlet algorithm and the predictor-corrector algorithms. The Verlet algorithm is probably the most widely used method for integrating the equations of motion. This algorithm uses positions and accelerations at time t and the positions at time $t - \delta t$ to calculate new positions at time $t + \delta t$,

$$\begin{aligned}
 r(t + \delta t) &= r(t) + v(t)\delta t + \frac{1}{2}a(t)\delta t^2 + \dots \\
 r(t - \delta t) &= r(t) - v(t)\delta t + \frac{1}{2}a(t)\delta t^2 - \dots
 \end{aligned}
 \tag{2.52}$$

After adding these two equations we obtain

$$r(t + \delta t) = 2r(t) - r(t - \delta t) + a(t)\delta t^2. \tag{2.53}$$

The Verlet algorithm is a direct solution of the second-order equation. This algorithm is straightforward and the storage requirements are modest. Nevertheless, the problem of this algorithm is that it is of moderate precision and the velocities are not explicitly generated, but can be calculated by using

$$v(t) = \frac{r(t + \delta t) - r(t - \delta t)}{2\delta t}. \tag{2.54}$$

Apart from the Verlet algorithm, Leap-frog algorithm is another commonly numerical algorithm used to generate system's trajectory. The steps can be summarized as followed

- | | | |
|---|---|--|
| → | 1. solve for a_i at t using | $-\frac{dE}{dr_i} = F_i = m_i a_i(t)$ |
| → | 2. update v_i at $t + \frac{\delta t}{2}$ using | $v_i(t + \frac{\delta t}{2}) = v_i(t - \frac{\delta t}{2}) + a_i(t)\delta t$ |
| → | 3. update r_i at $t + \delta t$ using | $r_i(t + \delta t) = r_i(t) + v_i(t + \frac{\delta t}{2})\delta t$ |

This algorithm can be derived from the velocity and position data successively alternate at $\frac{1}{2}$ time step intervals. According to this scheme, the velocities are explicitly calculated by

$$v(t) = \frac{1}{2} \left[v\left(t + \frac{1}{2} \delta t\right) + v\left(t - \frac{1}{2} \delta t\right) \right]. \quad (2.55)$$

The better supplement of the same basic algorithm is called velocity Verlet algorithm,

$$\begin{aligned} r(t + \delta t) &= r(t) + v(t)\delta t + \frac{1}{2} a(t)\delta t^2 \\ v(t + \delta t) &= v(t) + \frac{1}{2} \delta t [a(t) + a(t + \delta t)], \end{aligned} \quad (2.56)$$

which yields positions, velocities and accelerations at the same time and does not compromise precision.

Beeman's algorithm, also related to the Verlet algorithm, uses a more acute expression for the velocity. Since the kinetic energy is calculated directly from the velocities, thus it often gives better energy conservation. However, the expressions of this algorithm are more complex and expensive than those of the Verlet algorithm as

$$\begin{aligned} r(t + \delta t) &= r(t) + v(t)\delta t + \frac{2}{3} a(t)\delta t^2 - \frac{1}{6} a(t - \delta t)\delta t^2 \\ v(t + \delta t) &= v(t) + \frac{1}{3} a(t)\delta t + \frac{5}{6} a(t)\delta t - \frac{1}{6} a(t - \delta t)\delta t. \end{aligned} \quad (2.57)$$

The predictor-corrector algorithm contains three basic steps. In the first step, new positions, velocities, accelerations and high-order terms are predicted based on the Taylor series expansion:

$$\begin{aligned}
r^p(t + \delta t) &= r(t) + v(t)\delta t + \frac{1}{2}a(t)\delta t^2 + \frac{1}{6}b(t)\delta t^3 + \frac{1}{24}c(t)\delta t^4 + \dots \\
v^p(t + \delta t) &= v(t) + a(t)\delta t + \frac{1}{2}b(t)\delta t^2 + \frac{1}{6}c(t)\delta t^3 + \dots \\
a^p(t + \delta t) &= a(t) + b(t)\delta t + \frac{1}{2}c(t)\delta t^2 \dots \\
b^p(t + \delta t) &= b(t) + c(t)\delta t + \dots
\end{aligned} \tag{2.58}$$

The superscript p marks these as predicted values. Since r and v stand for the complete set of positions and velocities, a is short for all the accelerations and b denotes all the third time derivatives of r . In the second step, we can calculate the force at time $t + \delta t$ from the new position r^p to give the correct accelerations, $a^c(t + \delta t)$. Then, we can estimate the size of the error in the prediction step,

$$\Delta a(t + \delta t) = a^c(t + \delta t) - a^p(t + \delta t). \tag{2.59}$$

Then, the estimated error is employed in the corrector step,

$$\begin{aligned}
r^c(t + \delta t) &= r^p(t + \delta t) + c_0 \Delta a(t + \delta t) \\
v^c(t + \delta t) &= v^p(t + \delta t) + c_1 \Delta a(t + \delta t) \\
a^c(t + \delta t) &= a^p(t + \delta t) + c_2 \Delta a(t + \delta t) \\
b^c(t + \delta t) &= b^p(t + \delta t) + c_3 \Delta a(t + \delta t)
\end{aligned} \tag{2.60}$$

When the finite difference algorithm is chosen, the time step must be small enough such that the expansions can provide a reliable estimate of the atomic positions and velocities at each simulation step.

2.2.3.3 Periodic boundary conditions

In computer simulation, periodic boundary conditions are widely used in order to solve the problem of surface effects. A cubic box of particles is replicated throughout the space in all directions to form an infinite lattice. Figure 2.2 shows periodic boundary conditions in two dimensions.

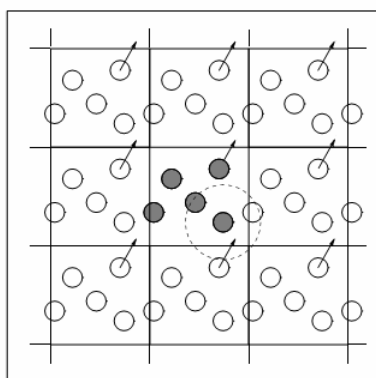


Figure 2.2 Periodic boundary conditions in two dimensions.

The key point is that each particle in the box interacts with the nearest particles in the same box and also with their images in nearby boxes. As a particle moves out of a central box during simulation, then an image particle moves in to replace it from the opposite side at the same time with the same velocity to conserve overall mass and momentum in the central box. Therefore, the number of

particles within the central box remains constant throughout the course of the simulation.

2.2.3.4 Cut-off limit and potential at cut-off

In classical MD simulation, the non-bonded interactions are of most time-consuming part of the energy and force calculations. Since the number of non-bonded terms involve a numerous interesting pairs due to the effect of periodic boundary condition (e.g., there are $N*(N-1)/2$ interactions for N atom system). To save computer resources, the most popular way is to use non-bonded cut-off along with the minimum image criterion. It is assumed that non-bonded interactions occurring between atoms separated by more than cut-off distance are set to zero. Thus, only the nearest images of distinguishable particles are taken into account in calculations of the energy or force, and the cut-off limit should be no more than half the length of the box, as illustrated in Figure 2.3.

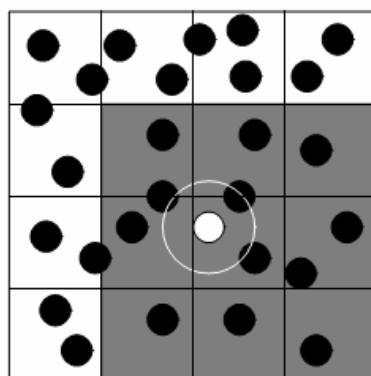


Figure 2.3 Cut-off limit.

Another problem can be occurrence since introduction of cut-off in both the potential energy and the force near the cut-off value makes a little jump, especially in the MD simulation where energy conservation is required. To avoid this problem, simple approach is to use a shifted potential in order to vanish at the cut-off radius,

$$V(r) = \begin{cases} \phi_{LJ}(r) - \phi_{LJ}(R_c) & \text{if } r \leq R_c \\ 0 & \text{if } r > R_c \end{cases}, \quad (2.61)$$

where R_c is the cut-off distance and $\phi_{LJ}(R_c)$ is equal to the value of the potential at the cut-off distance.

Although the shifted potential can be used to conserve the system's energy, the energy and force between a pair of molecules is still discontinuous at $r = R_c$. To eliminate discontinuities in the energy and force equations, an alternative way is using a switching function, such as

$$V^{SF}(r) = \begin{cases} \phi_{LJ}(r) - \phi_{LJ}(R_c) - \left(\frac{d\phi_{LJ}(r)}{dr} \right)_{r=R_c} (r - R_c) & r \leq R_c \\ 0 & r > R_c \end{cases}, \quad (2.62)$$

It should be noted that the use of switching function over the entire range may affect the equilibrium structures. Therefore, this function is usually applied over a narrow range, i.e., near the cut-off for eliminating the discontinuous problem.

2.2.3.5 Non-bonded neighbor lists

In fact, the simulation time may not dramatically reduce when cut-off limit is used for calculating the number of non-bonded interactions. This is true since the distance between every pair of atoms would still have calculated for each simulation step. With respect to this point, the Verlet neighbor list (see Figure 2.4) is used to store all atoms within the cut-off distance (solid circle) and all atoms that locate slightly further away than the cut-off distance (dashed circle).

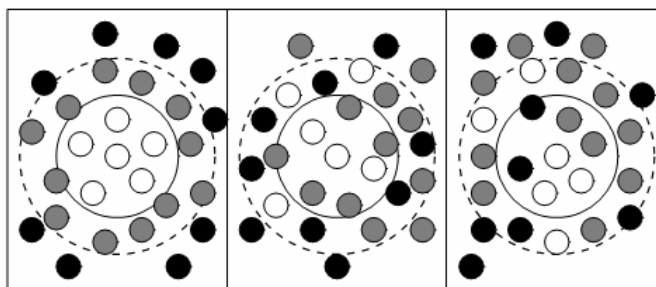


Figure 2.4 Verlet neighbor list.

In practice, the list of stored particles is commonly updated frequency between 10 and 20 steps according to the fact that atom's neighbors do not change significantly over 10 or 20 simulation steps. At the first step of the simulations, the list is constructed for all of the neighbors of each atom, for which the pair separation is within a list sphere. Therefore, only pairs appearing in the list of the next time step are checked in the force routine. The list must be reconstructed always before particles originally outside the list range (black) have penetrated the potential cut-off sphere.

2.2.3.6 Long-range interactions

The use of cut-off limit and shifted-force potentials neglects long-range Coulombic interaction. The van der Waals interactions can be neglected beyond the cut-off limit because these interactions converge to zero very quickly as the distance between the two atoms increases. In contrast, the charge-charge interactions are longer decay range as $1/r$. Therefore, the forces obtained from charge-charge interactions are serious problem since their range is greater than half of box length. There are two common methods used for the treatment of long-range forces. The Ewald summation (Heyes, 1981) is to study the energetics of ionic crystals by including the interaction of the particle with all the other particles in the simulation box and with all of their images in periodic cells. The potential energy of the Ewald summation can be written as

$$V^{ZZ} = \frac{1}{2} \sum_n' \left(\sum_{i=1}^N \sum_{j=1}^N Z_i Z_j |r_{ij} + n|^{-1} \right), \quad (2.63)$$

where Z_i and Z_j are charges. The sum over n is the sum over all simple cubic lattice points. The prime indicates that we omit $i = j$ for $n = 0$.

The problems of this summation are computationally quite expensive and it tends to reinforce artifacts due to the use of periodic boundary conditions. Another way is to apply reaction field method (Foulkes and Haydock, 1989). This method assumes that the interaction from molecules beyond a cut-off distance can be handled in an average way. The advantages of this method are the conceptually simple and computationally efficient. Within the sphere or cavity R , the

interaction with molecules is calculated explicitly. The size of the reaction field acting on molecule i is proportional to the moment of the cavity surrounding i ,

$$\xi_i = \frac{2(\epsilon_s - 1)}{2\epsilon_s + 1} \frac{1}{r_c^3} \sum_{j \in R} \mu_j. \quad (2.64)$$

According to equation (2.63), the summation extends over the molecules in the cavity, including i , and r_c is the radius of the cavity (Onsager, 1936). The contribution to the energy from the reaction field is $-\frac{1}{2} \mu_i \xi_i$.

2.3 Combined *ab initio* QM/MM MD simulation

In general, the classical simulation based on pairwise additive approximation can yield reasonable results for the structural and dynamical properties of condensed phase systems. In some cases, however, the many-body interactions often have significant influence, especially for the strongly interaction systems. On the basis of *ab initio* QM/MM approach, the system is partitioned into two parts, namely QM and MM regions, as shown in Figure 2.5.

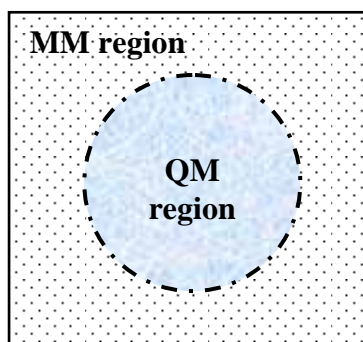


Figure 2.5 System's partition.

In this work, the most interesting region, the sphere includes NO_3^- and its surrounding water molecules, is treated by Born-Oppenheimer *ab initio* quantum mechanics, while the rest of the system is described by classical molecular mechanical potentials.

The total interaction energy (E_{tot}) of the system can be divided into three component parts,

$$E_{tot} = \left\langle \Psi_{QM} \mid \hat{H} \mid \Psi_{QM} \right\rangle + E_{MM} + E_{QM-MM}, \quad (2.65)$$

where $\left\langle \Psi_{QM} \mid \hat{H} \mid \Psi_{QM} \right\rangle$ refers to the interactions within the QM region and the later two terms, E_{MM} and E_{QM-MM} , represent the energy of interactions within the MM and between the QM and MM regions, respectively.

During the QM/MM simulation, water molecules can frequently exchange between QM and MM regions. In this case, forces acting on each particle in the

system are switched according to the defined region upon entering or leaving the QM region,

$$F_i = S_m(r)F_{QM} + (1 - S_m(r))F_{MM}, \quad (2.66)$$

where F_i refers to force on each particle in the system. r is the distance between the nitrate ion and the oxygen atom of water. F_{QM} and F_{MM} are quantum mechanical and molecular mechanical forces, respectively. $S_m(r)$ is a smoothing function (Brooks, Bruccoleri, Olafson, States, Swaminathan, and Karplus, 1983).

$$\begin{aligned} S_m(r) &= 1 \quad \text{for } r \leq r_1, \\ S_m(r) &= \frac{(r_0^2 - r^2)^2 (r_0^2 + 2r^2 - 3r_1^2)}{(r_0^2 - r_1^2)^3} \quad r_1 < r \leq r_0, \\ S_m(r) &= 0 \quad \text{for } r > r_0, \end{aligned} \quad (2.67)$$

where r_1 and r_0 are the distances characterizing the start and finish of the QM region. This smoothing function was applied to ensure a continuous change of forces at the transition between QM and MM regions, as shown in Figure 2.6.

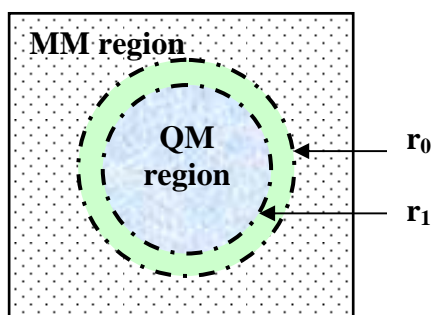


Figure 2.6 Smoothing of force at transition between QM and MM regions.

CHAPTER III

RESULTS AND DISCUSSION

This chapter begins with computational details, followed by detailed analysis on the solvation structure and dynamics of the NO_3^- ion in water. The hydration structure of NO_3^- and the characteristics of hydrogen bonding between NO_3^- and water will be discussed in terms of radial distribution functions (RDFs) and their corresponding integration numbers, as well as angular distribution functions and orientations of water molecules surrounding the ion. The dynamical properties of the hydrated NO_3^- will be analyzed by means of velocity autocorrelation functions (VACFs) and their Fourier transformations. The VACFs can provide direct insight into the dynamics as the time integrals are related to macroscopic transport coefficients, and their Fourier transformations are directly related to vibrational spectra. Other dynamical properties such as water exchange processes and mean residence times of water molecules in the bulk and in the hydration shell of ion will also be evaluated and discussed.

3.1 Computational details

3.1.1 Construction of NO_3^- - H_2O pair potential

In this work, a flexible BJH-CF2 model, which describes intermolecular (Stillinger and Rahman, 1978) and intramolecular interactions (Bopp, Jancso', and Heinzinger, 1983), was employed for water. This flexible water model

allows explicit hydrogen movements, thus ensuring a smooth transition, when water molecules move from the QM region with its full flexibility to the MM region. The pair potential function for describing nitrate-water interactions is newly constructed. Firstly, both NO_3^- and H_2O species were separately optimized at MP2 level of accuracy using aug-cc-pvdz basis set (Dunning, 1989; Kendall, Dunning, and Harrison, 1992; Woon and Dunning, 1993). Next, the NO_3^- ion was placed on the xy plane (see Figure 3.1), while a water molecule was allowed to move with respect to the variation of θ (*i.e.*, between 0 and 60°) and ϕ (*i.e.*, between 0 and 90°), associated with 9 different types of water orientation (see Figure 3.2). Examples of stabilization energies between the NO_3^- ion and water molecule are shown in Figures 3.3-3.9.

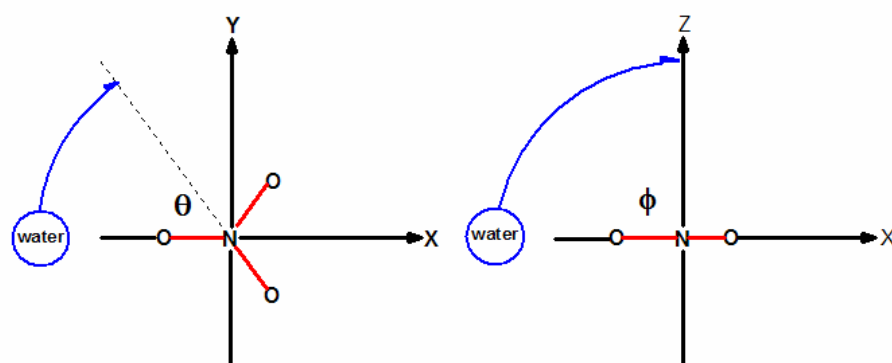


Figure 3.1 Variation of NO_3^- - H_2O configurations.

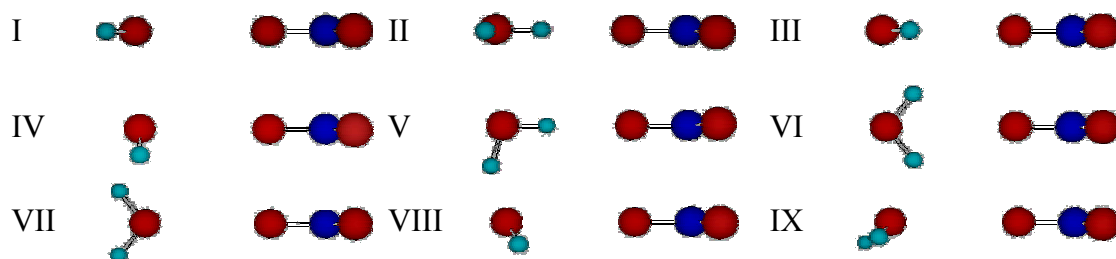


Figure 3.2 Variation of water's orientations.

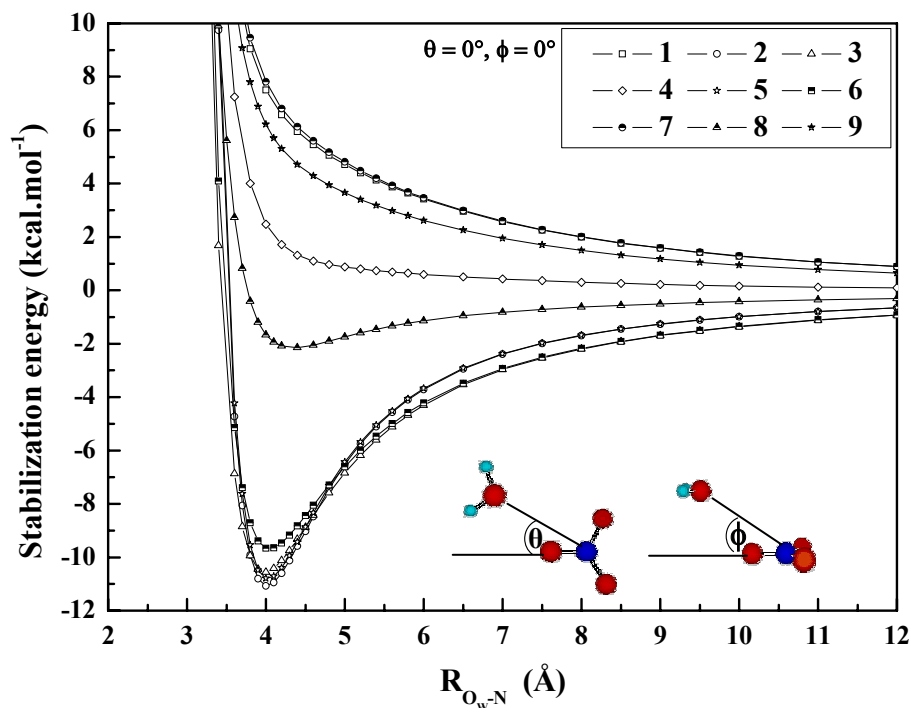


Figure 3.3 Plots of stabilization energies between the NO_3^- ion and water molecule, for $\theta = 0^\circ$ and $\phi = 0^\circ$.

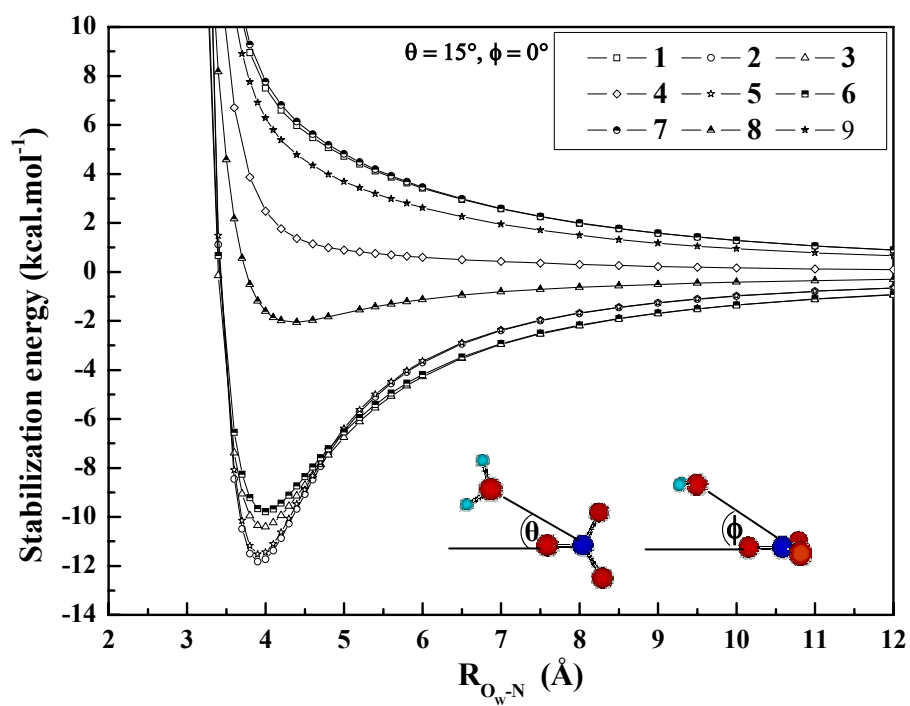


Figure 3.4 Plots of stabilization energies between the NO_3^- ion and water molecule, for $\theta = 15^\circ$ and $\phi = 0^\circ$.

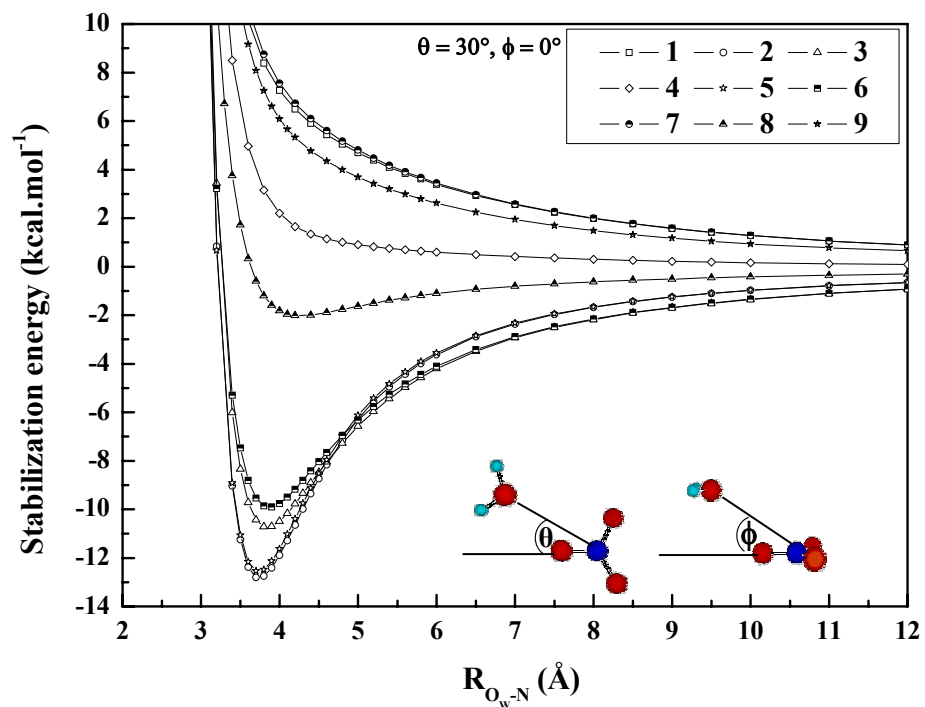


Figure 3.5 Plots of stabilization energies between the NO_3^- ion and water molecule, for $\theta = 30^\circ$ and $\phi = 0^\circ$.

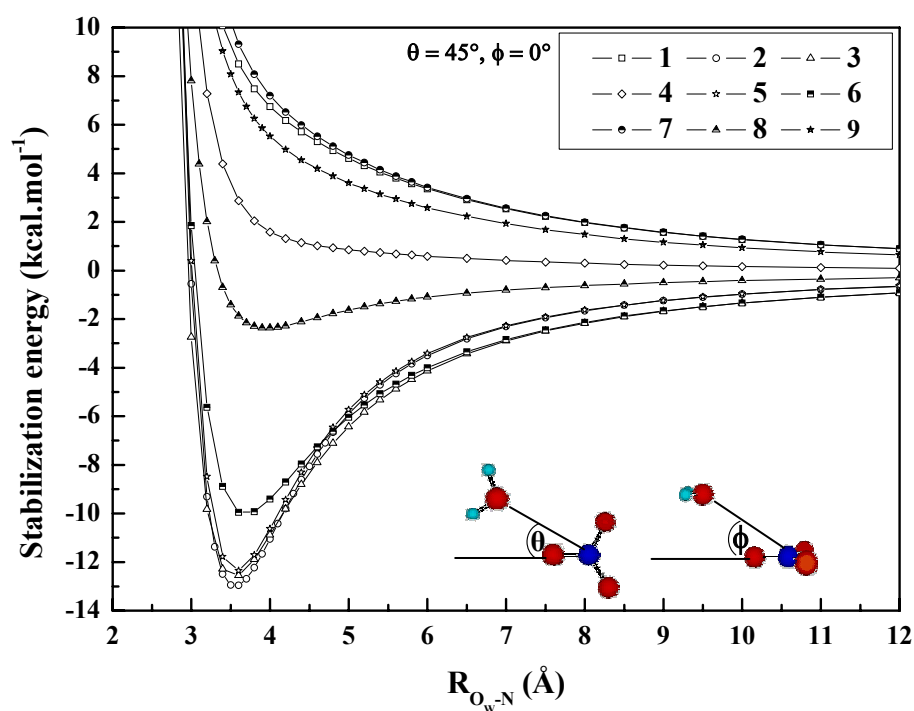


Figure 3.6 Plots of stabilization energies between the NO_3^- ion and water molecule, for $\theta = 45^\circ$ and $\phi = 0^\circ$.

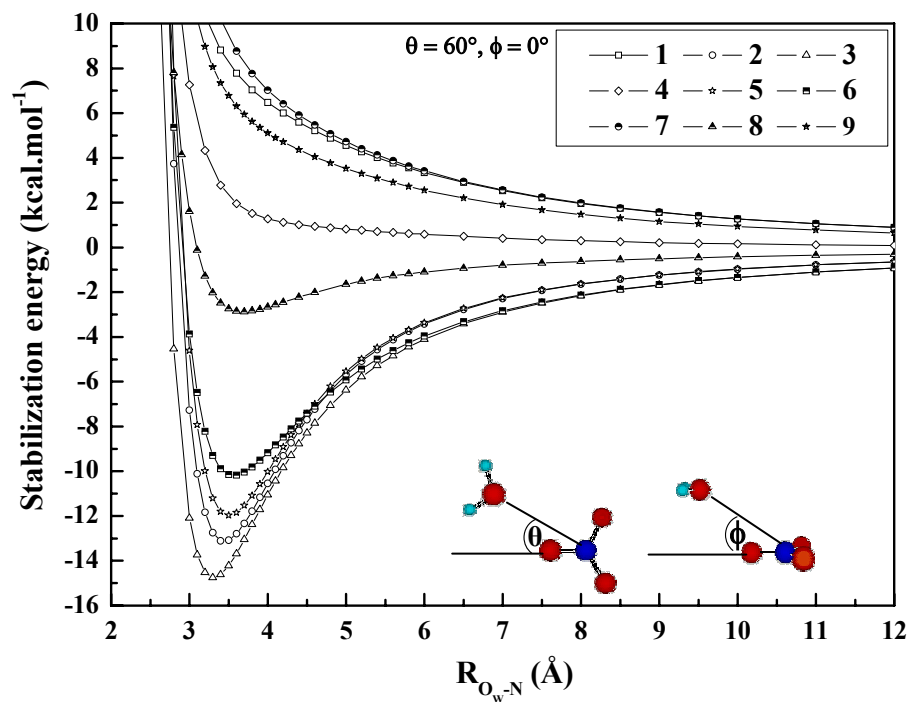


Figure 3.7 Plots of stabilization energies between the NO_3^- ion and water molecule, for $\theta = 60^\circ$ and $\phi = 0^\circ$.

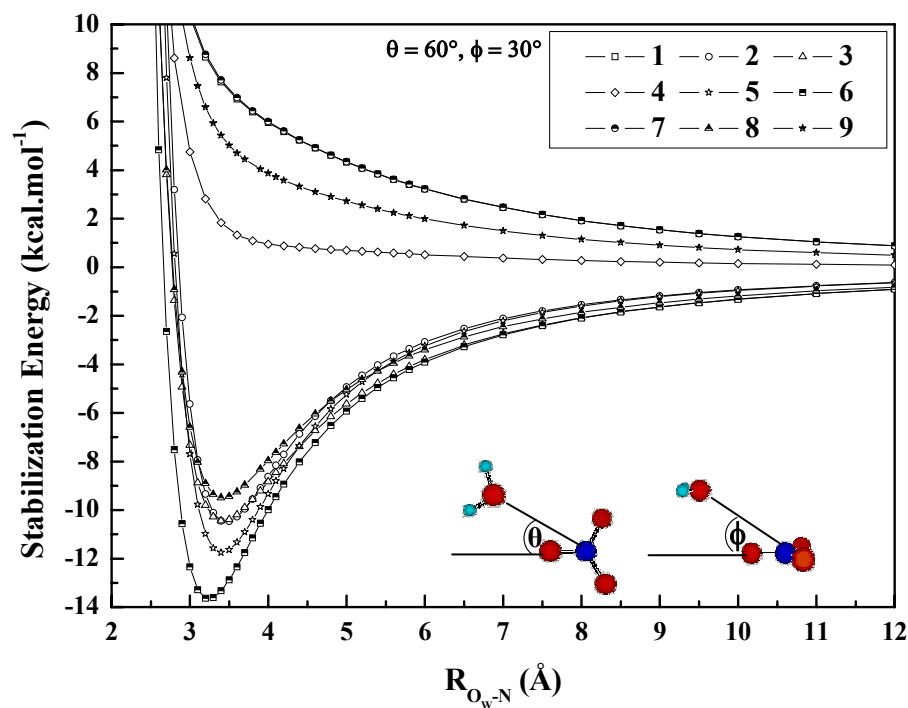


Figure 3.8 Plots of stabilization energies between the NO_3^- ion and water molecule, for $\theta = 60^\circ$ and $\phi = 30^\circ$.

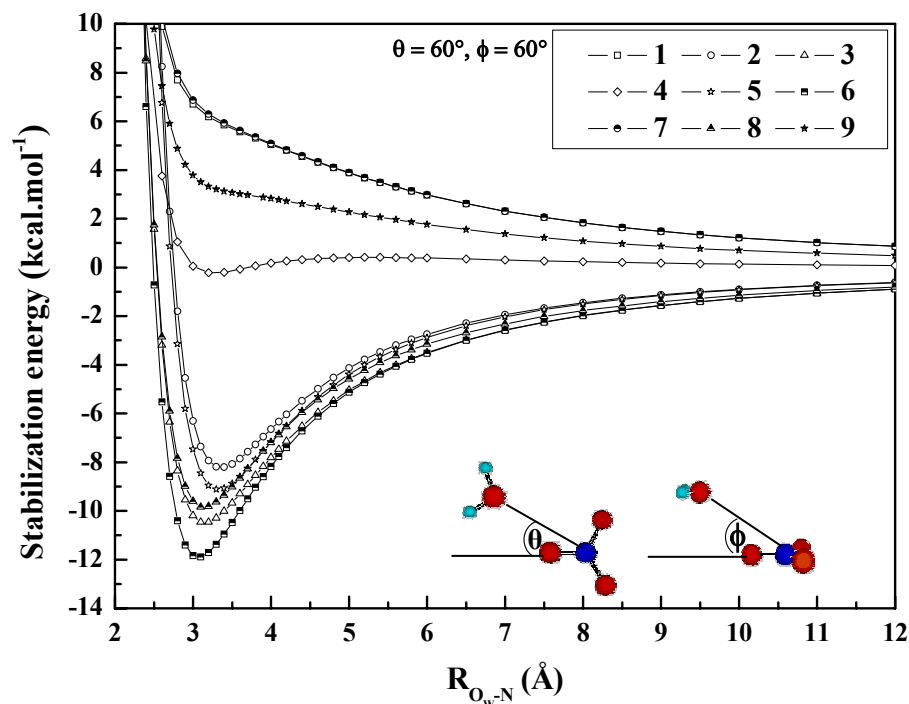


Figure 3.9 Plots of stabilization energies between the NO_3^- ion and water molecule, for $\theta = 60^\circ$ and $\phi = 60^\circ$.

Then, a total of 5,266 MP2 interaction energy points for various NO_3^- - H_2O configurations, obtained from MP2 calculations using aug-cc-pvdz basis set, were fitted to an analytical form of

$$\Delta E_{\text{NO}_3^- - \text{H}_2\text{O}} = \sum_{i=1}^4 \sum_{j=1}^3 \left[\frac{A_{ij}}{r_{ij}^4} + \frac{B_{ij}}{r_{ij}^5} + C_{ij} \cdot \exp(-D_{ij} r_{ij}) + \frac{q_i q_j}{r_{ij}} \right], \quad (3.1)$$

where A , B , C and D are fitting parameters (see Table 3.1), r_{ij} denotes the distances between the i -th atoms of NO_3^- and the j -th atoms of water molecule and q are atomic net charges. In the present study, the charges on N and O of NO_3^- were obtained from Mulliken population analysis (MPA) of MP2 calculations using aug-cc-pvdz basis set,

and the charges on O and H of water molecule were adopted from the flexible water model. They were set to 1.4996, -0.8332, -0.6598 and 0.3299, respectively. According to equation (3.1), all Coulombic terms were multiplied by factors of 0.529177 and 627.51. It is known that the MPA certainly depends on the basis set. However, when fitting a potential function to an energy surface, the absolute values of the charges are only of secondary importance since the other parameters will compensate (*i.e.*, as an energy surface is fitted, the r^n terms in the potential together with the Coulombic term are only an approximation to fit this surface). Moreover, it could be noticed that the short-range part of this potential ($r < 4.4$ Å) is less significant since the corresponding ion-water interactions within this region were obtained directly by QM calculations during the HF/MM and B3LYP/MM simulations.

Table 3.1 Optimized parameters of the analytical pair potential for the interaction of water with NO_3^- (interaction energies in kcal.mol^{-1} and distances in Å).

Pair	A	B	C	D
	($\text{kcal mol}^{-1} \text{Å}^4$)	($\text{kcal mol}^{-1} \text{Å}^5$)	(kcal mol^{-1})	(Å^{-1})
N- O_w	-1310.7757	10012.1163	-55579.5941	2.8288
N- H_w	-512.0615	209.1700	5811.3787	2.9891
O_N - O_w	332.9194	1807.6405	-722.8225	1.2542
O_N - H_w	-84.1666	132.7195	53.9955	1.1110

The quality of the fit is shown in Figure 3.10, where the stabilization energies obtained from the MP2 calculations (ΔE_{MP2}) and from the fitted potential function (ΔE_{FIT}) are compared for some configurations. In Figure 3.10, the MP2 interaction energies with BSSE correction (ΔE_{BSSE}) are also given for comparison. In this work, the counterpoise correction was not taken into consideration since the BSSE estimates suggest that a correction seems unnecessary.

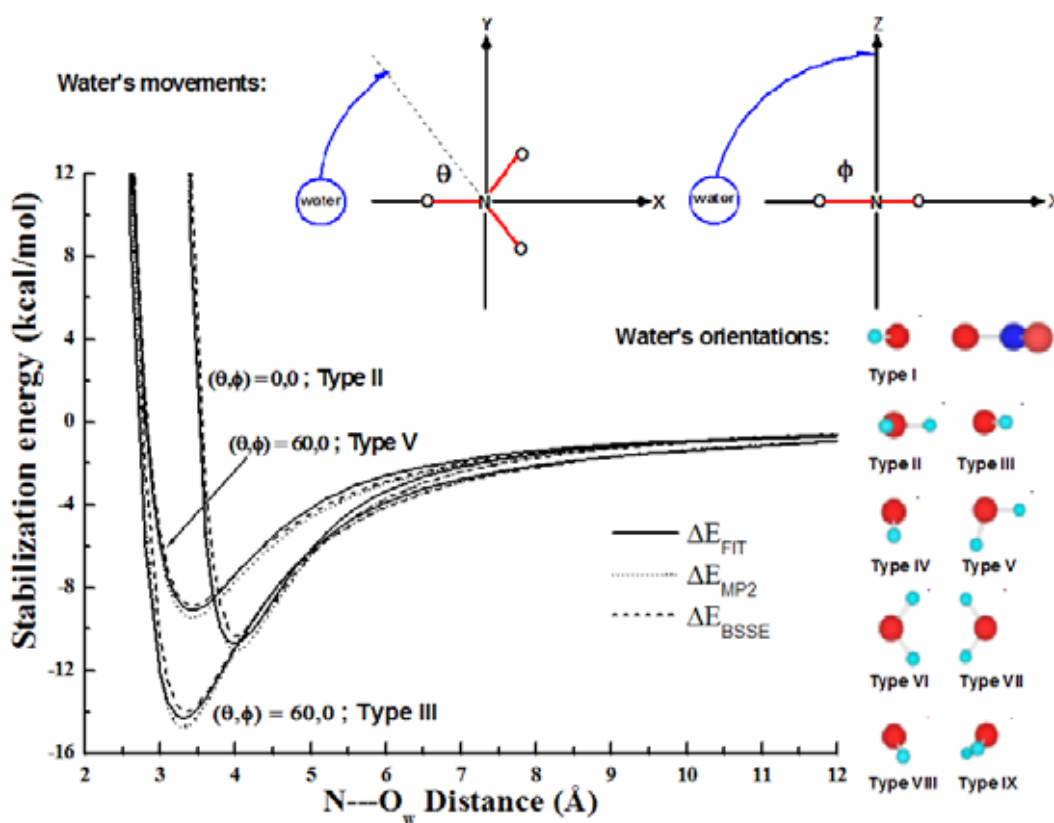


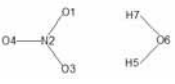
Figure 3.10 Comparison of the interaction energies obtained from the MP2 calculations with and without basis set superposition error (BSSE) correction, ΔE_{MP2} and ΔE_{BSSE} , and from the fitted potential function, ΔE_{FIT} , using the parameters given in Table 3.1 for some values of θ and ϕ .

3.1.2 Selection of QM method, basis set and QM size

With regard to the QM/MM scheme, besides the statistical requirement of a sufficiently long simulation time, the selection of QM method, basis set and QM size is crucial for obtaining a correct description on the structural and dynamical properties of solvated ions. As a matter of fact that the performance of QM/MM MD simulations in conjunction with correlated *ab initio* methods is still too time-consuming, making the HF and hybrid density functional B3LYP methods the possible alternatives for the present study. To simply test whether the HF or B3LYP methods are adequate for this particular system, geometry optimizations of NO_3^- - H_2O complex were carried out at HF, B3LYP, MP2 and CCSD levels of accuracy (see Table 3.2). The comparison to the data obtained by correlated methods indicated that the HF and B3LYP methods both appear reliable enough to achieve a sufficient level of accuracy in the QM/MM simulations, and that correlation effects are small and thus negligible. As can be seen from the data in Table 3.2, the stabilization energies, which are the most relevant data determining solute-solvent interactions, are considerably overrated by the B3LYP method, independent of the basis set. On the other hand, the ion-ligand distances show better agreement between correlated *ab initio* methods and B3LYP within the same basis set quality, but the distances obtained by HF with the DZV+ basis set to be employed in the QM/MM simulation are in fair agreement with the correlated distances obtained by the larger basis set and thus indicate this basis set to be a good compromise for the simulation if the HF method is used. The HF method has been well demonstrated in previous QM/MM studies (Kerdcharoen *et al.*, 1996; Tongraar *et al.*, 1998; Tongraar and Rode, 2003; Tongraar and Rode, 2005; Tongraar and Rode, 2005; Intharathep, Tongraar, and Sagarik, 2005; Rode, Schwenk, Hofer,

and Randolph, 2005; Rode and Hofer, 2006; Rode, Hofer, Randolph, Schwenk, Xenides, and Vchirawongkwin, 2005), even for the treatment of anions, also proving the assumption that the effects of electron correlation are small enough to be neglected (Tongraar *et al.*, 1998; Tongraar and Rode, 2003). In a recent QM/MM MD simulation of pure water (Rode *et al.*, 2005), it has been demonstrated that the HF method with a sufficiently large QM size could provide detailed information of pure water in good agreement with the MP2-based simulation. The B3LYP method was employed in order to test the adequacy of the DFT method for the description of hydrated anions. By several cases it has been well-documented that the DFT methods often give poor results for hydrated cations (Rode *et al.*, 2004; Rode *et al.*, 2005; Rode and Hofer, 2006). It should be realized that while the HF scheme could produce an error due to the neglect of electron correlation effects, the DFT methods, although including such effects to a certain (uncontrollable) extent, are often found to overestimate the correlation energy (Intharathep *et al.*, 2005; Rode *et al.*, 2005; Rode and Hofer, 2006). On the other hand, a comparison of the HF calculations with the DFT results could be helpful to estimate the methodical frameworks.

Table 3.2 Stabilization energies and some selected structural parameters of the optimized NO_3^- - H_2O complex, calculated at HF, B3LYP, MP2 and CCSD methods using DZV+ and aug-cc-pvdz (data in parentheses) basis sets.

Method	HF	B3LYP	MP2	CCSD
				
ΔE	-16.43	-18.60	-16.83	-16.78
(kcal.mol ⁻¹)	(-13.87)	(-15.82)	(-14.52)	(-14.19)
R_{2-1} (Å)	1.275 (1.228)	1.315 (1.267)	1.333 (1.272)	1.330 (1.252)
R_{2-3} (Å)	1.276 (1.228)	1.316 (1.267)	1.333 (1.272)	1.330 (1.252)
R_{2-4} (Å)	1.259 (1.216)	1.296 (1.252)	1.318 (1.260)	1.308 (1.239)
R_{1-7} (Å)	2.230 (2.198)	2.090 (2.051)	2.168 (2.035)	2.186 (2.071)
R_{3-5} (Å)	2.211 (2.200)	2.078 (2.060)	2.152 (2.047)	2.171 (2.055)
R_{6-5} (Å)	0.956 (0.949)	0.986 (0.975)	0.988 (0.976)	0.986 (0.970)
R_{6-7} (Å)	0.956 (0.949)	0.986 (0.975)	0.988 (0.976)	0.986 (0.970)
A_{5-6-7} (°)	105.87 (99.36)	102.30 (96.61)	103.22 (95.60)	103.39 (96.60)
A_{1-7-6} (°)	135.11 (139.24)	138.61 (142.35)	137.82 (143.36)	137.59 (141.21)
A_{3-5-6} (°)	136.52 (139.09)	139.43 (141.66)	139.07 (142.39)	138.81 (142.52)

In addition to the choice of the QM method, it is known that the use of larger basis set is a key factor for obtaining better results (see Table 3.2). In practice, however, the computational expense for QM force calculations using large basis sets is significant. In most of the previous QM/MM studies (Kerdcharoen *et al.*, 1996;

Tongraar *et al.*, 1998; Tongraar and Rode, 2003; Tongraar and Rode, 2005; Tongraar and Rode, 2005; Intharathep *et al.*, 2005; Rode, Schwenk *et al.*, 2005; Rode and Hofer, 2006; Rode *et al.*, 2005), therefore, a moderate basis set has been employed. In the present work, since a satisfactory description of anions requires diffuse basis functions, the DZV+ basis set (Dunning and Hay, 1976) was chosen, considered as a suitable compromise between the quality of the simulation results and the requirement of CPU time.

To define the size of QM region, a preliminary HF/MM simulation, *i.e.*, the simulation in which only the NO_3^- was treated quantum mechanically using HF method while the rest of the system is described by classical pair potentials, was performed (see Figure 3.11a). According to the resulting N- O_w RDF, the first minimum of the N- O_w peak is exhibited at around 5.0 Å. An integration up to first minimum of the N- O_w peak yields about 18-20 water molecules. This implies that a QM size with diameter of 10.0 Å seemed to be desirable for the present study. However, the evaluation of QM forces for all particles within this QM size is still beyond the limit of our current computational facility. Therefore, a slightly smaller QM size with diameter of 8.8 Å was chosen, which includes NO_3^- and about 14-16 water molecules. To ensure a continuous change of forces at the boundary between the QM and MM regions, a smoothing function (Brooks *et al.*, 1983) was employed within an interval of 0.2 Å (*i.e.*, between the N--- O_w distance of 4.4-4.6 Å).

3.1.3 Simulation protocol

All simulations were performed in a canonical ensemble at 298 K with a time step of 0.2 fs. The periodic box, with a box length of 18.17 Å, contained one

NO_3^- and 199 water molecules, corresponding to the experimental density of pure water. Long-range interactions were treated using the reaction-field procedure (Adams, Adams, and Hill, 1979). The system was initially equilibrated by performing a preliminary HF/MM MD simulation, in which only the NO_3^- was treated quantum mechanically using HF method, for 200,000 time steps. Then, the HF/MM and B3LYP/MM simulations were started independently with system's re-equilibration for 30,000 time steps, followed by another 75,000 (HF/MM) and 85,000 (B3LYP/MM) time steps to collect configurations every 10^{th} step.

3.2 Structural details

The solvation structure of NO_3^- in water is described by means of N-O_w , N-H_w , $\text{O}_N\text{-O}_w$ and $\text{O}_N\text{-H}_w$ RDFs, together with their corresponding integration numbers, as shown in Figure 3.11. According to the shape and height of the resulting N-O_w RDFs (Figure 3.11a), both HF/MM and B3LYP/MM simulations reveal broad and unsymmetrical first N-O_w peaks with maximum at 3.96 and 3.83 Å, respectively. Integrations up to the first minimum of the corresponding N-O_w peaks yield average coordination numbers of 21.6 and 20.9, respectively. The observed broad and unsymmetrical N-O_w RDFs clearly indicate a high flexibility of the NO_3^- hydration shell. In addition, the first minimum of the N-O_w peaks is not well separated from the bulk, indicating a large number of water molecules situated in between the hydration shell and bulk. This implies also that water molecules in the hydration shell of NO_3^- are quite mobile, *i.e.*, they can easily exchange with bulk water. Comparing the corresponding N-O_w RDF obtained by the preliminary HF/MM simulation (Figure 3.11a), it becomes obvious that the use of only classical NO_3^- - H_2O and H_2O - H_2O pair

potentials is inadequate to correctly describe the short-range ion-water and water-water interactions, producing a higher rigidity of the NO_3^- hydration shell.

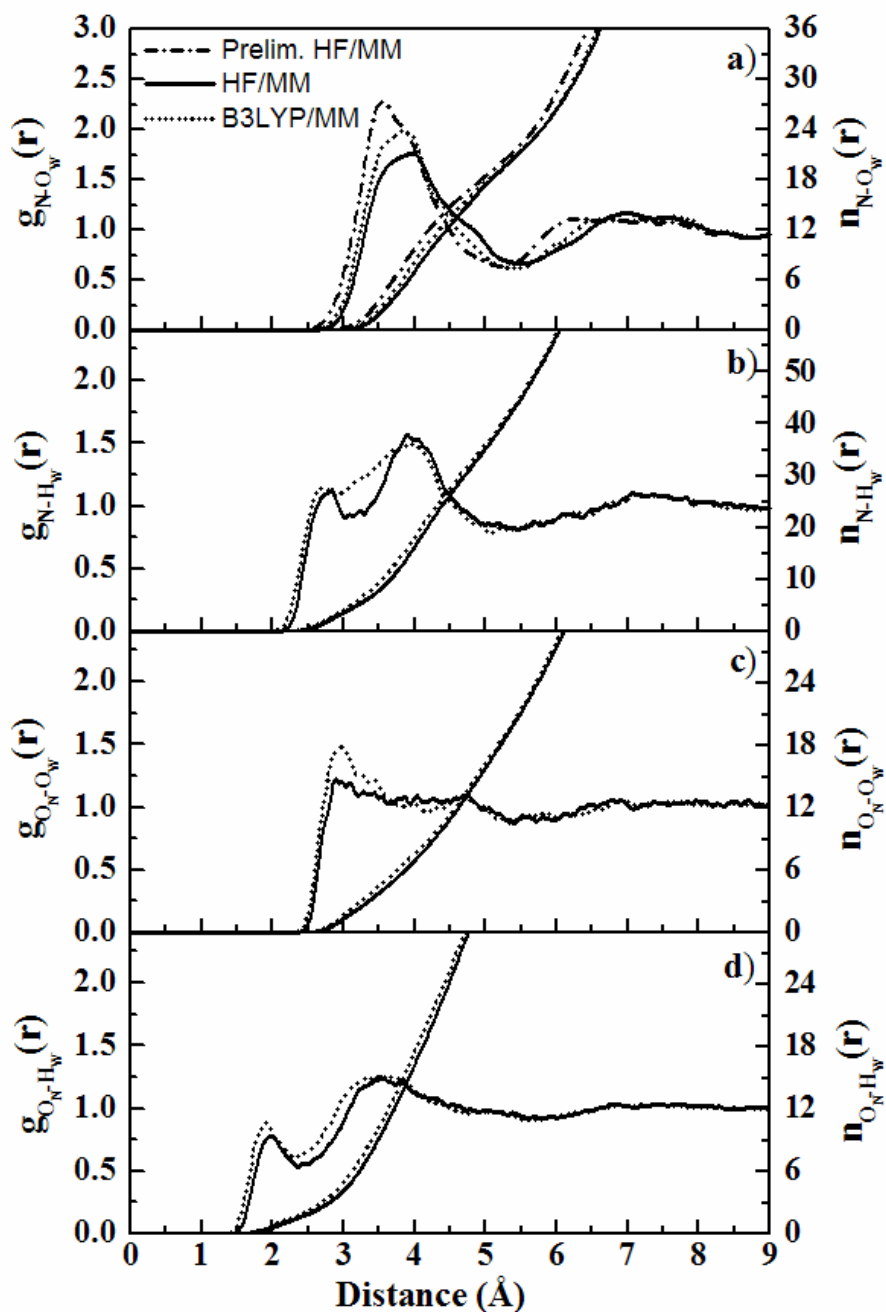


Figure 3.11 a) N-O_w, b) N-H_w, c) O_N-O_w and d) O_N-H_w radial distribution functions and their corresponding integration numbers.

In Figure 3.11b, the N-H_w RDFs obtained between the HF/MM and B3LYP/MM simulations are significantly different. The HF/MM simulation depicts two distinct peaks with maxima at distances of 2.62 and 4.03 Å. In the B3LYP/MM simulation, the first N-H_w peak is merged into a rather broad second peak, indicating that water molecules with somewhat distorted hydrogen bonding to oxygen atoms of NO₃⁻ are the main constituents of the first hydration shell. In Figure 3.11c, the O_N-O_w RDFs obtained from both HF/MM and B3LYP/MM simulations do not show distinct minima after the first shell, suggesting that a clear determination of the first shell coordination number for each of oxygen atoms of NO₃⁻ is not feasible. This also points at rather weak ion-water hydrogen bonds.

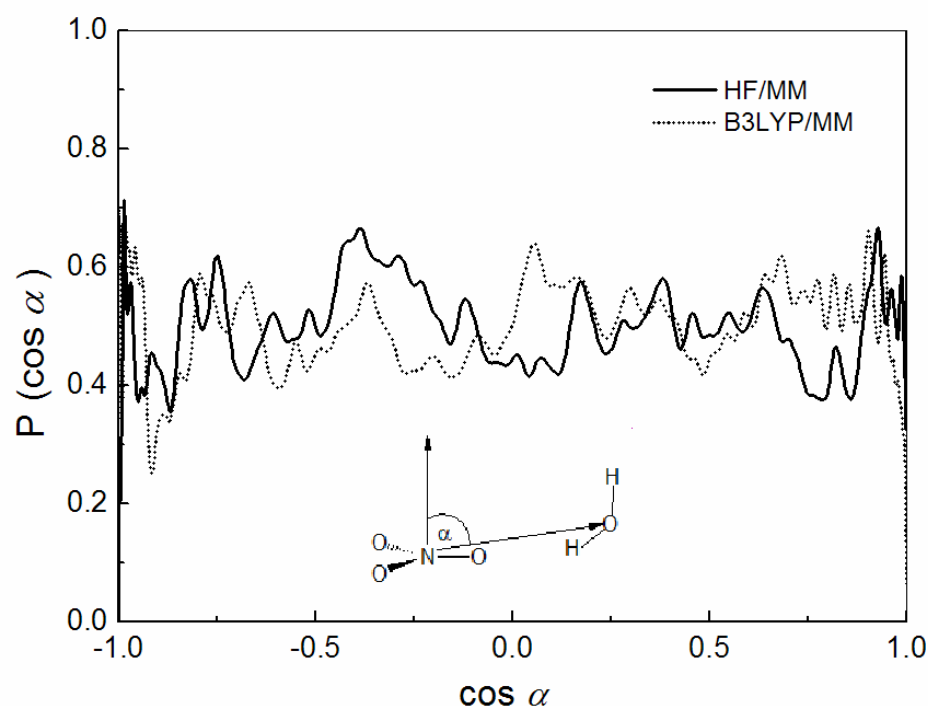


Figure 3.12 Distributions of the angle α between the vector perpendicular to NO₃⁻ plane and the vector along N---O_w distance, calculated within the first minimum of N-O_w RDFs.

Figure 3.12 shows the distributions of water molecules surrounding the ion as the distributions of the cosine of angle α between the vector perpendicular to NO_3^- plane and the vector along any $\text{N}\cdots\text{O}_w$ distance. Obviously, both HF/MM and B3LYP/MM simulations do not indicate specific features for the distribution of first shell water molecules, *i.e.*, they are mostly arranged with respect to $\text{N}-\text{O}_N\cdots\text{H}_w-\text{O}_w$ hydrogen bonds. Figure 3.13 shows some selected configurations of $\text{NO}_3^-(\text{H}_2\text{O})_n$ complexes obtained during the HF/MM and B3LYP/MM simulations. It is obvious that the first shell waters prefer to coordinate to oxygen atoms of NO_3^- , rather than to nitrogen atom from above and/or below the NO_3^- plane. As can be seen in Figure 3.13, each of first shell waters shares one hydrogen atom to linearly bind with oxygen atoms of NO_3^- . Nevertheless, it could be other possible arrangements, such as bifurcated hydrogen bonds as well as cyclic arrangements with two distorted hydrogen bonds, can temporarily be formed in aqueous solution.

More information on hydrogen bonds between NO_3^- and water can be obtained *via* the O_N-H_w RDFs (Figure 3.11d). Since the characteristics of hydrogen bonds in pure solvent represent a most important reference, the corresponding atom-atom RDFs for pure water obtained at similar QM/MM level of accuracy were utilized for comparison, as depicted in Figure 3.14. In this work, the HF/MM and B3LYP/MM simulations reveal first O_N-H_w peaks with maxima at 1.98 and 1.91 Å, respectively. These first O_N-H_w peaks are indicative of the hydrogen bonds between oxygen atoms of NO_3^- and their nearest-neighbor water molecules. Compared to the corresponding O-H RDF of pure water (Tongraar and Rode, 2004) (Figure 3.14), *e.g.*, in terms of shape and peak height, it is obvious that the $\text{O}_N\cdots\text{H}_w-\text{O}_w$ hydrogen bond interactions are rather weak.

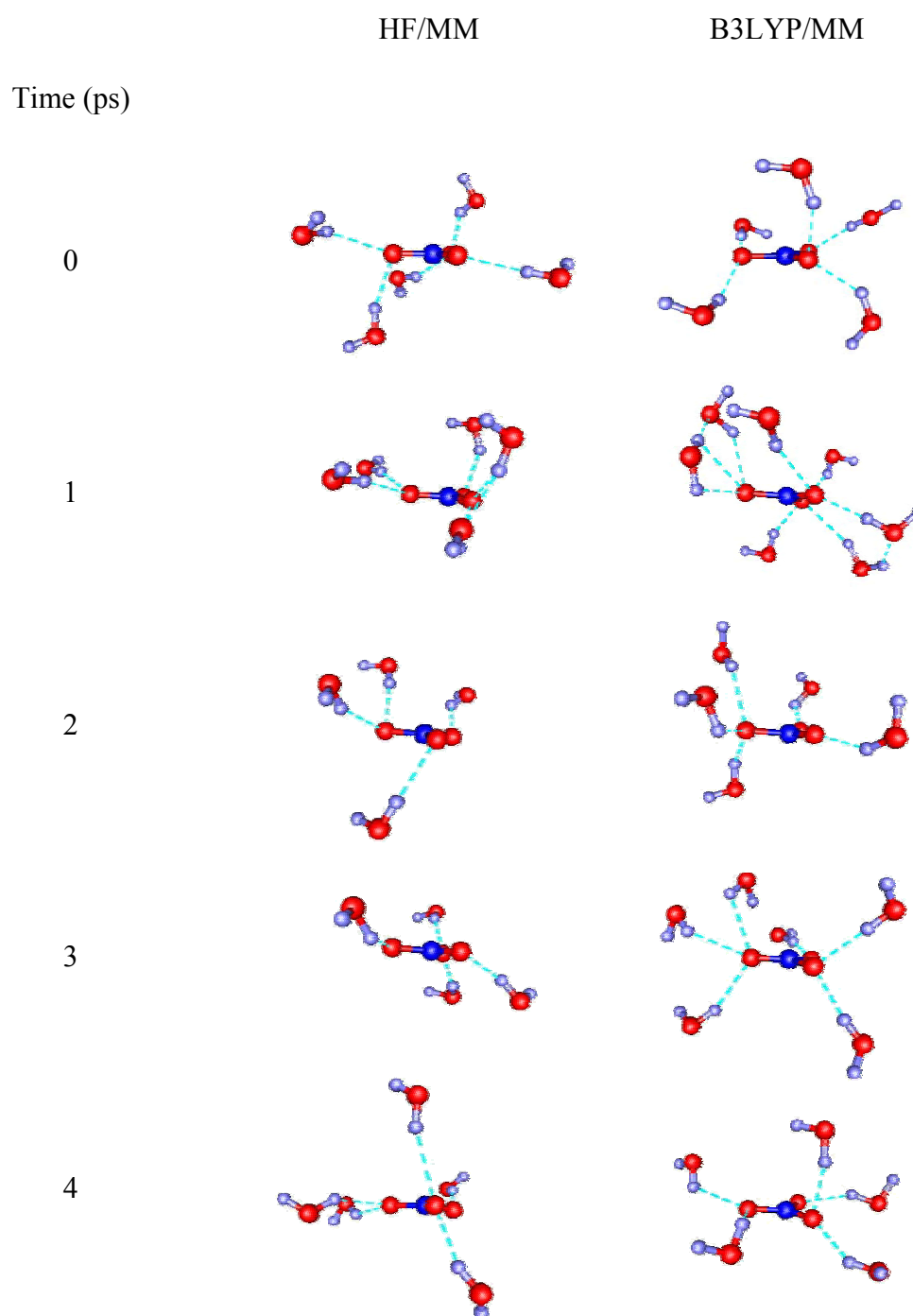


Figure 3.13 Arrangements of $\text{NO}_3^-(\text{H}_2\text{O})_n$ complexes obtained at 0, 1, 2, 3 and 4 ps of the HF/MM and B3LYP/MM simulations, plotted within the $\text{O}_N \cdots \text{H}_w$ distance of 2.5 Å.

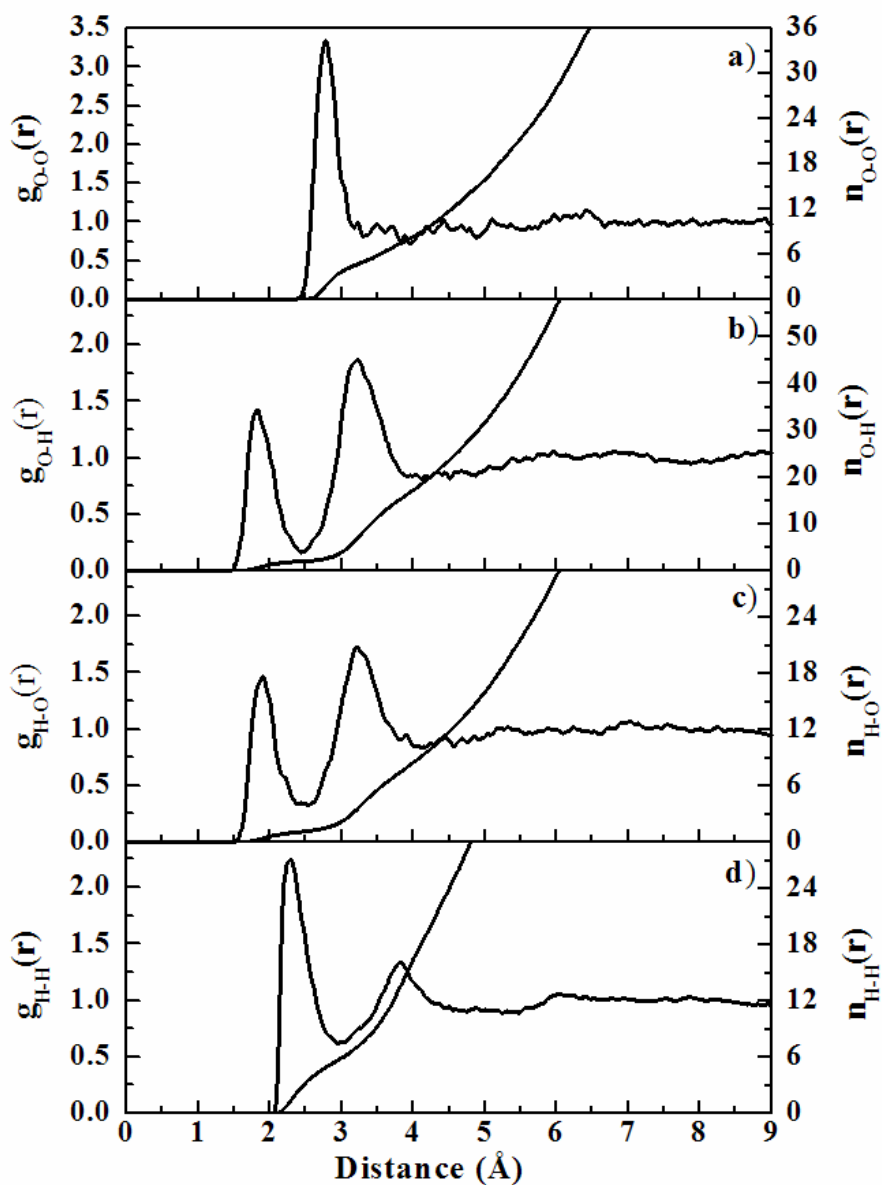


Figure 3.14 a) O-O, b) O-H, c) H-O and d) H-H radial distribution functions and their corresponding integration numbers. The first atom of each pair refers to the atoms of the water molecule, whose oxygen position was defined as center of the QM region during the QM/MM simulation (Tongraar *et al.*, 2004).

For a more detailed interpretation on the NO_3^- -water hydrogen bonds, the probability distributions of the cosine of the $\text{N}-\text{O}_\text{N}\cdots\text{H}_\text{w}$ and $\text{O}_\text{N}\cdots\text{H}_\text{w}-\text{O}_\text{w}$ angles calculated from the subset of configurations within the $\text{O}_\text{N}\cdots\text{H}_\text{w}$ distance of 2.5 Å are plotted in Figures 3.15 and 3.16, respectively. For an ideal hydrogen bond, the $\text{N}-\text{O}_\text{N}\cdots\text{H}_\text{w}-\text{O}_\text{w}$ interactions would be in a linear arrangement, *i.e.* a cosine equal or near to -1 for both $\text{N}-\text{O}_\text{N}\cdots\text{H}_\text{w}$ and $\text{O}_\text{N}\cdots\text{H}_\text{w}-\text{O}_\text{w}$ angles. With respect to the results obtained by the HF/MM and B3LYP/MM simulations, the distributions of $\text{N}-\text{O}_\text{N}\cdots\text{H}_\text{w}$ angles significantly deviate from linearity, whereas the distributions of $\text{O}_\text{N}\cdots\text{H}_\text{w}-\text{O}_\text{w}$ angle show a clear preference for the linear $\text{O}_\text{N}\cdots\text{H}_\text{w}-\text{O}_\text{w}$ arrangements. Figure 3.17 shows the distributions of the cosine of the angle θ , defined as the angle between the $\text{O}_\text{w}\cdots\text{O}_\text{N}$ vector and the dipole vector of water molecules surrounding the NO_3^- oxygens. Apparently, both HF/MM and B3LYP/MM simulations show a clear dipole-oriented arrangement of water molecules surrounding the NO_3^- oxygens (*e.g.*, the strong correlations between the nearest-neighbor water molecules and their lone pair direction), with maxima at $\cos \theta$ between 0.5 and 0.8. It is obvious that despite the fact that the interactions between NO_3^- and water are rather weak, the $\text{O}_\text{w}-\text{H}_\text{w}\cdots\text{O}_\text{N}$ bonds have a determining influence on the structure of hydrated NO_3^- .

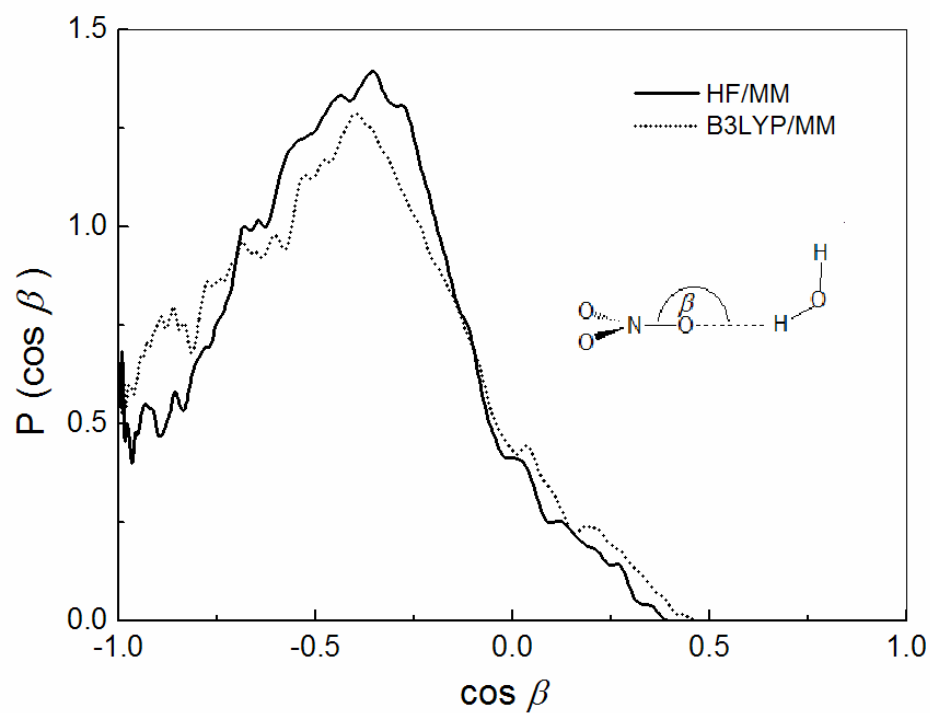


Figure 3.15 Distributions of the $\text{N-O}_N\cdots\text{H}_w$ angle, calculated within the $\text{O}_N\cdots\text{H}_w$ distance of 2.5 Å.

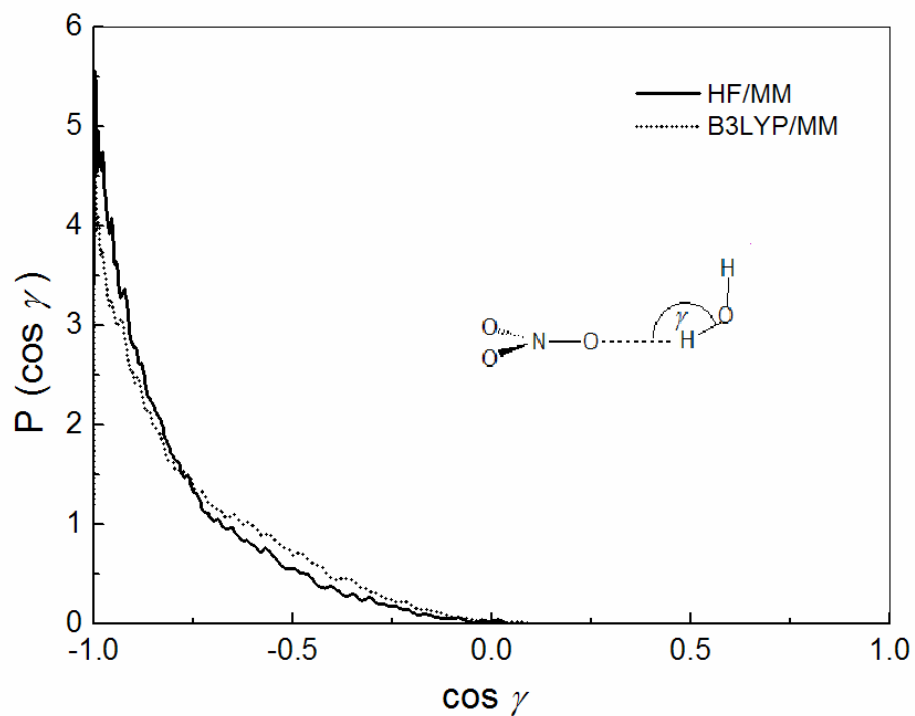


Figure 3.16 Distributions of the $\text{O}_N\cdots\text{H}_w\text{-O}_w$ angle, calculated within the $\text{O}_N\cdots\text{H}_w$ distance of 2.5 Å.

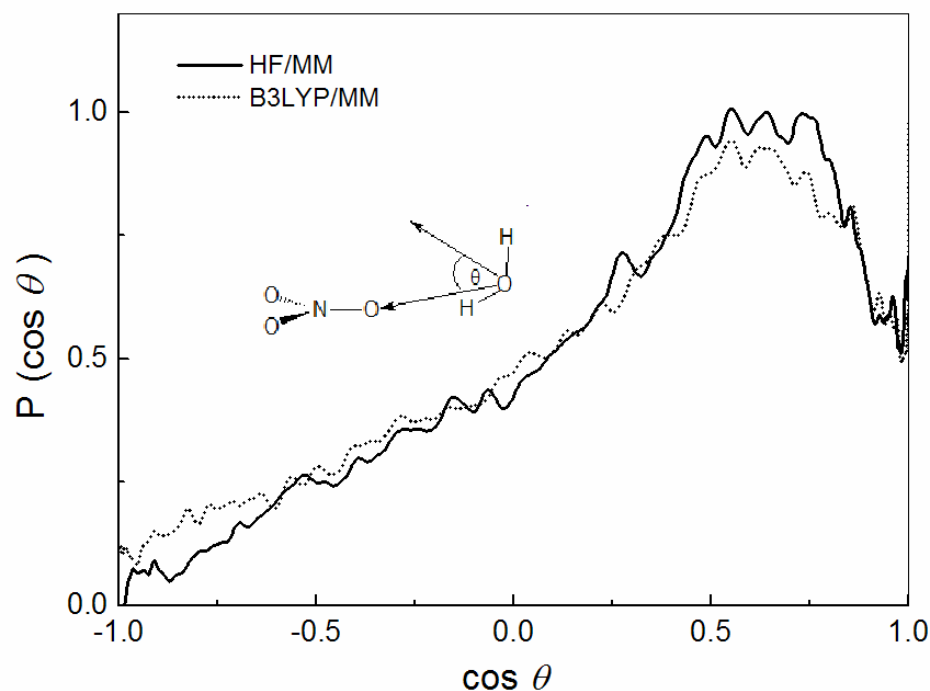


Figure 3.17 Distributions of the angle θ between the $O_w \cdots O_N$ vector and the vector of water's dipole moment, calculated within the $O_N \cdots H_w$ distance of 2.5 Å.

3.3 Dynamical details

3.3.1 Intramolecular geometry and vibrations of NO_3^-

The geometrical arrangement of NO_3^- in water is described in terms of distributions of N-O bond length and O-N-O angle, as shown in Figures 3.18a and b, respectively. Both HF/MM and B3LYP/MM simulations clearly indicate a flexibility of the NO_3^- structure, with half-height widths of about 1.26 ± 0.05 and 1.31 ± 0.06 Å for the distributions of N-O bonds, and of about 120 ± 4 and $120 \pm 5^\circ$ for the distributions of O-N-O angles, respectively. The observed difference between the HF/MM and B3LYP/MM simulations can probably be regarded more as a consequence of the approximations of the functional and the parametrizations of the B3LYP method than

as a consequence of correlation effects. The results obtained by both the HF/MM and B3LYP/MM simulations obviously suggest a substantial change in the local structure of NO_3^- , being either planar or non-planar geometry with equivalent and/or inequivalent N-O bonds, according to the influence of water environment. A useful indicator of the NO_3^- planarity in aqueous solution is the distribution of the angle ϕ , defined by a vector along any N-O bond and a vector pointing outwards between the other two N-O bonds, as shown in Figure 3.19, which illustrates that the intramolecular geometry of NO_3^- is slightly deviating from planarity, obviously because water molecules in the first hydration shell of NO_3^- oxygens break the D_{3h} symmetry of the ion.

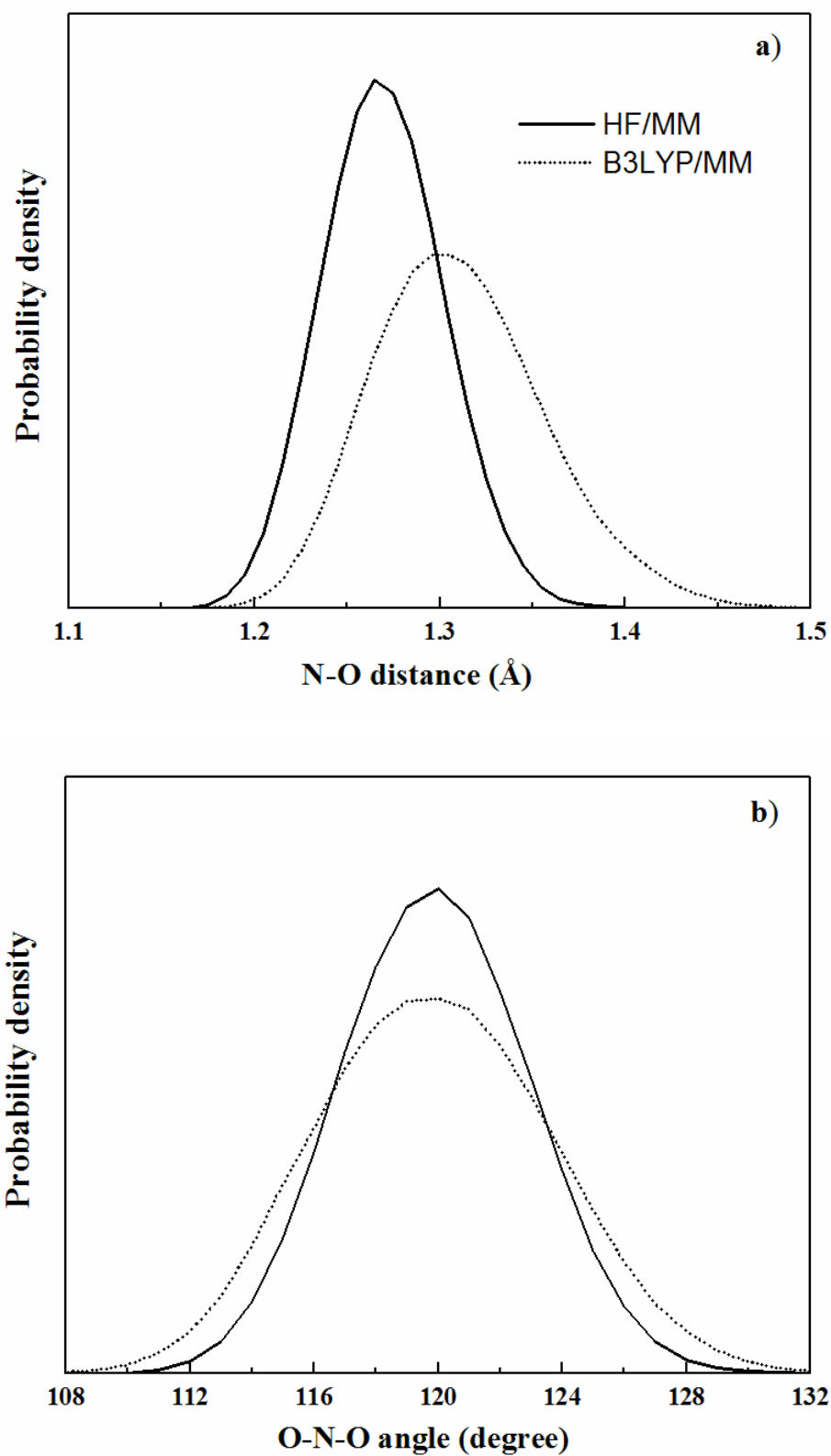


Figure 3.18 Distributions of a) N-O bond length and b) O-N-O angle of NO_3^- .

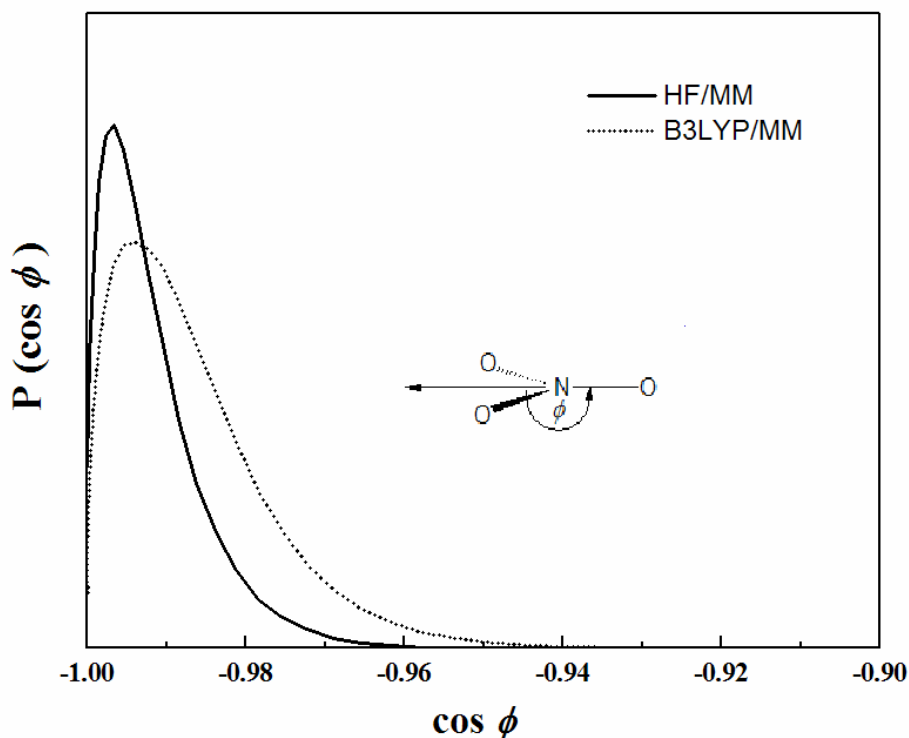


Figure 3.19 Distributions of ϕ , as defined by a vector along any N-O bond and a vector pointing outwards between the other two N-O bonds.

The power spectra, which correspond to symmetric stretching (ν_1), out-of-plane bending (ν_2), asymmetric stretching (ν_3) and asymmetric bending (ν_4) vibrations, of NO_3^- were evaluated using normal-coordinate analysis (Bopp, 1986). By Fourier transformations of three components of oxygen's velocity autocorrelation functions (VACFs), the corresponding ν_1 , ν_2 , ν_3 and ν_4 bands can be obtained, as summarized in Table 3.3. In this work, all calculated frequencies were multiplied by the standard scaling factors (Scott and Radom, 1996) of 0.9051 and 0.9614 for HF and B3LYP method, respectively. With respect to the spectral data in Table 3.3, both HF/MM and B3LYP/MM simulations produce all four vibrational modes, with spectral frequencies in the order $\nu_3 > \nu_1 > \nu_2 > \nu_4$. The B3LYP/MM simulation

produces the power spectra at lower frequencies than the HF/MM run. This corresponds to the observed higher flexibility of the NO_3^- structure (see Figures 3.18 and 3.19). In a qualitative sense, all frequencies obtained by both HF/MM and B3LYP/MM simulations are in reasonable agreement with the experimental data (Irish and Davis, 1968; Irish, Chang, and Nelson, 1970). In this context, it should be noted that most of the experimental measurements for spectral analysis on NO_3^- have to be performed with solutions of relatively high concentrations, whereas the present HF/MM and B3LYP/MM results refer to dilute solution.

Table 3.3 Vibrational frequencies of NO_3^- .

Method	Frequencies (cm^{-1})			
	ν_1	ν_2	ν_3	ν_4
HF/MM MD	1088	712	1401,1441	709
B3LYP/MM MD	965	710	1237,1313	649
Classical MD ^a	1009	814,833	1380,1393	704
Classical MD ^a	996	816	1379	689
MP4 (Gas phase) ^b	996	816	1379	689
B3LYP (Gas phase) ^b	1061	844	1364	707
Experiments ^{c,d}	1049	825	1348,1404	719
	-	-	1340,1460	720,740

Notes ^a taken from Ebner *et al.*, 1999. ^b taken from Ebner *et al.*, 1998. ^c taken from Irish and Davis, 1968. ^d taken from Irish *et al.*, 1970.

An interesting feature of the vibrational frequencies of NO_3^- is the experimentally observed ν_3 splitting in aqueous solutions. According to the experimental observations (Waterland and Kelley, 2000; Waterland *et al.*, 2001; Irish and Davis, 1968), the ν_3 asymmetric N-O stretching mode was found to consist of two distinctive peaks corresponding to the decrease of local symmetry of NO_3^- , *i.e.*, from D_{3h} to C_{2v} (or lower), due to its interaction with surrounding water molecules. In this work, the splitting of the ν_3 band is well reflected, being about 40 and 24 cm^{-1} for HF/MM and B3LYP/MM simulation, respectively. In addition, in both simulations, the ν_2 mode is less pronounced. This frequency mode is usually related to the change in the equilibrium geometry of NO_3^- from planar to pyramidal upon electronic excitation (Waterland and Kelley, 2000). In this context, the observed low intensity of ν_2 bands can be attributed to the fact that the structure of NO_3^- in aqueous solution is not too far from planarity (see Figure 3.19). This finding is in consistent with the lack of intensity of the out-of-plane deformation band in the resonance Raman spectrum of hydrated NO_3^- (Waterland and Kelley, 2000).

3.3.2 Intramolecular geometry and vibrations of water molecules in the hydration shell of NO_3^-

The intramolecular geometry of water molecules in the bulk and in the vicinity of NO_3^- is explained in terms of distributions of O-H bond length and H-O-H angle, as shown in Figures 3.20a and b, respectively. The B3LYP/MM simulation shows longer O-H bond lengths together with narrower H-O-H angles compared to the HF/MM results, with half-height widths of 0.98 ± 0.035 and 0.96 ± 0.03 Å for the distributions of O-H bonds, and of 103 ± 8 and $110 \pm 6.5^\circ$ for the distributions of H-O-H

angles, respectively. These differences can be a consequence of the higher coordination numbers resulting from the B3LYP/MM simulation, which will be discussed later.

With respect to the normal-coordinate analyses (Bopp, 1986), the three quantities, Q_1 , Q_2 and Q_3 , calculated from the VACFs of water's hydrogens for describing symmetric stretching and bending and asymmetric stretching motions, respectively, are reported in Table 3.4. To reliably describe the effect of NO_3^- on the vibrational motions of its surrounding water molecules, the corresponding data for pure water obtained from previous HF/MM (Tongraar and Rode, 2004) and B3LYP/MM (Xenides, Randolph, and Rode, 2005) simulations are given for comparison. In the HF/MM simulation, the bending and stretching frequencies of water molecules in the hydration shell of NO_3^- are slightly blue-shifted, by about 23, 3 and 15 cm^{-1} for Q_2 , Q_1 and Q_3 , respectively. The observed small changes in both the bending and stretching modes can be ascribed to a slight influence of NO_3^- on the vibrational motions of its surrounding water molecules. In the B3LYP/MM simulation, the corresponding Q_2 mode is blue-shifted by 15 cm^{-1} , while the Q_1 and Q_3 show significant red-shifts of 187 and 25 cm^{-1} , respectively. These data are in good accord with a generally more rigid structure of hydrated NO_3^- resulting from the DFT approach, which generally tends to exaggerate the strength of hydrogen bonds (Xenides *et al.*, 2005; Xenides, Randolph, and Rode, 2006).

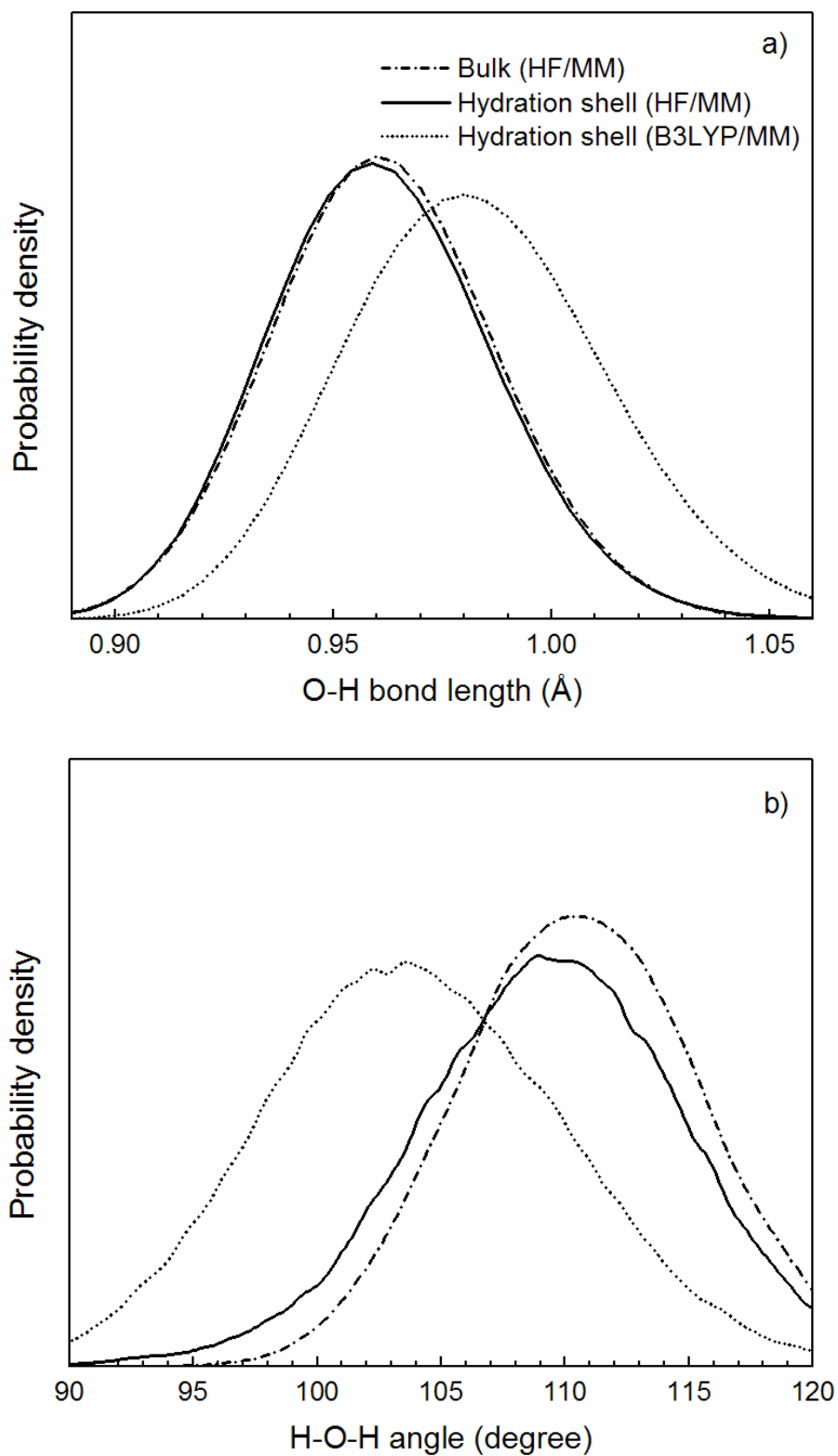


Figure 3.20 Distributions of a) O-H bond length and b) H-O-H angle of water molecules in the bulk and in the hydration shell of NO_3^- .

Table 3.4 Vibrational frequencies of water molecules in the bulk and in the hydration sphere of NO_3^- . Numbers in parentheses correspond to the data obtained by B3LYP/MM-based simulations.

Vibrations (cm^{-1})	Hydration shell of NO_3^-	Bulk *	H_2O (expt.) **
Q_2	1661 (1637)	1638 ^a , 1640 ^{b,c} (1622) ^c	1645 ^d , 1643 ^e
Q_1	3566 (3393)	3563 ^a , 3770 ^b , 3774 ^c (3580) ^c	3345 ^d ,
Q_3	3691 (3528)	3676 ^a , 3775 ^b , 3773 ^c (3553) ^c	3400 ^{e,f} 3445 ^d

Notes * values obtained from previous HF/MM and B3LYP/MM (i.e., numbers in parentheses) MD simulations of pure water using DZV (^a taken from Tongraar and Rode, 2004.) and DZP (^b taken from Xenides *et al.*, 2006 and ^c taken from Xenides *et al.*, 2005.) basis sets. ** experimental values of liquid water. ^d taken from Murphy and Berstein, 1972. ^e taken from Lock and Bakker, 2002. ^f taken from Deák *et al.*, 2000.

3.3.3 Translational motion and exchange process of water molecules in the hydration shell of NO_3^-

The self-diffusion coefficients (D) for water molecules in the bulk and in the hydration sphere of NO_3^- were calculated from the water's center-of-mass VACFs using the Green-Kubo relation (McQuarrie, 1976),

$$D = \frac{1}{3} \lim_{t \rightarrow \infty} \int_0^t C_v(t) dt . \quad (3.2)$$

All of the calculated D values are summarized in Table 3.5. In comparison to the data for bulk water obtained by a compatible QM/MM simulation (Tongraar and Rode, 2004), the D values obtained from the HF/MM and B3LYP/MM simulations clearly indicate a high mobility of water molecules in the vicinity of NO_3^- . This phenomenon is in consistent with the observed high flexibility of the NO_3^- -water complex, because of the weak ion-water interactions.

Table 3.5 Diffusion coefficients of water molecules in the bulk and in the hydration shell of NO_3^- .

Method	Hydration shell of NO_3^- ($\times 10^{-5} \text{ cm}^2 \text{ s}^{-1}$)	Bulk ($\times 10^{-5} \text{ cm}^2 \text{ s}^{-1}$)
HF/MM MD	5.09	3.31 ^a
B3LYP/MM MD	4.14	-
Experiment	-	2.30 ^b

Notes ^a taken from Tongraar and Rode, 2004. ^b taken from Woolf, 1975.

According to the N-O_w (Figure 3.11a) and the $\text{O}_N\text{-O}_w$ RDFs (Figure 3.11c), the non-zero first minimum of the RDFs obtained in both HF/MM and

B3LYP/MM simulations suggests an easy exchange of water molecules in the vicinity of NO_3^- . Numerous water exchange processes, following either associative (*A*) or dissociative (*D*) as well as associative (*I_a*) and dissociative (*I_d*) interchange mechanisms, were indeed observed when the $\text{O}_\text{N} \cdots \text{O}_\text{w}$ distances were plotted against simulation time for the HF/MM and B3LYP/MM simulations, as shown in Figures 3.20 and 3.21, respectively. The variability of water exchange process mechanisms observed can be considered as indication toward weak ion-water hydrogen bond interactions.

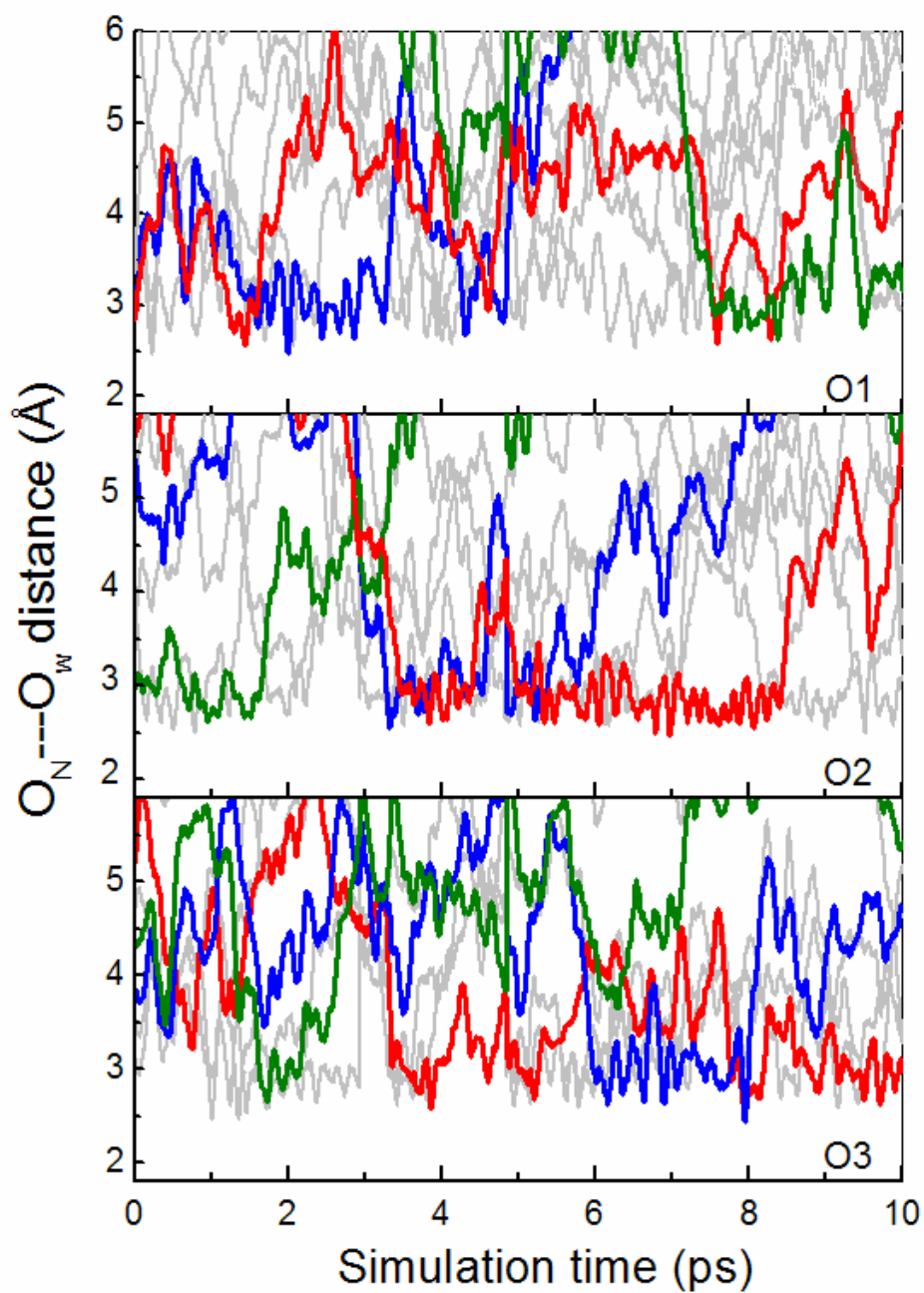


Figure 3.21 Time dependence of $O_N \cdots O_W$ distances, selecting only for the first 10 ps of the HF/MM simulation.

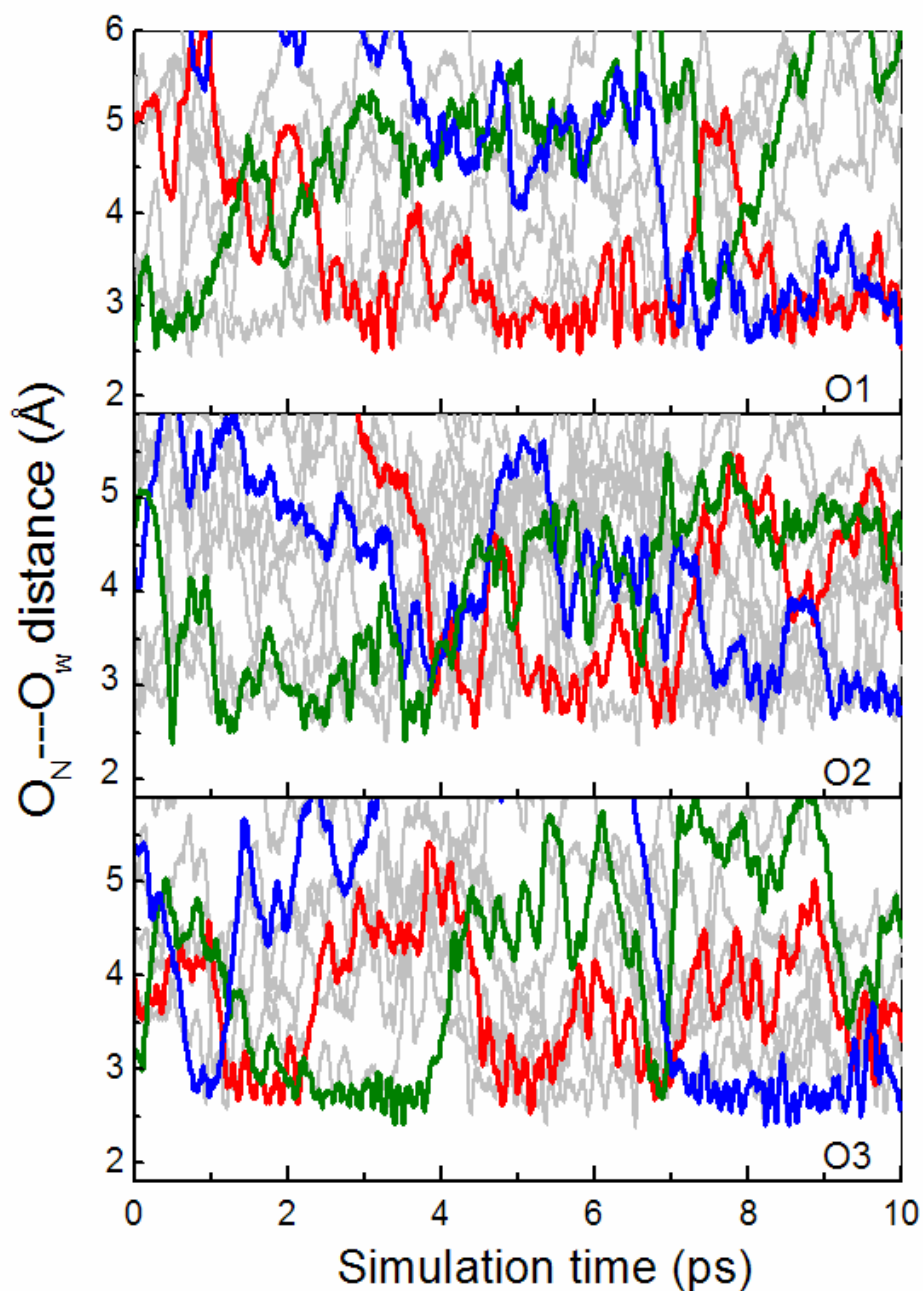


Figure 3.22 Time dependence of $O_N\text{---}O_w$ distances, selecting only for the first 10 ps of the B3LYP/MM simulation.

The rate of water exchange processes at each of the NO_3^- oxygens was evaluated via mean residence times (MRT) of the water molecules. In this work, the MRT data were calculated using the direct method (Hofer, Tran, Schwenk, and Rode,

2004), as the product of the average number of nearest-neighbor water molecules located within the $O_N\text{---}O_w$ distance of 3.5 Å with the duration of the simulation, divided by the number of exchange events, *i.e.*,

$$\tau = \frac{t_{sim} \times CN_{av}}{N_{ex}} . \quad (3.3)$$

Since the $O_N\text{---}O_w$ RDFs are less pronounced (see Figure 3.11c), the $O_N\text{---}O_w$ distance of 3.5 Å was selected, assuming to be a rough estimate of the first minimum of $O_N\text{---}O_w$ RDFs and a limit for a significantly stabilizing anion-water interaction. Applying this evaluation limit, significantly different coordination numbers result from HF and B3LYP framework: while the HF method predicts average coordination numbers of 3.74 to 3.78 for the oxygens, the same data for the B3LYP method are 4.75-4.99 (cf. Table 3.6). While all other data reported so far could be considered similar for both methods, these coordination numbers make a significant difference for the structure of the hydrated anion. Following the reported tendency of DFT methods to overestimate hydrogen bonding, the HF values are considered to be more reliable, but a better evaluation of this assumption appears only possible by a substantial increase of the QM diameter to a value including a second shell of water molecules, thus including also hydrogen bonding between ligands and bulk into the same quantum mechanical description. Such an evaluation will be performed, when the necessary computational facilities will be available.

Table 3.6 Mean residence time of water molecules in the bulk and in the vicinity of NO_3^- oxygens, calculated within the $\text{O}_\text{N} \cdots \text{O}_\text{w}$ distance of 3.5 Å.

Atom/solute	CN	t_{sim}	$t^* = 0.0$ ps		$t^* = 0.5$ ps	
			$N_{ex}^{0.0}$	$\tau_{H_2O}^{0.0}$	$N_{ex}^{0.5}$	$\tau_{H_2O}^{0.5}$
HF/MM MD						
O1	3.76	15.0	492	0.11	44	1.28
O2	3.74	15.0	464	0.12	39	1.44
O3	3.84	15.0	498	0.11	47	1.26
Pure H_2O^a	4.6	12.0	292	0.2	31	1.8
Pure H_2O^b	4.2	40.0	-	0.33	-	1.51
B3LYP/MM MD						
O1	4.77	17.0	554	0.15	52	1.56
O2	4.99	17.0	613	0.14	61	1.39
O3	4.75	17.0	562	0.14	59	1.37
Pure H_2O^b	4.2	30.0	-	1.07	-	7.84

Notes ^a taken from Tongraar and Rode, 2004. ^b taken from Xenides *et al.*, 2005.

With respect to time parameters t^* (*i.e.*, the minimum duration of a ligand's displacement from its original coordination shell to be accounted) of 0.0 and 0.5 ps, the calculated MRT values are summarized in Table 3.6. In general, the MRT data obtained using $t^* = 0.0$ ps are used for an estimation of hydrogen bond lifetimes, whereas the data obtained with $t^* = 0.5$ ps are considered as a good estimate for

sustainable ligand exchange processes (Hofer *et al.*, 2004). In this work, $\tau_{H_2O}(O_i) < \tau_{H_2O}(H_2O)$ results from both the HF/MM and B3LYP/MM simulations, without much differences in the values. However, as can be seen in Table 3.6, the previous B3LYP/MM simulation (Xenides *et al.*, 2005) of pure water had predicted much too slow exchange rates (while the HF values are close to the experimental values), proving the overestimation of hydrogen-bond strength by the B3LYP method. Hence, the anion-induced MRT differences obtained from the B3LYP/MM results are surely correct for the description, but most probably too high in the amount. All MRT values obtained in both simulations make it obvious, however, that water molecules binding to NO_3^- oxygens are quite labile and that the hydrogen bonds between NO_3^- and water are weak, thus enabling very frequent water exchange processes within the hydration sphere of NO_3^- . The observed differences between the MRT values of the NO_3^- oxygens are related to the solvation structure of NO_3^- . On the other hand, this also implies that the time of simulation may not be sufficient for a complete sampling of all possible structures at each of these oxygens. However, the variation width is small enough to assume reliability of the average value.

The MRT data are characteristic for a “structure-breaking” substance, and the ability of NO_3^- to act as structure-breaker in aqueous solution is also in accordance with all the previously reported data from our simulations.

CHAPTER IV

CONCLUSION

In this work, two combined QM/MM molecular dynamics simulations, namely HF/MM and B3LYP/MM, have been performed to investigate structural and dynamical properties of NO_3^- in aqueous solution. By the QM/MM approach, the first hydration shell of NO_3^- was treated quantum mechanically, while the rest of the system was described by means of classical pair potentials. Within the current computational facility, the HF and B3LYP methods together with the D95V+ basis set and the QM size with diameter of 8.8 Å employed in the present study have been considered as a suitable compromise between the quality of the simulation results and the requirement of CPU time. In addition, as a matter of fact that the performance of QM/MM MD simulations in conjunction with correlated *ab initio* methods is still too time-consuming, it was assumed that the effects of electron correlation would have small influence on the NO_3^- -water interactions, and thus negligible. On the other hand, it was postulated that the *ab initio* calculations at the HF and B3LYP levels using D95V+ basis set are accurate enough to produce reliable structural and dynamical details of the hydrated NO_3^- .

In terms of structural properties, the simulation results have shown a substantial influence of quantum mechanical forces for the structural description of this weakly interacting system. The detailed analysis on the RDFs clearly indicated a well-defined first hydration shell of NO_3^- , but the hydrogen-bond interactions between

NO_3^- and water are rather weak, in particular when compared to that of water hydrogen-bond network. For the geometrical arrangement of NO_3^- itself, both HF/MM and B3LYP/MM simulations predicted broad distributions of N-O distances and O-N-O angles, indicating that the structure of NO_3^- in aqueous solution is rather flexible. With respect to the observed high flexibility of NO_3^- , the calculated power spectra of the NO_3^- vibrations are in good accord with the experimentally observed solvent-induced symmetry breaking of this ion in aqueous solution. In addition, the “structure-breaking” behavior of NO_3^- is well reflected by the observed shifts in the corresponding bending and stretching frequencies as well as the mean residence time of water molecules surrounding the ion.

Finally, a remark should be made with respect to the QM/MM results obtained in this study. Comparing the HF and B3LYP methods for the QM part of the system, most of the structural and dynamical data appear rather similar at a first glance, but coordination numbers and dynamical data finally indicate a certain superiority of the *ab initio* HF formalism. Possible weaknesses of the B3LYP scheme could be attributed to the incompleteness of the kinetic energy term, the self-interaction error and the parameterization of the B3LYP method which did not contain any H-bonded system. When better computational facilities allow, a further improvement of the quantitative values can be expected from extending the size of the QM region as well as from using *ab initio* correlated methods.

REFERENCES

REFERENCES

- Adams, D. J., Adams, E. H., and Hill, G. J. (1979). The computer simulation of polar liquids. **Molecular Physics** 38: 387-400.
- Aker, P. M., Zhang, J. X., and Nichols, W. (1999). Nitrate ion detection in aerosols using morphology-dependent stimulated Raman scattering. **The Journal of Chemical Physics** 110: 2202-2207.
- Åqvist, J., and Warshel, A. (1993). Simulation of enzyme reactions using valence bond force fields and other hybrid quantum/classical approaches. **Chemical Reviews** 93: 2523-2544.
- Armunanto, R., Schwenk, C. F., Randolph, B. R., and Rode, B. M. (2004). Structure and dynamics of Co^{2+} in liquid ammonia: *Ab initio* QM/MM molecular dynamics simulation. **Chemical Physics** 305: 135-140.
- Armunanto, R., Schwenk, C. F., and Rode, B. M. (2003). Structure and dynamics of hydrated Ag(I) : *Ab initio* quantum mechanical-molecular mechanical molecular dynamics simulation. **The Journal of Physical Chemistry A** 107: 3132-3138.
- Armunanto, R., Schwenk, C. F., and Rode, B. M. (2004). Gold(I) in liquid ammonia: *Ab initio* QM/MM molecular dynamics simulation. **Journal of the American Chemical Society** 126: 9934-9935.

- Armunanto, R., Schwenk, C. F., Setiaji, A. H. B., and Rode, B. M. (2003). Classical and QM/MM molecular dynamics simulations of Co^{2+} in water. **Chemical Physics** 295: 63-70.
- Bartlett, R. J. (1989). Coupled-cluster approach to molecular structure and spectra: A step toward predictive quantum chemistry.
- Bauschlicher, C. W., Langhoff, S. R., and Taylor, P. R. (1990). Accurate quantum chemical calculations. **Advances in Chemical Physics** 77: 103-161.
- Becke, A. D. (1993). Density-functional thermochemistry. . The role of exact exchange. **The Journal of Chemical Physics** 98: 5648-5652.
- Berendren, H., Postma, J., van Gunsteren, W., and Hermans, J. (1981). Interaction models for water in relation to proteins hydration. In B. Pullman (ed.). **Intermolecular forces** (pp. 311-342). Reidel: Dordrecht.
- Bernardi, F., Olivucci, M., and Robb, M. A. (1992). Simulation of MC-SCF results on covalent organic multi-bond reactions: Molecular mechanics with valence bond (MM-VB). **Journal of the American Chemical Society** 114: 1606-1616.
- Bopp, P. (1986). A study of the vibrational motions of water in an aqueous CaCl_2 solution. **Chemical Physics** 106: 205-212.
- Bopp, P., Jancsó, G., and Heinzinger, K. (1983). An improved potential for non-rigid water molecules in the liquid phase. **Chemical Physics Letters** 98: 129-133.
- Born, M., and Oppenheimer, R. (1927). Quantum theory of the molecules. **Annalen der Physik** 84: 457-484.

- Boys, S. F. (1950). Electronic wavefunctions. I. A general method of calculation for stationary states of any molecular system. **Proceedings of the Royal Society of London Series A** 200: 542-554.
- Brooks, B. R., Bruccoleri, R. E., Olafson, B. D., States, D. J., Swaminathan, S., and Karplus, M. (1983). CHARMM: A program for macromolecular energy, minimization and dynamics calculations. **Journal of Computational Chemistry** 4: 187-217.
- Burke., C. A. E., Adya, A. K., and Neilson, G. W. (1991). A structural study of the aqua-anions NO_3^- , BrO_3^- , ClO_3^- by difference methods of X-ray diffraction. **Journal Physics: Condensed Matter** 3: 837-850.
- Caminiti, R., Licheri, G., Paschina, G., Piccaluga, G., and Pinna, G. (1980). Interactions and structure in aqueous NaNO_3 solutions. **The Journal of Chemical Physics** 72: 4522-4528.
- Car, R., and Parrinello, M. (1985). Unified approach for molecular dynamics and density-functional theory. **Physical Review Letters** 55: 2471-2474.
- Carravetta, V., and Clementi, E. (1984). Water-water interaction potential: An approximation of the electron correlation contribution by a functional of the SCF density matrix. **The Journal of Chemical Physics** 81: 2646-2651.
- Collins, J. B., Schleyer, P. v. R., Stephen Binkley, J., and Pople, J. A. (1976). Self-consistent molecular orbital methods. XVII. Geometries and binding energies of second-row molecules. A comparison of three basis sets. **The Journal of Chemical Physics** 64: 5142-5151.

- Cummins, P. L., and Gready, J. E. (1997). Coupled semiempirical molecular orbital and molecular mechanics model (QM/MM) for organic molecules in aqueous solution. **Journal of Computational Chemistry** 18: 1496-1512.
- Deák, J. C., Rhea, S. T., Iwaki, L. K., and Dlott, D. D. (2000). Vibrational energy relaxation and spectral diffusion in liquid water and deuterated water. **The Journal Physical Chemistry** 104: 4866-4875.
- Dolg, M., Stoll, H., Preuss, H., and Pitzer, R. M. (1993). Relativistic and correlation effects for element 105 (hahnium, Ha): a comparative study of M and MO (M = Nb, Ta, Ha) using energy-adjusted *ab initio* pseudopotentials. **The Journal of Physical Chemistry** 97: 5852-5859.
- Dunning, T. H. (1989). Gaussian basis sets for use in correlated molecular calculations. I. The atoms boron through neon and hydrogen. **The Journal of Chemical Physics** 90: 1007-1023.
- Dunning, T. H., Jr., and Hay, P. J. (1976). In H.F. Schaefer (ed.). **Modern theoretical chemistry**. New York: Plenum Press.
- Earras-Hanauer, H., Clark, T., and van Eldik, R. (2003). Molecular orbital and DFT studies on water exchange mechanisms of metal ions. **Coordination Chemistry Reviews** 233: 238-239.
- Ebner, C., Sansone, R., Hengrasmee, S., and Probst, M. (1999). Molecular dynamics study of an aqueous potassium nitrate solution. **International Journal of Quantum Chemistry** 75: 805-814.
- Ebner, C., Sansone, R., and Probst, M. (1998). Quantum chemical study of the interaction of nitrate anion with water. **International Journal of Quantum Chemistry** 70: 877-886.

- Elrod, M. J., and Saykally, R. J. (1994). Many-body effects in intermolecular forces. **Chemical Reviews** 94: 1975-1997.
- Ferguson, E. E., Fehsenfeld, F. C., and Albritton, D. L. (1979). In M.T. Bowers (ed.). **Gas phase ion chemistry**. New York: Academic Press.
- Field, M. J., Bash, P. A., and Karplus, M. (1990). A combined quantum mechanical and molecular mechanical potential for molecular dynamics simulations. **Journal of Computational Chemistry** 11: 700-733.
- Frank, H. (1956). **Chemical physics of ionic solutions**. New York: John Wiley & Sons.
- Foulkes, W. MC., and Haydock, R. (1989). Tight-binding models and density-functional theory. **Physical Review B** 39: 12520-12536.
- Gao, J. (1996). Methods and applications of combined quantum mechanical and molecular mechanical potentials. **Reviews in Computational Chemistry** 7: 119-185.
- Guilbaud, P., and Wipff, G. (1993). Hydration of UO_2^{2+} cation and its NO_3^- and 18-crown-6 adducts studied by molecular dynamics simulations. **The Journal Physical Chemistry** 97: 5685-5692.
- Hannongbua, S. (1997). The role of nonadditive effects in the first solvation shell of Na^+ and Mg^{2+} in liquid ammonia: Monte Carlo studies including three-body corrections. **The Journal of Chemical Physics** 106: 6076-6081.
- Hehre, W. J., Stewart, R. F., and Pople, J. A. (1969). Self-consistent molecular-orbital methods. I. Use of gaussian expansions of slater-type atomic orbitals. **The Journal of Chemical Physics** 51: 2657-2664.

- Heyes, D. M. (1981). Electrostatic potentials and fields in infinite point charge lattices. **The Journal of Chemical Physics** 74: 1924-1929.
- Hille, B. (1992). **Ionic channels of excitable membranes** (2nd ed.). Sunderland, MA: Sinauer.
- Hofer, T. S., Tran, H. T., Schwenk, C. F., and Rode, B. M. (2004). Characterization of dynamics and reactivities of solvated ions by *ab initio* simulations. **Journal of Computational Chemistry** 25: 211-217.
- Hohenberg, P., and Kohn, W. (1964). Inhomogeneous electron gas. **Physical Review** 136: B864-B871.
- Howell, J. M., Sapse, A. M., Singman, E., and Synder, G. (1982). *Ab initio* self-consistent field calculations of $\text{NO}_2^-(\text{H}_2\text{O})_n$ and $\text{NO}_3^-(\text{H}_2\text{O})_n$ clusters. **The Journal of Physical Chemistry** 86: 2345-2349.
- Hser, M., and Ahlrichs, R. (1989). Improvements of the direct SCF method. **Journal of Computational Chemistry** 10: 104-111.
- Ikushima, Y., Saito, N., and Arai, M. (1998). Raman spectral studies of aqueous zinc nitrate solution at high temperatures and at a high pressure of 30 MPa. **The Journal of Physical Chemistry B** 102: 3029-3035.
- Inada, Y., Loeffler, H. H., and Rode, B. M. (2002). Librational, vibrational and exchange motions of water molecules in aqueous Ni(II) solution: Classical and QM/MM molecular dynamics simulations. **Chemical Physics Letters** 358: 449-458.
- Intharathep, P., Tongraar, A., and Sagarik, K. (2005). Structure and dynamics of hydrated NH_4^+ : An *ab initio* QM/MM molecular dynamics simulation. **Journal of Computational Chemistry** 26: 1329-1338.

- Irish, D., Chang, G., and Nelson, D. (1970). Cation-nitrate ion contact in aqueous solutions. **Inorganic Chemistry** 9: 425-426.
- Irish, D., and Davis, A. (1968). Interactions in aqueous alkali metal nitrate solutions. **Canadian Journal of Chemistry** 46: 943-951.
- Jakobsen, H.J., Bildsøe, H., Skibsted, J., and Giavani, T. (2001). ^{14}N MAS NMR spectroscopy: The nitrate ion. **Journal of the American Chemical Society** 123: 5098-5099.
- Jones, R. O., and Gunnarsson, O. (1989). The density functional formalism, its applications and prospects. **Reviews of Modern Physics** 61: 689-746.
- Kahn, L. R., Baybutt, P., and Truhlar, D. G. (1976). *Ab initio* effective core potentials: Reduction of all-electron molecular structure calculations to calculations involving only valence electrons. **The Journal of Chemical Physics** 65: 3826-3853.
- Kapinus, E. N., Revelsky, I. A., Ulogov, V. O., and Lyalikov, Y. A. (2004). Simultaneous determination of fluoride, chloride, nitrite, bromide, nitrate, phosphate and sulfate in aqueous solutions at 10^{-9} to 10^{-8} % level by ion chromatography. **Journal Chromatography B** 800: 321-323.
- Kataoka, Y. (1993). Bulletin of the Chemical Society of Japan 66: 2478 Quoted in Ebner, C., Sansone, R., Hengrasmee, S., and Probst, M. (1999). Molecular dynamics study of an aqueous potassium nitrate solution. **International Journal of Quantum Chemistry** 75: 805-814.
- Kato, T., Machida, K., Oobatake, M., and Hayashi, S. (1988). Ionic dynamics in computer simulated molten LiNO_3 . II. Tumbling and spinning motions of nitrate ions. **The Journal of Chemical Physics** 89: 7471-7477.

- Kato, T., Machida, K., Oobatake, M., and Hayashi, S. (1990). Vibrational dephasing in computer simulated molten LiNO_3 . **The Journal of Chemical Physics** 93: 3970-3977.
- Kato, T., Hayashi, S., Oobatake, M., and Machida, K. (1993). Cation dependence of the ionic dynamics in computer simulated molten nitrates. **The Journal of Chemical Physics** 99: 3966-3975.
- Kendall, R. A., Dunning, T. H., and Harrison, R. J. (1992). Electron affinities of the first-row atoms revisited. Systematic basis sets and wave functions. **The Journal of Chemical Physics** 96: 6796-6806.
- Kerdcharoen, T., Liedl, K. R., and Rode, B. M. (1996). A QM/MM simulation method applied to the solution of Li^+ in liquid ammonia. **Chemical Physics** 211: 313-323.
- Kistenmacher, H., Popkie, H., and Clementi, E. (1974). Study of the structure of molecular complexes. VIII. Small clusters of water molecules surrounding Li^+ , Na^+ , K^+ , F^- and Cl^- ions. **The Journal of Chemical Physics** 61: 799-815.
- Kritayakornpong, C., Plankensteiner, K., and Rode, B. M. (2003). Dynamics in the hydration shell of Hg^{2+} ion: Classical and *ab initio* QM/MM molecular dynamics simulations. **Chemical Physics Letters** 371: 438-444.
- Laaksonen, A., and Kovacs, H. (1994). Canadian Journal Chemistry 72: 2278 Quoted in Ebner, C., Sansone, R., Hengrasmee, S., and Probst, M. (1999). Molecular dynamics study of an aqueous potassium nitrate solution. **International Journal of Quantum Chemistry** 75: 805-814.

- Lebrero, M. C. G., Bikiel, D. E., Elola, M. D., and Estrin, D. A. (2002). Solvent-induced symmetry breaking of nitrate ion in aqueous clusters: A quantum-classical simulation study. **The Journal of Chemical Physics** 117: 2718-2725.
- Lee, S. H., and Rasaiah, J. C. (1996). Molecular dynamics simulation of ion mobility. 2. Alkali metal and halide ions using the SCP/E model for water at 25 °C. **The Journal of Physical Chemistry** 100: 1420-1425.
- Lee, C., Yang, W., Parr, R. G. (1988). Development of the Colle-Salvetti correlation-energy formula into a functional of the electron density. **Physic Review B** 37: 785. Levine, I. N. (2000). **Quantum chemistry**. (5th ed.). New York: Prentice-Hall, Inc.
- Lie, G. C., and Clementi, E. (1986). Molecular-dynamics simulation of liquid water with an *ab initio* flexible water-water interaction potential. **Physical Review A** 33: 2679-2693.
- Lock, A. J., Bakker, H. J. (2002). Temperature dependence of vibrational relaxation in liquid H₂O. **The Journal of Chemical Physics** 117: 1708-1722.
- Loeffler, H. H., Yagüe, J. I., and Rode, B. M. (2002). QM/MM-MD simulation of hydrated vanadium(II) ion. **Chemical Physics Letters** 363: 367-371.
- Loeffler, H. H., Yagüe, J. I., and Rode, B. M. (2002). Many-body effects in combined quantum mechanical/molecular mechanical simulations of the hydrated manganous ion. **The Journal of Physical Chemistry A** 106: 9529-9532.

- Martínez, J. M., Hernández-Cobos, J., Saint-Martin, H., Pappalardo, R. R., Ortega-Blake, I., and Marcos, E. S. (1994). Coupling a polarizable water model to the hydrated ion–water interaction potential: A test on the Cr^{3+} hydration. **The Journal of Chemical Physics** 112: 2339-2347.
- McQuarrie, D. A. (1976). **Statistical mechanics**. Harper Row: New York.
- Mezei, M., and Beveridge, D. L. (1981). Monte Carlo studies of the structure of dilute aqueous solutions of Li^+ , Na^+ , K^+ , F^- and Cl^- . **The Journal of Chemical Physics** 74: 6902-6910.
- Møller, C., and Plesset, M. S. (1934). Note on an approximation treatment for many-electron systems. **Physical Review** 46: 618-622.
- Muller, R. P., and Warshel, A. (1995). *Ab initio* calculations of free energy barriers for chemical reactions in solution. **The Journal of Physical Chemistry** 99: 17516-17524.
- Murphy, W. F., and Bernstein, H. J. (1972). Raman spectra and an assignment of the vibrational stretching region of water. **The Journal Physical Chemistry** 76: 1147-1152.
- Murphy, R. B., Philipp, D. M., and Friesner, R. A. (2000). Frozen orbital QM/MM methods for density functional theory. **Chemical Physics Letters** 321: 113-120.
- Nakahara, M., and Emi, K. (1993). Effect of dielectric friction on the perpendicular reorientation of the nitrate ion in water and organic solvents. **The Journal of Chemical Physics** 99: 5418-5425.

- Nicholas, A. M. de. P., and Wasylishen, R. E. (1985). Rotations of the nitrate and carbonate anions in aqueous solution by NMR spectroscopy. **The Journal of Physical Chemistry** 89: 5446-5450.
- Obst, S., and Bradaczek, H. (1996). Molecular dynamics study of the structure and dynamics of hydration shell of alkaline and alkaline-earth metal cations. **The Journal of Physical Chemistry** 100: 15677-15687.
- Ohtaki, H., and Radnai, T. (1993). Structure and dynamics of hydrated ions. **Chemical Reviews** 93: 1157-1204.
- Onsager, L. (1936). Electric moments of molecules in liquids. **Journal of the American Chemical Society** 58: 1486-1493.
- Probst, M. M., Spohr, E., Heinzinger, K., and Bopp, P. (1991). A molecular dynamics simulation of an aqueous beryllium chloride solution. **Molecular Simulation** 7: 43-57.
- Pauli, W. (1925). On the Connexion between the completion of electron groups in an atom with the complex structure of spectra. **Zeitschrift fur Physik** 31: 765-783.
- Remsungnern, T., and Rode, B. M. (2003). Dynamical properties of the water molecules in the hydration shells of Fe(II) and Fe(III) ions: *Ab initio* QM/MM molecular dynamics simulations. **Chemical Physics Letters** 367: 586-592.
- Remsungnern, T., and Rode, B. M. (2004). Molecular dynamics simulation of the hydration of transition metal ions: The role of non-additive effects in the hydration shells of Fe²⁺ and Fe³⁺ ions. **Chemical Physics Letters** 385: 491-497.

- Robinson, R.A., and Stokes, R.H. (1959). **Electrolyte solutions** (2nd ed.). London: Butter-worth.
- Rode, B.M., and Hofer, T.S. (2006). How to access structure and dynamics of solutions: The capabilities of computational methods. **Pure & Applied Chemistry** 78: 525-539.
- Rode, B. M., Schwenk, C. F., and Tongraar, A. (2004). Structure and dynamics of hydrated ions-new insights through quantum mechanical simulations. **Journal of Molecule Liquids** 110: 105-122.
- Rode, B. M., Schwenk, C.F., Hofer, T. S., and Randolf, B. R. (2005). Coordination and ligand exchange dynamics of solvated metal ions. **Coordination Chemistry Reviews** 249: 2993-3006.
- Rode, B. M., Hofer, T. S., Randolf, B. R., Schwenk, C. F., Xenides, D., and Vchirawongkwin, V. (2005). Quantum mechanical/molecular mechanical simulations of the Ti (III) ion in water. **Theoretical Chemistry Accounts** 249: 2993.
- Rosi, B., and Fontana, M.P. (1987). Molecular reorientations and local structure in nitrate aqueous solutions. **The Journal of Chemical Physics** 87: 6406-6415.
- Salvador, P., Curtis, J. E., Tobias, D. J., and Jungwirth, P. (2003). Polarizability of the nitrate anion and its solvation at the air/water interface. **Physical Chemistry Chemical Physics** 5: 3752-3757.
- Schrödinger, E. (1926). Quantisierung als Eigenwertproblem, **Annalen der Physik** 79: 361-376.

- Schwenk, C. F., Loeffler, H. H., and Rode, B. M. (2001). Molecular dynamics simulations of Ca^{2+} in water: Comparison of a classical simulation including three-body corrections and Born-Oppenheimer *ab initio* and density functional theory quantum mechanical/molecular mechanics simulations. **The Journal of Chemical Physics** 115: 10808-10813.
- Schwenk, C. F., Loeffler, H. H., and Rode, B. M. (2003). Structure and dynamics of metal ions in solution: QM/MM molecular dynamics simulations of Mn^{2+} and V^{2+} . **Journal of the American Chemical Society** 125: 1618-1624.
- Scott, A. P., and Random, L. J. (1996). Harmonic vibrational frequencies: An evaluation of Hartree-Fock, Møller-Plesset, Quadratic Configuration Interaction, Density Functional Theory and Semiempirical Scale Factors. **The Journal Physical Chemistry** 100: 16502-16513.
- Shen, M., Xie, Y., Deakyne, C. A., and Schaefer, H. F. (1990). Hydrogen bonding between the nitrate anion (conventional and peroxy forms) and the water molecule. **The Journal of Chemical Physics** 93: 3379-3388.
- Singh, U. C., and Kollman, P. A. (1986). A combined *ab initio* quantum mechanical and molecular mechanical method for carrying out simulations on complex molecular system: Applications to the $\text{CH}_3\text{Cl}+\text{Cl}^-$ exchange reaction and gas phase protonation of polyethers. **Journal of Computational Chemistry** 7: 718-730.
- Skipper, N. T., and Neilson, G. W. (1989). X-ray and neutron diffraction studies on concentrated aqueous solutions of sodium nitrate and silver nitrate. **Journal Physics: Condensed Matter** 1: 4141-4154.
- Slater, J. C. (1929). The theory of complex spectra, **Physical Review** 34: 1293-1322.

- Slater, J. C. (1930). Atomic shielding constants. **Physical Review** 36: 57-64.
- Stanton, R. V., Hartsough, D. S., and Merz, K. M., Jr. (1995). An examination of a density functional/molecular mechanical coupled potential. **Journal of Computational Chemistry** 16: 113-128.
- Stephens, P. J., Devlin, F. J., Chabalowski, C. F., and Frisch, M. J. (1994). *Ab initio* calculation of vibrational absorption and circular dichroism spectra using density functional force fields. **The Journal of Chemical Physics** 98: 11623-11627.
- Stillinger, F. H., and Rahman, A. (1978). Revised central force potentials for water. **The Journal of Chemical Physics** 68: 666-670.
- Texler, N. R., Holdway, S., Neilson, G. W., and Rode, B. M. (1998). Monte Carlo simulations and neutron diffraction studies of the peptide forming system 0.5 mol kg⁻¹ CuCl₂ -5 mol kg⁻¹ NaCl-H₂O at 293 and 353 K. **Journal of Chemical Society, Faraday Transaction** 94: 59-65.
- Texler, N. R., and Rode, B. M. (1997). Monte Carlo simulations of copper chloride solutions at various concentrations including full 3-body correction terms. **Chemical Physics** 222: 281-288.
- Tomasi, J., and Persico, M. (1994). Molecular interactions in solution: An overview of methods based on continuous distributions of the solvent. **Chemical Reviews** 94: 2027-2094.
- Tongraar, A. (1998). *Ab initio* QM/MM dynamics simulations of cations in aqueous solution. Ph. D. Thesis, Innsbruck University, Innsbruck, Austria.

- Tongraar, A., Hannongbua, S., and Rode, B. M. (1997). Molecular dynamics simulations of a potassium ion and iodide ion in liquid ammonia. **Chemical Physics** 219: 279-290.
- Tongraar, A., Liedl, K. R., and Rode, B. M. (1997). Solvation of Ca^{2+} in water studied by Born-Oppenheimer *ab initio* QM/MM dynamics. **The Journal of Physical Chemistry A** 101: 6299-6309.
- Tongraar, A., Liedl, K. R., and Rode, B.M. (1998). Born-Oppenheimer *ab initio* QM/MM dynamics simulations of Na^+ and K^+ in water: From structure making to structure breaking effects. **The Journal of Physical Chemistry A** 102: 10340-10347.
- Tongraar, A., Liedl, K. R., and Rode, B. M. (1998). The hydration shell structure of Li^+ investigated by Born-Oppenheimer *ab initio* QM/MM dynamics. **Chemical Physics Letters** 286: 56-64.
- Tongraar, A., and Rode, B. M. (1999). Preferential solvation of Li^+ in 18.45 % aqueous ammonia: A Born-Oppenheimer *ab initio* quantum mechanics/molecular mechanics MD simulation. **The Journal of Physical Chemistry A** 103: 8524-8527.
- Tongraar, A., and Rode, B. M. (2001). A Born-Oppenheimer *ab initio* quantum mechanical/molecular mechanical molecular dynamics simulation on preferential solvation of Na^+ in aqueous ammonia solution. **The Journal of Physical Chemistry A** 105: 506-510.

- Tongraar, A., and Rode, B. M. (2001). The role of non-additive contributions on the hydration shell structure of Mg^{2+} studied by Born-Oppenheimer *ab initio* quantum mechanical/molecular mechanical molecular dynamics simulation. **Chemical Physics Letters** 346: 485-491.
- Tongraar, A., and Rode, B. M. (2003). The hydration structures of F^- and Cl^- investigated by *ab initio* QM/MM molecular dynamics simulations. **Physical Chemistry Chemical Physics** 5: 357-362.
- Tongraar, A., and Rode, B. M. (2004). *Ab initio* QM/MM molecular dynamics simulation of preferential K^+ solvation in aqueous ammonia solution. **Physical Chemistry Chemical Physics** 6: 411-416.
- Tongraar, A., and Rode, B. M. (2004). Dynamical properties of water molecules in the hydration shells of Na^+ and K^+ : *Ab initio* QM/MM molecular dynamics simulations. **Chemical Physics Letters** 385: 378-383.
- Tongraar, A., and Rode, B. M. (2005). *Ab initio* QM/MM dynamics of anion-water hydrogen bonds in aqueous solution. **Chemical Physics Letters** 403: 314-319.
- Tongraar, A., and Rode, B. M. (2005). Structural arrangement and dynamics of the hydrated Mg^{2+} : An *ab initio* QM/MM molecular dynamics simulation. **Chemical Physics Letters** 409: 304-309.
- Tongraar, A., Sagarik, K., and Rode, B. M. (2001). Effects of many-body interactions on the preferential solvation of Mg^{2+} in aqueous ammonia solution: A Born-Oppenheimer *ab initio* QM/MM dynamics study. **The Journal of Physical Chemistry B** 105: 10559-10564.

- Tongraar, A., Sagarik, K., and Rode, B. M. (2002). Preferential solvation of Ca^{2+} in aqueous ammonia solution: Classical and combined *ab initio* quantum mechanical/molecular mechanical molecular dynamics simulations. **Physical Chemistry Chemical Physics** 4: 628-634.
- Wang, X. B., Yang, X., Wang, L. S., and Nicholas, J. B. (2002). Photodetachment and theoretical study of free and water-solvated nitrate anions, $\text{NO}_3^-(\text{H}_2\text{O})_n$ ($n=0-6$). **The Journal of Chemical Physics** 116: 561-570.
- Waterland, M. R., and Kelley, A. M. (2000). Far-ultraviolet resonance Raman spectroscopy of nitrate ion in solution. **The Journal of Chemical Physics** 113: 6760-6773.
- Waterland, M. R., Stockwell, D., and Kelley, A. M. (2001). Symmetry breaking effects in NO_3^- : Raman spectra of nitrate salts and *ab initio* resonance Raman spectra of nitrate-water complexes. **The Journal of Chemical Physics** 114: 6249-6258.
- William, R. J. P. (1971). In R. F. Gould (ed.). **Bio-inorganic chemistry**. Washington, DC: American Chemical Society.
- Woolf, L. A. (1975). **Journal of the Chemical Society Faraday Transactions** 71: 784.
- Woon, D. E., and Dunning, T. H., Jr. (1993). Gaussian basis sets for use in correlated molecular calculations. III. The atoms aluminum through argon. **The Journal of Chemical Physics** 98: 1358-1371.
- Xenides, D., Randolf, B.R., and Rode, B.M. (2005). Structure and ultrafast dynamics of liquid water. **The Journal of Chemical Physics** 122: 174506.

Xenides, D., Randolf, B. R., and Rode, B. M. (2006). Hydrogen bonding in liquid water: An *ab initio* QM/MM MD simulation study. **Journal of Molecular Liquids** 123: 61-67.

Yagüe, J. I., Mohammed, A. M., Loeffler, H., and Rode, B. M. (2001). Classical and mixed quantum mechanical/molecular mechanical simulation of hydrated manganous ion. **The Journal of Physical Chemistry A** 105: 7646-7650.

APPENDIX

APPENDIX A

PUBLICATION

A Combined QM/MM Molecular Dynamics Simulations Study of Nitrate Anion (NO_3^-) in Aqueous Solution

Anan Tongraar,^{*,†} Piyawan Tangkawanwanit,[†] and Bernd Michael Rode[‡]

School of Chemistry, Institute of Science, Suranaree University of Technology, Nakhon Ratchasima 30000, Thailand, and Department of Theoretical Chemistry, Institute of General, Inorganic and Theoretical Chemistry, University of Innsbruck, Innrain 52a, A-6020 Innsbruck, Austria

Received: July 26, 2006; In Final Form: September 22, 2006

The structural and dynamical properties of NO_3^- in dilute aqueous solution have been investigated by means of two combined quantum mechanics/molecular mechanics (QM/MM) molecular dynamics simulations, namely HF/MM and B3LYP/MM, in which the ion and its surrounding water molecules were treated at HF and B3LYP levels of accuracy, respectively, using the DZV+ basis set. On the basis of both HF and B3LYP methods, a well-defined first hydration shell of NO_3^- is obtainable, but the shell is quite flexible and the hydrogen-bond interactions between NO_3^- and water are rather weak. With respect to the detailed analysis of the geometrical arrangement and vibrations of NO_3^- , the experimentally observed solvent-induced symmetry breaking of the ion is well reflected. In addition, the dynamical information, i.e., the bond distortions and shifts in the corresponding bending and stretching frequencies as well as the mean residence time of water molecules surrounding the NO_3^- ion, clearly indicates the “structure-breaking” ability of this ion in aqueous solution. From a methodical point of view it seems that both the HF and B3LYP methods are not too different in describing this hydrated ion by means of a QM/MM simulation. However, the detailed analysis of the dynamics properties indicates a better suitability of the HF method compared to the B3LYP-DFT approach.

1. Introduction

Due to the key role ions play in many chemical and biological processes,^{1,2} a number of experimental and theoretical studies have been carried out to obtain detailed knowledge about ions in aqueous electrolyte solutions.^{3–5} Considering the structural feature of ions solvated in aqueous solution, cations usually have simple solvation geometries due to their relatively large binding energies between the cation and water. Unlike cations, anion solvation is more complicated since most of the anion–water interactions are generally weaker than those of cations and energetically comparable with the water–water interactions. As a consequence, a delicate balance between anion–water and water–water interactions is crucial in determining bulk vs surface solvation, i.e., structures with the anion on the “surface” of water clusters.

Nitrate anion (NO_3^-) is one of the important ions in solution chemistry and biology, which is frequently encountered as a terminal anion in the series of reactions involving nitrogen.⁶ In the gas phase, the isolated NO_3^- ion is nominally planar and has D_{3h} symmetry. In polar solvents, however, its D_{3h} symmetry is expected to be broken by the influence of solvent environment. These effects have already been explored via resonance Raman spectroscopy studies.^{7,8} Recently, the Raman spectra of aqueous solutions of $\text{Mg}(\text{NO}_3)_2$ have been reported,⁹ providing a detailed picture of the NO_3^- ion in different salt concentrations. In aqueous solution, the hydration shell structure of NO_3^- has been studied both by experiments and computer simulations. Experimental studies, in particular neutron and X-ray diffrac-

tions,^{3,10,11} have reported a wide variety of coordination numbers, ranging from about 2 to 18. The observed large discrepancy has been attributed to the interference of counterions. In conjunction with experiments, computer simulations of aqueous solutions containing NO_3^- have provided structural and dynamical details of this solvated ion at molecular level.^{9,12–17} However, most of the early simulation works had relied on classical molecular mechanical models. It has been demonstrated that the hydration shell structure as well as the orientations of water molecules surrounding the ion depend quite sensitively on the interaction potentials employed in the simulations.¹⁶

As a result of the continuous increase in computer capacity and performance, more sophisticated molecular dynamics (MD) techniques based on a combined quantum mechanics/molecular mechanics (QM/MM) approach have become an elegant tool to elucidate microscopic details of solvation structure and dynamics of various ions in solution.^{5,18–25} In the QM/MM approach, the most interesting region, a sphere which includes the ion and its surrounding solvent molecules, is treated quantum mechanically. By this scheme, the complicated many-body contributions as well as the polarization effects, which are hardly accessible through the basic assumptions underlying the classical models, can be reliably included into the specific region. For small anions, like F^- and Cl^- , our previous QM/MM studies have pointed out the importance of QM treatment for obtaining a realistic picture of these ions.^{5,19} For example, the QM/MM results clearly demonstrated a substantial decrease of the F^- coordination number compared to that predicted by pair potential simulation. In the case of Cl^- , it has been shown that the orientation of first shell water molecules was considerably changed by quantum effects, although the pair potential simulation supplied an almost identical coordination number. In addition, with respect to detailed analysis on the dynamics of

* Corresponding author fax: 0066-44-224017; e-mail: anan_tongraar@yahoo.com.

[†] Suranaree University of Technology.

[‡] University of Innsbruck.

TABLE 1: Stabilization Energies and Some Selected Structural Parameters of the Optimized NO_3^- - H_2O Complex, Calculated at HF, B3LYP, MP2, and CCSD Methods Using DZV+ and aug-cc-pvtz (Data in Parentheses) Basis Sets

method	HF	B3LYP	MP2	CCSD
ΔE (kcal \cdot mol $^{-1}$)	-16.43 (-13.58)	-18.60 (-15.76)	-16.83 (-13.96)	-16.78 (-14.19)
R_{2-1} (Å)	1.275 (1.224)	1.315 (1.263)	1.333 (1.265)	1.330 (1.252)
R_{2-3} (Å)	1.276 (1.224)	1.316 (1.263)	1.333 (1.265)	1.330 (1.252)
R_{2-4} (Å)	1.259 (1.212)	1.296 (1.247)	1.318 (1.251)	1.308 (1.239)
R_{1-7} (Å)	2.230 (2.217)	2.090 (2.062)	2.168 (2.028)	2.186 (2.071)
R_{3-5} (Å)	2.211 (2.219)	2.078 (2.071)	2.152 (2.039)	2.171 (2.055)
R_{6-5} (Å)	0.956 (0.946)	0.986 (0.972)	0.988 (0.972)	0.986 (0.970)
R_{6-7} (Å)	0.956 (0.946)	0.986 (0.972)	0.988 (0.972)	0.986 (0.970)
A_{5-6-7} (deg)	105.87 (99.94)	102.30 (97.13)	103.22 (95.81)	103.39 (96.60)
A_{1-7-6} (deg)	135.11 (138.76)	138.61 (141.93)	137.82 (143.15)	137.59 (141.21)
A_{3-5-6} (deg)	136.52 (138.61)	139.43 (141.22)	139.07 (142.17)	138.81 (142.52)

these hydrated ions, it has been proven that F^- clearly acted as a "structure-maker", while the characteristics of Cl^- solvation led to a more flexible structure with frequent rearrangements of the hydrogen bonds.²⁰

With respect to the previous QM/MM studies for simple anions, it was our increased interest to apply the more accurate QM/MM technique for studying more complicated anions, like NO_3^- . In the present study, therefore, two combined QM/MM MD simulations, namely HF/MM and B3LYP/MM, have been performed in order to obtain better knowledge about the solvation structure and dynamics of NO_3^- in water.

2. Methods

Details of the QM/MM MD technique have been reported elsewhere in the literature.^{5,18-25} With regard to the QM/MM scheme, besides the statistical requirement of a sufficiently long simulation time, the selection of the QM method, basis set, and QM size is crucial for obtaining a correct description on the structural and dynamical properties of solvated ions. As a matter of fact, the performance of QM/MM MD simulations in conjunction with correlated ab initio methods is still too time-consuming, making the HF and hybrid density functional B3LYP methods the possible alternatives for the present study. To simply test whether the HF or B3LYP methods are adequate for this particular system, geometry optimizations of the NO_3^- - H_2O complex were carried out at HF, B3LYP, MP2, and CCSD levels of accuracy (see Table 1). The comparison to the data obtained by correlated methods indicated that the HF and B3LYP methods both appear reliable enough to achieve a sufficient level of accuracy in the QM/MM simulations and that the correlation effects are small and thus negligible. As can be seen from the data in Table 1, the stabilization energies, which are the most relevant data determining solute-solvent interactions, are considerably overrated by the B3LYP method, independent of the basis set. On the other hand, the ion-ligand distances show better agreement between correlated ab initio methods and B3LYP within the same basis set quality, but the distances obtained by HF with the DZV+ basis set to be employed in the QM/MM simulation are in fair agreement with the correlated distances obtained by the larger basis set and thus indicate this basis set to be a good compromise for the simulation if the HF method is used. The HF method has been well validated in previous QM/MM studies,¹⁸⁻²⁶ even for the treatment of anions, also proving the assumption that the effects of electron correlation are small enough to be neglected.^{19,20} In a recent QM/MM MD simulation of pure water,²⁶ it has been demonstrated that the HF method with a sufficiently large QM

size could provide detailed information of pure water in good agreement with the MP2-based simulation and with experimental data concerning H-bond structure and lifetime. The B3LYP method proved inferior in this case, but it was also employed in this work in order to test its adequacy for the description of hydrated anions, as several cases have shown that the DFT methods can give poor results for hydrated cations.^{5,24,25} It should be realized that while the HF scheme could produce an error due to the neglect of electron correlation effects, the DFT methods, although including such effects to a certain (uncontrollable) extent, are often found to overestimate the correlation energy.²³⁻²⁶ On the other hand, a comparison of the HF calculations with the DFT results could be helpful to give a qualitative estimate of a possible influence of correlation effects.

In addition to the choice of the QM method, it is known that the use of a larger basis set is a key factor for obtaining better results (see Table 1). In practice, however, the computational expense for QM force calculations using large basis sets is significant. In most of the previous QM/MM studies,¹⁸⁻²⁶ a moderate basis set has been employed, therefore. In the present work, since a satisfactory description of anions requires diffuse basis functions, the DZV+ basis set²⁷ was chosen, considered as a suitable compromise between the quality of the simulation results and the requirement of CPU time. To define the size of the QM region, a preliminary HF/MM simulation, i.e., the simulation in which only the NO_3^- was treated quantum mechanically using the HF method while the rest of the system is described by classical pair potentials, was performed (see Figure 2a). According to the resulting N- O_w radial distribution function (RDF), the first minimum of the N- O_w peak is exhibited at around 5.0 Å. An integration up to the first minimum of the N- O_w peak yields about 18-20 water molecules. This implies that a QM size with diameter of 10.0 Å seemed to be desirable for the present study. However, the evaluation of QM forces for all particles within this QM size is still beyond the limit of our current computational facility. Therefore, a slightly smaller QM size with diameter of 8.8 Å was chosen, which includes NO_3^- and about 14-16 water molecules.

To ensure a continuous change of forces at the boundary between the QM and MM regions, a smoothing function²⁸ was employed within an interval of 0.2 Å (i.e., between the N- O_w distances of 4.4-4.6 Å). A flexible model, which describes intermolecular²⁹ and intramolecular³⁰ interactions, was employed for water. This flexible water model allows explicit hydrogen movements, thus ensuring a smooth transition, when water molecules move from the QM region with its full flexibility to

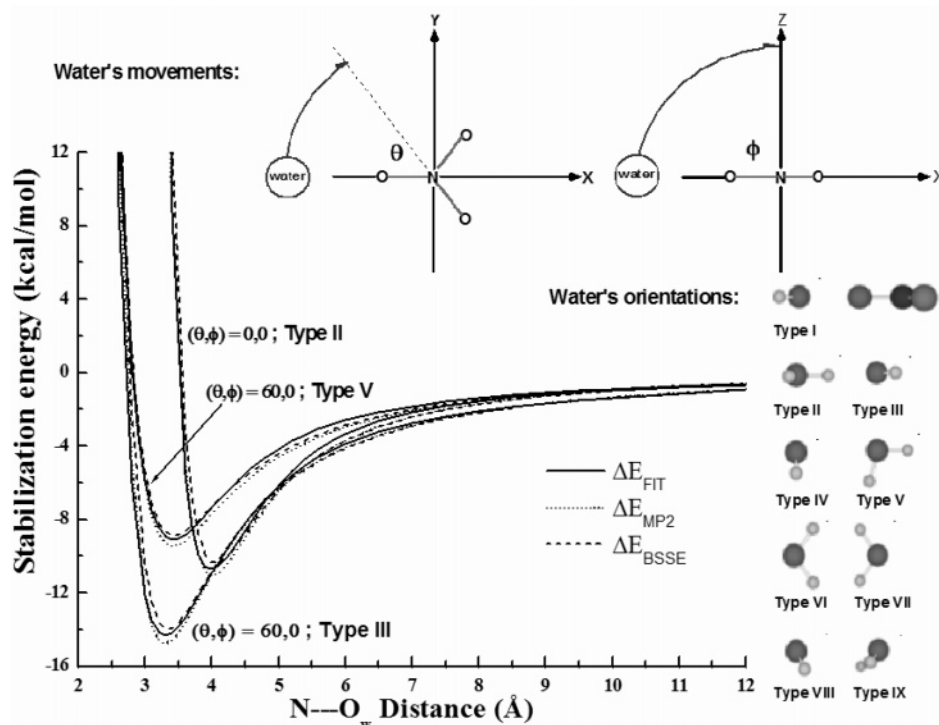


Figure 1. Comparison of the interaction energies obtained from the MP2 calculations with and without basis set superposition error (BSSE) correction, ΔE_{MP2} and ΔE_{BSSE} , and from the fitted potential function, ΔE_{FIT} , using the parameters given in Table 2 for some values of θ and ϕ .

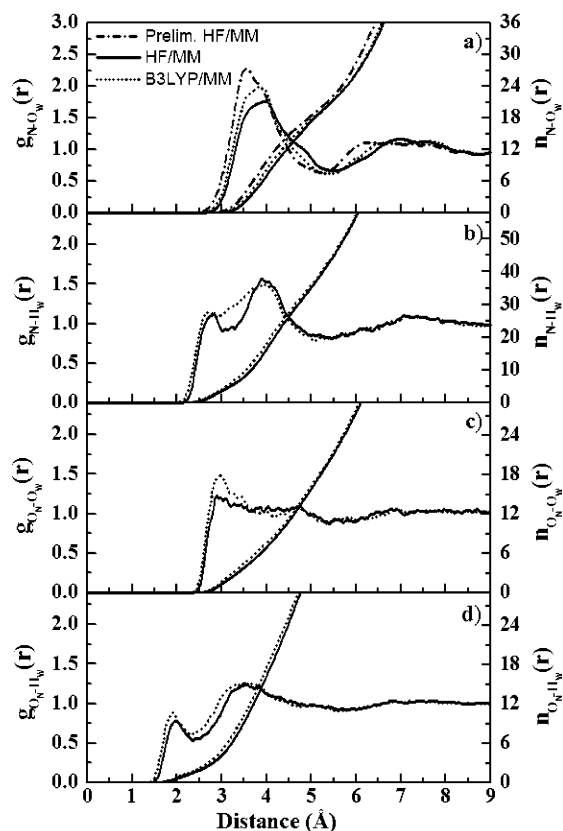


Figure 2. (a) N-O_w, (b) N-H_w, (c) O_N-O_w, and (d) O_N-H_w radial distribution functions and their corresponding integration numbers.

the MM region. The pair potential function for NO_3^- - H_2O interactions was newly constructed. The procedure is as follows: the NO_3^- ion was placed on the xy plane (see Figure 1), while a water molecule was allowed to move with respect to

TABLE 2: Optimized Parameters of the Analytical Pair Potential for the Interaction of Water with NO_3^- (Interaction Energies in $\text{kcal}\cdot\text{mol}^{-1}$ and Distances in Å)

pair	A ($\text{kcal mol}^{-1}\text{Å}^4$)	B ($\text{kcal mol}^{-1}\text{Å}^5$)	C (kcal mol^{-1})	D (Å^{-1})
N-O _w	-1310.7757	10012.1163	-55579.5941	2.8288
N-H _w	-512.0615	209.1700	5811.3787	2.9891
O _N -O _w	332.9194	1807.6405	-722.8225	1.2542
O _N -H _w	-84.1666	132.7195	53.9955	1.1110

the variation of θ (i.e., between 0 and 60°) and ϕ (i.e., between 0 and 90°), associated with 9 different types of water orientation. Then, a total of 5266 MP2 interaction energy points for various NO_3^- - H_2O configurations, obtained from Gaussian98³¹ calculations using the aug-cc-pvdz basis set,³²⁻³⁴ were fitted to an analytical form of

$$\Delta E_{\text{NO}_3^- - \text{H}_2\text{O}} = \sum_{i=1}^4 \sum_{j=1}^3 \left[\frac{A_{ij}}{r_{ij}^4} + \frac{B_{ij}}{r_{ij}^5} + C_{ij} \exp(-D_{ij}r_{ij}) + \frac{q_i q_j}{r_{ij}} \right] \quad (1)$$

where A , B , C , and D are fitting parameters (see Table 2), r_{ij} denotes the distances between the i th atoms of NO_3^- and the j th atoms of water molecule, and q are atomic net charges. In the present study, the charges on N and O of NO_3^- were obtained from the Mulliken population analysis (MPA) of MP2 calculations using the aug-cc-pvdz basis set, and the charges on O and H of the water molecule were adopted from the flexible water model.³⁰ They were set to 1.4996, -0.8332, -0.6598, and 0.3299, respectively. It is known that the MPA certainly depends on the basis set. However, when fitting a potential function to an energy surface, the absolute values of the charges are only of secondary importance since the other parameters will compensate (i.e., as an energy surface is fitted, the r^{-n} terms in the potential together with the Coulombic term

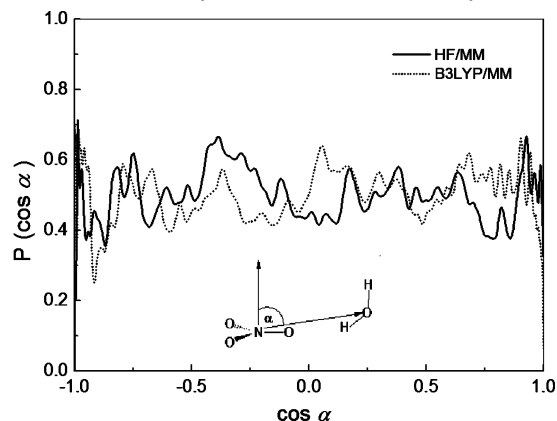


Figure 3. Distributions of the angle α between the vector perpendicular to the NO_3^- plane and the vector along the $\text{N}\cdots\text{O}_w$ distance, calculated within the first minimum of $\text{N}\cdots\text{O}_w$ RDFs.

are only an approximation to fit this surface). The quality of the fit is shown in Figure 1, where the stabilization energies obtained from the MP2 calculations (ΔE_{MP2}) and from the fitted potential function (ΔE_{FIT}) are compared for some configurations. In Figure 1, the MP2 interaction energies with BSSE correction (ΔE_{BSSE}) are also given for comparison. In this work, the counterpoise correction was not taken into consideration since the BSSE estimates suggest that a correction seems unnecessary.

All simulations were performed in a canonical ensemble at 298 K with a time step of 0.2 fs. The periodic box, with a box length of 18.17 Å, contained one NO_3^- and 199 water molecules, corresponding to the experimental density of pure water. Long-range interactions were treated using the reaction-field procedure.³⁵ The system was initially equilibrated by performing a preliminary HF/MM MD simulation, in which only the NO_3^- was treated quantum mechanically using the HF method, for 200 000 time steps. Then, the HF/MM and B3LYP/MM simulations were started independently with the system's re-equilibration for 30 000 time steps, followed by another 75 000 (HF/MM) and 85 000 (B3LYP/MM) time steps to collect configurations every 10th step.

3. Results and Discussion

3.1. Structural Details. The solvation structure of NO_3^- in water is described by means of $\text{N}\cdots\text{O}_w$, $\text{N}\cdots\text{H}_w$, $\text{O}_N\cdots\text{O}_w$, and $\text{O}_N\cdots\text{H}_w$ RDFs, together with their corresponding integration numbers, as shown in Figure 2. According to the shape and height of the resulting $\text{N}\cdots\text{O}_w$ RDFs (Figure 2a), both HF/MM and B3LYP/MM simulations reveal broad and unsymmetrical first $\text{N}\cdots\text{O}_w$ peaks with maximum at 3.96 and 3.83 Å, respectively. Integrations up to the first minimum of the corresponding $\text{N}\cdots\text{O}_w$ peaks yield average coordination numbers of 21.6 and 20.9, respectively. The observed broad and unsymmetrical $\text{N}\cdots\text{O}_w$ RDFs clearly indicate a high flexibility of the NO_3^- hydration shell. In addition, the first minimum of the $\text{N}\cdots\text{O}_w$ peaks is not well separated from the bulk, indicating a large number of water molecules situated between the hydration shell and bulk. This implies also that water molecules in the hydration shell of NO_3^- are quite mobile, i.e., they can easily exchange with bulk water. Comparing the corresponding $\text{N}\cdots\text{O}_w$ RDF obtained by the preliminary HF/MM simulation (Figure 2a), it becomes obvious that the use of only classical NO_3^- - H_2O and $\text{H}_2\text{O}\cdots\text{H}_2\text{O}$ pair potentials is inadequate to correctly describe the short-range ion-water and water-water interactions, producing a higher rigidity of the NO_3^- hydration shell.

In Figure 2b, the $\text{N}\cdots\text{H}_w$ RDFs obtained between the HF/MM and B3LYP/MM simulations are significantly different.

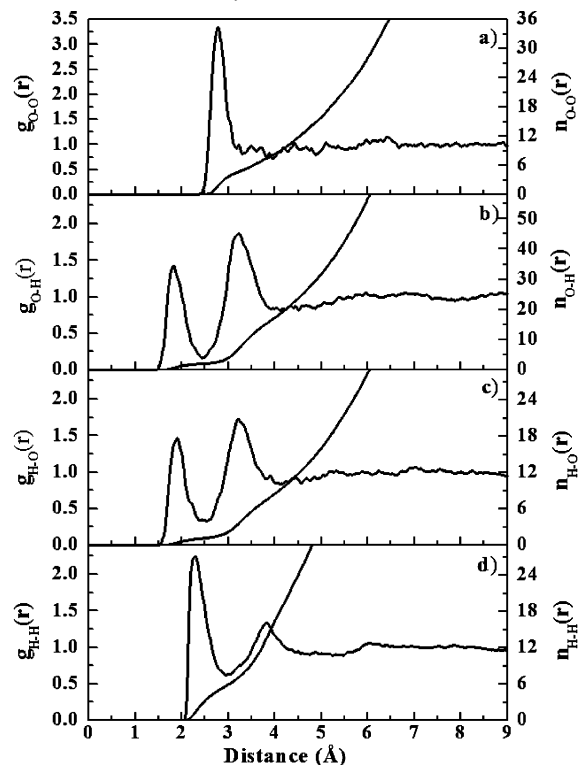


Figure 4. (a) O-O, (b) O-H, (c) H-O, and (d) H-H radial distribution functions and their corresponding integration numbers. The first atom of each pair refers to the atoms of the water molecule, whose oxygen position was defined as the center of the QM region during the QM/MM simulation.

The HF/MM simulation depicts two distinct peaks with maxima at distances of 2.62 and 4.03 Å. In the B3LYP/MM simulation, the first $\text{N}\cdots\text{H}_w$ peak is merged into a rather broad second peak, indicating that water molecules with somewhat distorted hydrogen bonding to oxygen atoms of NO_3^- are the main constituents of the first hydration shell. In Figure 2c, the $\text{O}_N\cdots\text{O}_w$ RDFs obtained from both HF/MM and B3LYP/MM simulations do not show distinct minima after the first shell, suggesting that a clear determination of the first shell coordination number for each of the oxygen atoms of NO_3^- is not feasible. This also points at rather weak ion-water hydrogen bonds. Figure 3 shows the distributions of water molecules surrounding the ion as the distributions of the cosine of angle α between the vector perpendicular to NO_3^- plane and the vector along any $\text{N}\cdots\text{O}_w$ distance. Obviously, both HF/MM and B3LYP/MM simulations do not indicate specific features for the distribution of first shell water molecules, i.e., they are mostly arranged with respect to $\text{N}\cdots\text{O}_N\cdots\text{H}_w\cdots\text{O}_w$ hydrogen bonds. The first shell waters prefer to coordinate to oxygen atoms of NO_3^- , rather than to the nitrogen atom from above and/or below the NO_3^- plane. In addition, it is expected that numerous possible arrangements, such as bifurcated hydrogen bonds as well as cyclic arrangements with two distorted hydrogen bonds, can temporarily be formed in aqueous solution.

More information on hydrogen bonds between NO_3^- and water can be obtained via the $\text{O}_N\cdots\text{H}_w$ RDFs (Figure 2d). Since the characteristics of hydrogen bonds in pure solvent represent a most important reference, the corresponding atom-atom RDFs for pure water obtained at a similar QM/MM level of accuracy³⁶ were utilized for comparison, as depicted in Figure 4. In this work, the HF/MM and B3LYP/MM simulations reveal first $\text{O}_N\cdots\text{H}_w$ peaks with maxima at 1.98 and 1.91 Å, respectively. These first $\text{O}_N\cdots\text{H}_w$ peaks are indicative of the hydrogen bonds between

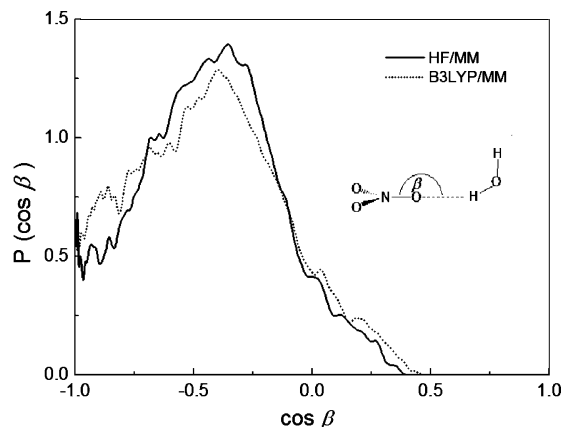


Figure 5. Distributions of the $N-O_N\cdots H_w$ angle, calculated within the $O_N\cdots H_w$ distance of 2.5 Å.

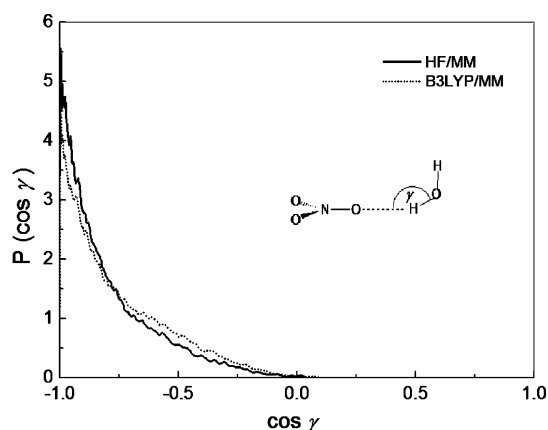


Figure 6. Distributions of the $O_N\cdots H_w-O_w$ angle, calculated within the $O_N\cdots H_w$ distance of 2.5 Å.

oxygen atoms of NO_3^- and their nearest-neighbor water molecules. Compared to the corresponding O–H RDF of pure water (Figure 4), e.g., in terms of shape and peak height, it is obvious that the $O_N\cdots H_w-O_w$ hydrogen bond interactions are rather weak.

For a more detailed interpretation on the NO_3^- –water hydrogen bonds, the probability distributions of the cosine of the $N-O_N\cdots H_w$ and $O_N\cdots H_w-O_w$ angles calculated from the subset of configurations within the $O_N\cdots H_w$ distance of 2.5 Å are plotted in Figures 5 and 6, respectively. For an ideal hydrogen bond, the $N-O_N\cdots H_w-O_w$ interactions would be in a linear arrangement, i.e. a cosine equal or near to -1 for both $N-O_N\cdots H_w$ and $O_N\cdots H_w-O_w$ angles. With respect to the results obtained by the HF/MM and B3LYP/MM simulations, the distributions of $N-O_N\cdots H_w$ angles significantly deviate from linearity, whereas the distributions of the $O_N\cdots H_w-O_w$ angle show a clear preference for the linear $O_N\cdots H_w-O_w$ arrangements. Figure 7 shows the distributions of the cosine of the angle θ , defined as the angle between the $O_w\cdots -O_N$ vector and the dipole vector of water molecules surrounding the NO_3^- oxygens. Apparently, both HF/MM and B3LYP/MM simulations show a clear dipole-oriented arrangement of water molecules surrounding the NO_3^- oxygens (e.g., the strong correlations between the nearest-neighbor water molecules and their lone pair direction), with maxima at $\cos \theta$ between 0.5 and 0.8. It is obvious that despite the fact that the interactions between NO_3^- and water are rather weak, the $O_w-H_w\cdots O_N$ bonds have a determining influence on the structure of hydrated NO_3^- .

3.2. Dynamical Details. 3.2.1. Intramolecular Geometry and Vibrations of NO_3^- . The geometrical arrangement of NO_3^-

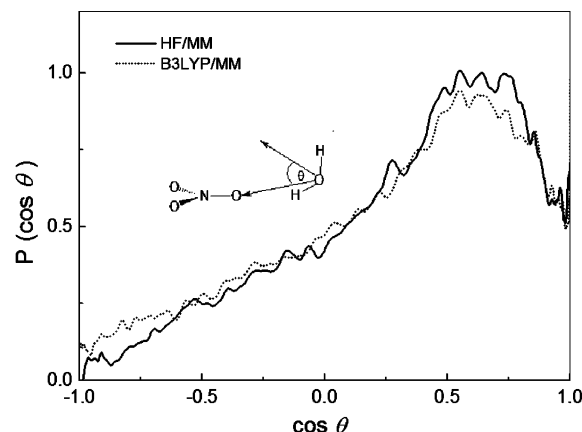


Figure 7. Distributions of the angle θ between the $O_w\cdots -O_N$ vector and the vector of water's dipole moment, calculated within the $O_N\cdots H_w$ distance of 2.5 Å.

in water is described in terms of distributions of the N–O bond length and the O–N–O angle, as shown in Figure 8 (parts a and b, respectively). Both HF/MM and B3LYP/MM simulations clearly indicate a flexibility of the NO_3^- structure, with half-height widths of about 1.26 ± 0.05 and 1.31 ± 0.06 Å for the distributions of N–O bonds and of about 120 ± 4 and $120 \pm 5^\circ$ for the distributions of O–N–O angles, respectively. The observed difference between the HF/MM and B3LYP/MM simulations can probably be regarded more as a consequence of the approximations of the functional and the parametrizations of the B3LYP method than as a consequence of correlation effects. The results obtained by both the HF/MM and B3LYP/MM simulations obviously suggest a substantial change in the local structure of NO_3^- , being either planar or nonplanar geometry with equivalent and/or inequivalent N–O bonds, according to the influence of water environment. A useful indicator of the NO_3^- planarity in aqueous solution is the distribution of the angle ϕ , defined by a vector along any N–O bond and a vector pointing outward between the other two N–O bonds, as shown in Figure 9, which illustrates that the intramolecular geometry of NO_3^- is slightly deviating from planarity, obviously because water molecules in the first hydration shell of NO_3^- oxygens break the D_{3h} symmetry of the ion.

The power spectra, which correspond to symmetric stretching (ν_1), out-of-plane bending (ν_2), asymmetric stretching (ν_3), and asymmetric bending (ν_4) vibrations, of NO_3^- were evaluated using normal-coordinate analysis.³⁷ By Fourier transformations of three components of oxygen's velocity autocorrelation functions (VACFs), the corresponding ν_1 , ν_2 , ν_3 , and ν_4 bands can be obtained, as summarized in Table 3. In this work, all calculated frequencies were multiplied by the standard scaling factors³⁸ of 0.9051 and 0.9614 for HF and B3LYP methods, respectively. With respect to the spectral data in Table 3, both HF/MM and B3LYP/MM simulations produce all four vibrational modes, with spectral frequencies in the order $\nu_3 > \nu_1 > \nu_2 > \nu_4$. The B3LYP/MM simulation produces the power spectra at lower frequencies than the HF/MM run. This corresponds to the observed higher flexibility of the NO_3^- structure (see Figures 8 and 9). In a qualitative sense, all frequencies obtained by both HF/MM and B3LYP/MM simulations are in reasonable agreement with the experimental data.^{40,41} In this context, it should be noted that most of the experimental measurements for spectral analysis on NO_3^- have to be performed with solutions of relatively high concentrations, whereas the present HF/MM and B3LYP/MM results refer to dilute solution.

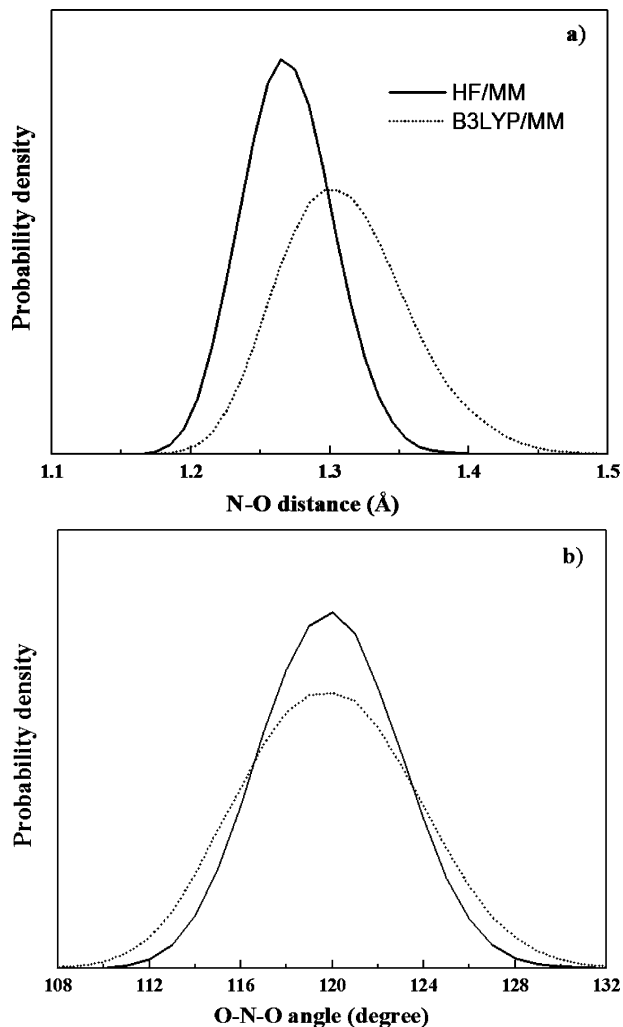


Figure 8. Distributions of (a) the N–O bond length and (b) the O–N–O angle of NO_3^- .

An interesting feature of the vibrational frequencies of NO_3^- is the experimentally observed ν_3 splitting in aqueous solutions. According to the experimental observations,^{7,8,40} the ν_3 asymmetric N–O stretching mode was found to consist of two distinctive peaks corresponding to the decrease of local symmetry of NO_3^- , i.e., from D_{3h} to C_{2v} (or lower), due to its interaction with surrounding water molecules. In this work, the splitting of the ν_3 band is well reflected, being about 40 and 24 cm^{-1} for HF/MM and B3LYP/MM simulations, respectively. In addition, in both simulations, the ν_2 mode is less pronounced. This frequency mode is usually related to the change in the equilibrium geometry of NO_3^- from planar to pyramidal upon electronic excitation.⁷ In this context, the observed low intensity of ν_2 bands can be attributed to the fact that the structure of NO_3^- in aqueous solution is not too far from planarity (see Figure 9). This finding is inconsistent with the lack of intensity of the out-of-plane deformation band in the resonance Raman spectrum of hydrated NO_3^- .⁷

3.2.2. Intramolecular Geometry and Vibrations of Water Molecules in the Hydration Shell of NO_3^- . The intramolecular geometry of water molecules in the bulk and in the vicinity of NO_3^- is explained in terms of distributions of O–H bond length and H–O–H angle, as shown in Figure 10 (parts a and b, respectively). The B3LYP/MM simulation shows longer O–H bond lengths together with narrower H–O–H angles compared to the HF/MM results, with half-height widths of 0.98 ± 0.035 and 0.96 ± 0.03 Å for the distributions of O–H bonds and of

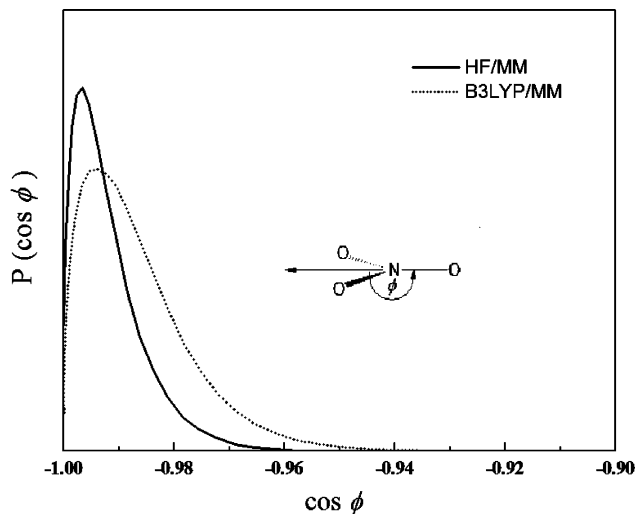


Figure 9. Distributions of ϕ , as defined by a vector along any N–O bond and a vector pointing outwards between the other two N–O bonds.

TABLE 3: Vibrational Frequencies of NO_3^-

method	frequencies (cm^{-1})			
	ν_1	ν_2	ν_3	ν_4
HF/MM MD	1088	712	1401, 1441	709
B3LYP/MM MD	965	710	1237, 1313	649
classical MD ¹⁶	1009	814, 833	1380, 1393	704
classical MD ¹⁶	996	816	1379	689
MP4 (gas phase) ³⁹	996	816	1379	689
B3LYP (gas phase) ³⁹	1061	844	1364	707
experiments ^{40,41}	1049	825	1348, 1404	719
			1340, 1460	720, 740

103 ± 8 and $110 \pm 6.5^\circ$ for the distributions of H–O–H angles, respectively. These differences can be a consequence of the higher coordination numbers resulting from the B3LYP/MM simulation, which will be discussed later.

With respect to the normal-coordinate analyses,³⁷ the three quantities, Q_1 , Q_2 , and Q_3 , calculated from the VACFs of water's hydrogens for describing symmetric stretching and bending and asymmetric stretching motions, respectively, are reported in Table 4. To reliably describe the effect of NO_3^- on the vibrational motions of its surrounding water molecules, the corresponding data for pure water obtained from previous HF/MM³⁶ and B3LYP/MM⁴³ simulations are given for comparison. In the HF/MM simulation, the bending and stretching frequencies of water molecules in the hydration shell of NO_3^- are slightly blue-shifted, by about 23, 3, and 15 cm^{-1} for Q_2 , Q_1 , and Q_3 , respectively. The observed small changes in both the bending and stretching modes can be ascribed to a slight influence of NO_3^- on the vibrational motions of its surrounding water molecules. In the B3LYP/MM simulation, the corresponding Q_2 mode is blue-shifted by 15 cm^{-1} , while the Q_1 and Q_3 show significant red-shifts of 187 and 25 cm^{-1} , respectively. These data are in good accord with a generally more rigid structure of hydrated NO_3^- resulting from the DFT approach, which generally tends to exaggerate the strength of hydrogen bonds.^{42,43}

3.2.3. Translational Motion and Exchange Process of Water Molecules in the Hydration Shell of NO_3^- . The self-diffusion coefficients (D) for water molecules in the bulk and in the hydration sphere of NO_3^- were calculated from the water's center-of-mass VACFs using the Green-Kubo relation⁴⁷

$$D = \frac{1}{3} \lim_{t \rightarrow \infty} \int_0^t C_v(t) dt \quad (2)$$

TABLE 4: Vibrational Frequencies of Water Molecules in the Bulk and in the Hydration Sphere of NO_3^- ^c

vibrations (cm^{-1})	hydration shell of NO_3^-	^a bulk	H_2O (expt) ^b
Q_2	1661 (1637)	1638, ³⁶ 1640 ^{42,43} (1622) ⁴³	1645, ⁴⁴ 1643 ⁴⁵
Q_1	3566 (3393)	3563, ³⁶ 3770, ⁴² 3774 ⁴³ (3580) ⁴³	3345, ⁴⁴ 3400 ^{45,46}
Q_3	3691 (3528)	3676, ³⁶ 3775, ⁴² 3773 ⁴³ (3553) ⁴³	3445 ⁴⁴

^a Values obtained from previous HF/MM and B3LYP/MM (i.e., numbers in parentheses) MD simulations of pure water using DZV (ref 36) and DZP (refs 42 and 43) basis sets. ^b Experimental values of liquid water. ^c Numbers in parentheses correspond to the data obtained by B3LYP/MM-based simulations.

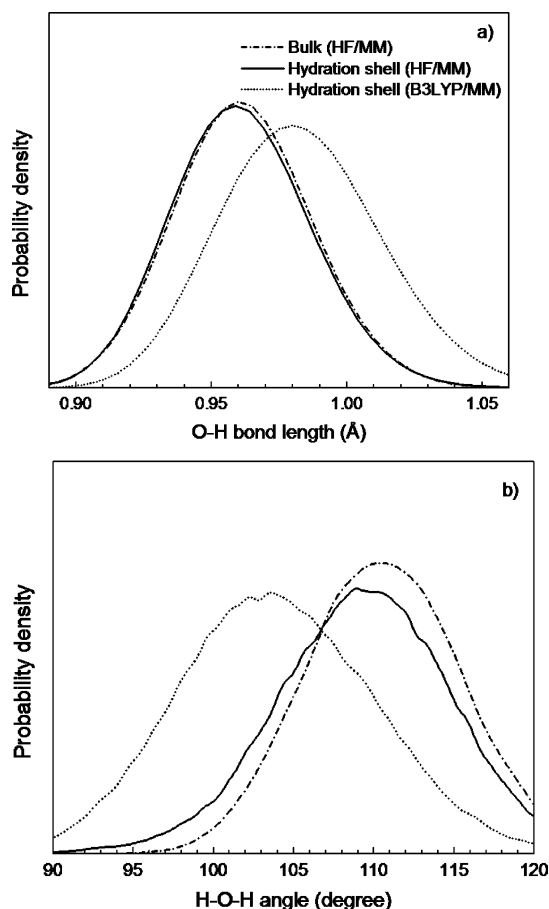


Figure 10. Distributions of (a) the O–H bond length and (b) the H–O–H angle of water molecules in the bulk and in the hydration shell of NO_3^- .

TABLE 5: Diffusion Coefficients of Water Molecules in the Bulk and in the Hydration Shell of NO_3^-

method	hydration shell of NO_3^- ($\times 10^{-5} \text{ cm}^2 \text{ s}^{-1}$)	bulk ($\times 10^{-5} \text{ cm}^2 \text{ s}^{-1}$)
HF/MM MD	5.09	3.31 ³⁶
B3LYP/MM MD	4.14	
experiment		2.30 ⁴⁸

All of the calculated D values are summarized in Table 5. In comparison to the data for bulk water obtained by a compatible QM/MM simulation,³⁶ the D values obtained from the HF/MM and B3LYP/MM simulations clearly indicate a high mobility of water molecules in the vicinity of NO_3^- . This phenomenon is inconsistent with the observed high flexibility of the NO_3^- –water complex because of the weak ion–water interactions.

According to the $\text{N}-\text{O}_w$ (Figure 2a) and the O_N-O_w RDFs (Figure 2c), the nonzero first minimum of the RDFs obtained in both HF/MM and B3LYP/MM simulations suggests an easy exchange of water molecules in the vicinity of NO_3^- . Numerous water exchange processes, following either associative (A) or

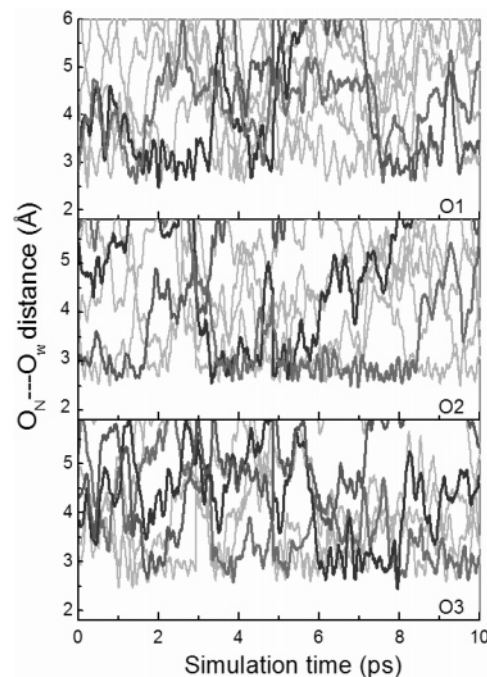


Figure 11. Time dependence of O_N-O_w distances, selecting only for the first 10 ps of the HF/MM simulation.

dissociative (D) as well as associative (I_a) and dissociative (I_d) interchange mechanisms, were indeed observed when the O_N-O_w distances were plotted against simulation time for the HF/MM and B3LYP/MM simulations, as shown in Figures 11 and 12, respectively. The variability of water exchange process mechanisms observed can be considered as indication toward weak ion–water hydrogen bond interactions.

The rate of water exchange processes at each of the NO_3^- oxygens was evaluated via mean residence times (MRT) of the water molecules. In this work, the MRT data were calculated using the direct method,⁴⁹ as the product of the average number of nearest-neighbor water molecules located within the O_N-O_w distance of 3.5 Å with the duration of the simulation, divided by the number of exchange events. Since the O_N-O_w RDFs are less pronounced (see Figure 2c), the O_N-O_w distance of 3.5 Å was selected, assuming to be a rough estimate of the first minimum of O_N-O_w RDFs and a limit for a significantly stabilizing anion–water interaction. Applying this evaluation limit, significantly different coordination numbers result from HF and B3LYP framework: while the HF method predicts average coordination numbers of 3.74–3.78 for the oxygens, the same data for the B3LYP method are 4.75–4.99 (cf. Table 6). While all other data reported so far could be considered similar for both methods, these coordination numbers make a significant difference for the structure of the hydrated anion. Following the reported tendency of DFT methods to overestimate hydrogen bonding, the HF values are considered to be more reliable, but a better evaluation of this assumption appears only possible by a substantial increase of the QM diameter to

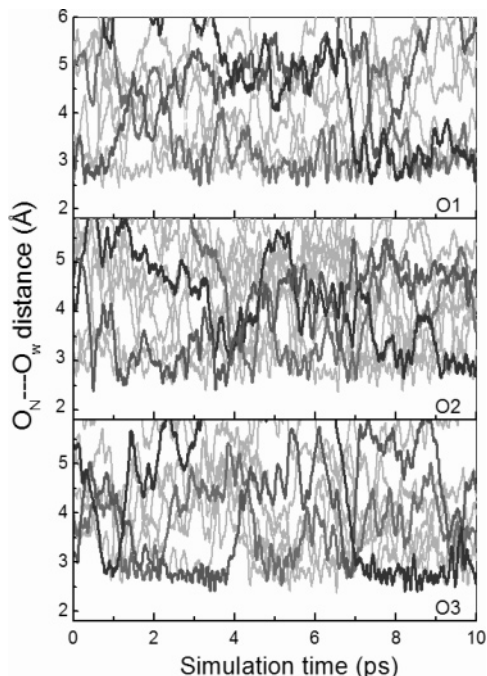


Figure 12. Time dependence of $\text{O}_N\text{---O}_w$ distances, selecting only for the first 10 ps of the B3LYP/MM simulation.

TABLE 6: Mean Residence Time of Water Molecules in the Bulk and in the Vicinity of NO_3^- Oxygens, Calculated within the $\text{O}_N\text{---O}_w$ Distance of 3.5 Å

atom/solute	CN	t_{sim}	$t^* = 0.0$ ps		$t^* = 0.5$ ps	
			$N_{\text{ex}}^{0.0}$	$\tau_{\text{H}_2\text{O}}^{0.0}$	$N_{\text{ex}}^{0.5}$	$\tau_{\text{H}_2\text{O}}^{0.5}$
HF/MM MD						
O1	3.76	15.0	492	0.11	44	1.28
O2	3.74	15.0	464	0.12	39	1.44
O3	3.84	15.0	498	0.11	47	1.26
pure H_2O^{36}	4.6	12.0	292	0.2	31	1.8
pure H_2O^{43}	4.2	40.0		0.33		1.51
B3LYP/MM MD						
O1	4.77	17.0	554	0.15	52	1.56
O2	4.99	17.0	613	0.14	61	1.39
O3	4.75	17.0	562	0.14	59	1.37
pure H_2O^{43}	4.2	30.0		1.07		7.84

a value including a second shell of water molecules, thus including also hydrogen bonding between ligands and bulk into the same quantum mechanical description. Such an evaluation will be performed, when the necessary computational facilities will be available.

With respect to time parameters t^* (i.e., the minimum duration of a ligand's displacement from its original coordination shell to be accounted) of 0.0 and 0.5 ps, the calculated MRT values are summarized in Table 6. In general, the MRT data obtained using $t^* = 0.0$ ps are used for an estimation of hydrogen bond lifetimes, whereas the data obtained with $t^* = 0.5$ ps are considered as a good estimate for sustainable ligand exchange processes.⁴⁹ In this work, $\tau_{\text{H}_2\text{O}}(\text{O}_i) < \tau_{\text{H}_2\text{O}}(\text{H}_2\text{O})$ results from both the HF/MM and B3LYP/MM simulations, without much differences in the values. However, as can be seen in Table 6, the previous B3LYP/MM simulation⁴³ of pure water had predicted much too slow exchange rates (while the HF values are close to the experimental values), proving the overestimation of hydrogen-bond strength by the B3LYP method. Hence, the anion-induced MRT differences obtained from the B3LYP/MM results are surely correct for the description but most probably too high in the amount. All MRT values obtained in both simulations make it obvious, however, that water molecules

binding to NO_3^- oxygens are quite labile and that the hydrogen bonds between NO_3^- and water are weak, thus enabling very frequent water exchange processes within the hydration sphere of NO_3^- . The observed differences between the MRT values of the NO_3^- oxygens are related to the solvation structure of NO_3^- . On the other hand, this also implies that the time of simulation may not sufficient for a complete sampling of all possible structures at each of these oxygens. However, the variation width is small enough to assume reliability of the average value.

The MRT data are characteristic for a "structure-breaking" substance, and the ability of NO_3^- to act as structure-breaker in aqueous solution is also in accordance with all the previously reported data from our simulations.

4. Conclusion

The QM/MM MD simulations of this work have once more shown the capability of this approach in providing details of solvation structure and dynamics of ions, in this case specifically for the weakly interacting NO_3^- in dilute aqueous solution. Comparing the HF and B3LYP methods for the QM part of the system, most of the structural and dynamical data appear rather similar at a first glance, but coordination numbers and dynamical data finally indicate a certain superiority of the ab initio HF formalism. Possible weaknesses of the B3LYP scheme could be attributed to the incompleteness of the kinetic energy term, the self-interaction error, and the parametrization of the B3LYP method which did not contain any H-bonded system. The vibrations of NO_3^- clearly reflect the experimentally observed solvent-induced symmetry breaking of this ion in aqueous solution. The anion forms a distinct but very loosely bound first hydration shell, based on weak nitrate oxygen–water hydrogen bonds. The lability of this shell results in frequent exchanges of water molecules and causes a typical structure-breaking behavior of this ion in aqueous solution. When computational facilities allow, a further improvement of the quantitative values can be expected from extending the size of the QM region as well as from using ab initio correlated methods.

Acknowledgment. This work was supported by the Thailand Research Fund, under the TRF Basic Research Grant (Project No. BRG4880010). B.M.R. acknowledges support by the Austrian Science Foundation (FWF Project P16221-N08).

References and Notes

- (1) Frank, H. *Chemical Physics of Ionic Solutions*; John Wiley & Sons: New York, 1956.
- (2) Williams, R. J. P. *Bio-inorganic Chemistry*; American Chemical Society: Washington, DC, 1971.
- (3) Ohtaki, H.; Radnai, T. *Chem. Rev.* **1993**, *93*, 1157.
- (4) Bopp, P. In *The Physics and Chemistry of Aqueous Ionic Solutions*; Reidel Publishing Company: 1987; p 217.
- (5) Rode, B. M.; Schwenk, C. F.; Tongraar, A. *J. Mol. Liq.* **2004**, *110*, 105.
- (6) Ferguson, E. E.; Fehsenfeld, F. C.; Albritton, D. L. *Gas-Phase Ion Chemistry*; Academic: New York, 1979.
- (7) Waterland, M. R.; Kelley, A. M. *J. Chem. Phys.* **2000**, *113*, 6760.
- (8) Waterland, M. R.; Stockwell, D.; Kelley, A. M. *J. Chem. Phys.* **2001**, *114*, 6249.
- (9) Wahab A.; Mahiuddin, S.; Hefter, G.; Kunz, W.; Minofar, B.; Jungwirth, P. *J. Phys. Chem. B* **2005**, *109*, 24108.
- (10) Nakahara, M.; Emi, K. *J. Chem. Phys.* **1993**, *99*, 5418.
- (11) Ikushima, Y.; Saito, N.; Arai, M. *J. Phys. Chem. B* **1998**, *102*, 3029.
- (12) Laaksonen, A.; Kovacs, H. *Can. J. Chem.* **1994**, *72*, 2278.
- (13) Kataoka, Y. *Bull. Chem. Soc. Jpn.* **1993**, *66*, 2478.
- (14) Guilbaud, P.; Wipff, G. *J. Phys. Chem.* **1993**, *97*, 5685.
- (15) Kato, T.; Hayashi, S.; Oobatake, M.; Katsunosuke, K. *J. Chem. Phys.* **1993**, *99*, 3966.

- (16) Ebner, C.; Sansone, R.; Hengrasmee, S.; Probst, M. *Int. J. Quantum Chem.* **1999**, *75*, 805.
- (17) Dang, L. X.; Chang, T.-M.; Roeselova, M.; Garrett, B. C.; Tobias, D. *J. Chem. Phys.* **2006**, *124*, 66101.
- (18) Kercharoen, T.; Liedl, K. R.; Rode, B. M. *Chem. Phys.* **1996**, *211*, 313.
- (19) Tongraar, A.; Liedl, K. R.; Rode, B. M. *J. Phys. Chem. A* **1998**, *102*, 10340.
- (20) Tongraar, A.; Rode, B. M. *Phys. Chem. Chem. Phys.* **2003**, *5*, 357.
- (21) Tongraar, A.; Rode, B. M. *Chem. Phys. Lett.* **2005**, *403*, 314.
- (22) Tongraar, A.; Rode, B. M. *Chem. Phys. Lett.* **2005**, *409*, 304.
- (23) Intharathap, P.; Tongraar, A.; Sagarik, K. *J. Comput. Chem.* **2005**, *26*, 1329.
- (24) Rode, B. M.; Schwenk, C. F.; Hofer, T. S.; Randolph, B. R. *Coor. Chem. Rev.* **2005**, *249*, 2993.
- (25) Rode, B. M.; Hofer, T. S. *Pure Appl. Chem.* **2006**, *78*, 525.
- (26) Rode, B. M.; Hofer, T. S.; Randolph, B. R.; Schwenk, C. F.; Xenides, D.; Vchirawongkwin, V. *Theor. Chem. Acc.* **2005**, *249*, 2993.
- (27) Dunning, T. H., Jr.; Hay, P. J. In *Modern Theoretical Chemistry, III*; Plenum: New York, 1976.
- (28) Brooks, B. R.; Bruccoleri, R. E.; Olafson, B. D.; States, D. J.; Swaminathan, S.; Karplus, M. *J. Comput. Chem.* **1983**, *4*, 187.
- (29) Stillinger, F. H.; Rahman, A. *J. Chem. Phys.* **1976**, *68*, 666.
- (30) Bopp, P.; Jancsó, G.; Heinzinger, K. *Chem. Phys. Lett.* **1983**, *98*, 129.
- (31) Frisch, M. J.; Trucks, G. W.; Schlegel, H. B.; Scuseria, G. E.; Robb, M. A.; Cheeseman, J. R.; Zakrewski, V. G.; Montgomery, J. A.; Stratmann, R. E.; Burant, J. C.; Dapprich, S.; Millam, J. M.; Daniels, A. D.; Kudin, K. N.; Strain, M. C.; Farkas, O.; Tomasi, J.; Barone, V.; Cossi, M.; Cammi, R.; Mennucci, B.; Pomelli, C.; Adamo, C.; Clifford, S.; Ochterski, J.; Peterson, G. A.; Ayala, P. Y.; Cui, Q.; Morokuma, K.; Malick, D. K.; Rabuck, A. D.; Raghavachari, K.; Foresman, J. B.; Cioslowski, J.; Ortiz, J. V.; Stefanov, B. B.; Liu, G.; Liashenko, A.; Piskorz, P.; Komaromi, I.; Gomperts, R.; Martin, R. L.; Fox, D. J.; Keith, T.; Al-Laham, M. A.; Peng, C. Y.; Nanayakkara, A.; Gonzalez, C.; Challacombe, M.; Gill, P. M. W.; Johnson, B. G.; Chen, W.; Wong, M. W.; Andres, J. L.; Head-Gordon, M.; Replogle, E. S.; Pople, J. A. *GAUSSIAN 98*; Gaussian, Inc.: Pittsburgh, PA, 1998.
- (32) Dunning, T. H. *J. Chem. Phys.* **1989**, *90*, 1007.
- (33) Kendall, R. A.; Dunning, T. H.; Harrison, R. J. *J. Chem. Phys.* **1992**, *96*, 6769.
- (34) Woon, D. E.; Dunning, T. H. *J. Chem. Phys.* **1993**, *98*, 1358.
- (35) Adams, D. J.; Adams, E. H.; Hills, G. J. *Mol. Phys.* **1979**, *38*, 387.
- (36) Tongraar, A.; Rode, B. M. *Chem. Phys. Lett.* **2004**, *385*, 378.
- (37) Bopp, P. *Chem. Phys.* **1986**, *106*, 205.
- (38) Scott, A. P.; Radom, L. *J. Phys. Chem.* **1996**, *100*, 16502.
- (39) Ebner, C.; Sansone, R.; Probst, M. *Int. J. Quantum Chem.* **1998**, *70*, 877.
- (40) Irish, D.; Davis, A. *Can. J. Chem.* **1968**, *46*, 943.
- (41) Irish, D.; Chang, G.; Nelson, D. *Inorg. Chem.* **1970**, *9*, 2.
- (42) Xenides, D.; Randolph, B. R.; Rode, B. M. *J. Mol. Liq.* **2006**, *123*, 61.
- (43) Xenides, D.; Randolph, B. R.; Rode, B. M. *J. Chem. Phys.* **2005**, *122*, 174506.
- (44) Murphy, W. F.; Berstein, H. J. *J. Phys. Chem.* **1972**, *76*, 1147.
- (45) Lock, A. J.; Bakker, H. J. *J. Chem. Phys.* **2002**, *117*, 1708.
- (46) Deák, J. C.; Rhea, S. T.; Iwaki, L. K.; Dlott, D. D. *J. Phys. Chem. A* **2000**, *104*, 4866.
- (47) McQuarrie, D. A. *Statistical Mechanics*; Harper Row: New York, 1976.
- (48) Woolf, L. A. *J. Chem. Soc., Faraday Trans.* **1975**, *71*, 784.
- (49) Hofer, T. S.; Tran, H. T.; Schwenk, C. F.; Rode, B. M. *J. Comput. Chem.* **2004**, *25*, 211.

CIRRICULUM VITAE

Piyawan Tangkawanwanit

Education:

- 1995-1998 B.Sc. (Chemistry), Rajabhat Institute of Ubon Rachathani, Ubon Ratchathani, Thailand
- 1998-2001 M.Sc. (Applied Chemistry), King Mungkut's Institute of Technology Ladkrabang, Bangkok, Thailand
- 2001-2006 Ph.D. (Chemistry), Suranaree University of Technology, Nakhon Ratchasima, Thailand

Experience:

- 1997 Teaching Assistant, Department of Chemistry, Faculty of Science, King Mungkut's Institute of Technology Ladkrabang, Bangkok, Thailand
- 1999 Lecturer, Faculty of Engineering, Rachathani University, Ubon Ratchathani, Thailand
- 2004-2005 Teaching Assistant, Department of Chemistry, Faculty of Science, Suranaree University of Technology, Nakhon Ratchasima, Thailand
- 2004 Lecturer, Faculty of Science and Technology, Nakhon Ratchasima Rajabhat University, Nakhon Ratchasima, Thailand
- 2005 Lecturer, Faculty of Engineering, Rajamangala University of Technology Isan, Nakhon Ratchasima, Thailand